AB INITIO STUDIES OF THE GROUND STATE STRUCTURE AND PROPERTIES OF BORON CARBIDES AND RUTHENIUM CARBIDES

Thesis

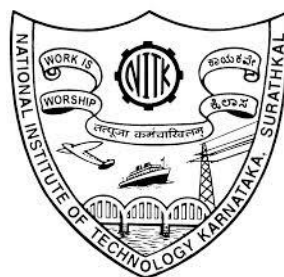Submitted in partial fulfilment of the requirements for the degree of

DOCTOR OF PHILOSOPHY

By

HARIKRISHNAN G.
(Roll No. 102022 PH10P02)

DEPARTMENT OF PHYSICS

NATIONAL INSTITUTE OF TECHNOLOGY KARNATAKA

SURATHKAL, INDIA -575 025

August, 2016

DECLARATION

I hereby declare that the Research Thesis entitled "**AB INITIO STUDIES OF THE GROUND STATE STRUCTURE AND PROPERTIES OF BORON CARBIDES AND RUTHENIUM CARBIDES**" which is being submitted to the National Institute of Technology Karnataka, Surathkal in partial fulfilment of the requirements for the award of the degree of **Doctor of Philosophy** in **Physics**, is a bonafide report of the research work carried out by me. The material contained in this thesis has not been submitted to any university or institution for the award of any degree.

Place : NITK Surathkal

Date : 18.08.2016

HARIKRISHNAN G.

102022 PH10P02
Department of Physics

CERTIFICATE

This is to certify that the Research Thesis entitled "**AB INITIO STUDIES OF THE GROUND STATE STRUCTURE AND PROPERTIES OF BORON CARBIDES AND RUTHENIUM CARBIDES**" submitted by **Harikrishnan G.** (Register Number: 102022 PH10P02) as the record of research work carried out by him, is accepted as the Research Thesis submission in partial fulfilment of the requirements for the award of the degree of **Doctor of Philosophy**.

Dr. Ajith K. M.   Chairperson-DRPC

Research Guide   (Signature with date and seal)

(Signature with date and seal)

To Valsa sir

ACKNOWLEDGEMENTS

ABSTRACT

This work investigates the ground state structure and properties of Boron Carbides ($B_{12}C_3$ and $B_{13}C_2$ stoichiometries) and Ruthenium Carbides (RuC, Ru_2C and Ru_3C stoichiometries), each belonging to a class of hard materials. Exhaustive crystal structure search using evolutionary algorithm and density functional theory is performed in each of these stoichiometries. The lowest energy structures emerging from the structure search are further relaxed and their ground properties are computed using DFT. The work in $B_{12}C_3$ stoichiometry provides the first independent confirmation using structure search that $B_{11}C^p$(CBC) is the ground state structure of this stoichiometry. It is established that mechanically and dynamically stable structures with base-centered monoclinic symmetry can be at thermodynamical equilibrium at temperatures up to 660 K in $B_{12}C_3$, raising the possibility of identifying the monoclinic symmetry in experimental measurements. A demonstration of experimentally identifiable signatures of monoclinic symmetry is provided through the computed cumulative infrared spectrum of some of the systems. The work in $B_{13}C_2$ stoichiometry has conclusively solved the long standing problem of the discrepancy between the DFT calculations and the experimental observations over the semiconducting nature of $B_{13}C_2$. The remarkable success of a newly identified 30-atom-cell structure in explaining many of the experimental data on $B_{12}C_3$ and $B_{13}C_2$ provides the first definitive evidence that structures with larger unit cells, are associated with crystals of these stoichiometries even at the ground state. The work in Ruthenium Carbide stoichiometries has gathered into a coherent perspective the widely varying structures proposed from experimental reports of synthesis, computational modeling and crystal structure search and provided conclusive structural candidates to be pursued in experiments. The study of the pressure-induced variation of their stability and properties has set indicators and benchmarks for future experimental investigations. The estimation of hardness of all the systems has underlined their importance in many applications, with nearly superhard values for some of them.

KEYWORDS : Evolutionary Algorithm, Density Functional Theory, Hardness.

TABLE OF CONTENTS

LIST OF FIGURES

LIST OF TABLES

NOMENCLATURE

B	Boron
B$_4$C	Boron Carbides
BaTiO$_3$	Barium Titanate
BEC	Born Effective Charges
B$_H$	Bulk Modulus in Hill approximation
B$_R$	Bulk Modulus in Reuss approximation
B$_V$	Bulk Modulus in Voigt approximation
BZ	Brillouin Zone
C	Carbon
C-BN	Cubic Boron Nitride
C$_v$	Heat Capacity
C$_{\alpha\beta}$	Matrix elements of elastic stiffness constant matrix
DFPT	Density Functional Perturbation Theory'
DFT	Density Functional Theory
DOS	Density of States
F	Helmholtz Free Energy
GGA	Generalized Gradient Approximation
G$_H$	Shear Modulus in Hill approximation
GPa	Gigapascal
G$_R$	Shear Modulus in Reuss approximation
G$_V$	Shear Modulus in Voigt approximation
IR	Infra-Red
KS	Kohn-Sham
LDA	Local Density Approximation

MD	Molecular Dynamics
n(r)	Electron density
NMR	Nuclear Magnetic Resonance
PAW	Projected Augmented Wave
PBE	Perdew-Burke-Ernzerhof
PtC	Platinum Carbide
PtN	Platinum Nitride
ReB$_2$	Rhenium diboride
RuC	Ruthenium Carbide
RuN	Ruthenium Nitride
S	Entropy
SIESTA	Spanish Initiative for Electronic Simulations with Thousands of Atoms
SrTiO$_3$	Strontium Titanate
USPEX	Universal Structure Predictor: Evolutionary Xtallography
VASP	Vienna Ab initio Simulation Package
VESTA	Visualization for Electronic and Structural Analysis
V$_H$(r)	Hartree potential energy
$V_n(r)$	Coulomb potential of the nuclei as experienced by the electrons
V$_{xc}$(r)	Exchange-correlation potential
WC	Tungsten Carbide
Y	Young's Modulus
Z	Partition Function
ν	Poisson's ratio
Ψ	Many particle wave function
φ	Single particle wave function

Chapter 1

INTRODUCTION

One system each from two classes of hard materials will be studied in this work. The first one to be identified as such a class consists of insulators or semiconductors of light elements B, C, N and O, having covalent bonds of short bond lengths and high cohesive energies (Gilan,2009; Veprek *et al*., 2000). Diamond with the highest measured Vickers hardness (H_V ~ 96 GPa, Field, 1992), cubic Boron Nitride (c–BN; H_V ~ 50 GPa) and Boron Carbide ($B_{12}C_3$; H_V ~ 30 GPa, Werheit *et al*., 2004) are some of the familiar superhard (H_V > 40 GPa, Gilan, 2009) and hard materials belonging to this class. The study of Boron Carbide from this class forms the first half of this work. Compounds of transition metal atoms with atoms of B, C or N constitute the more recently recognized second class of hard materials (Kaner *et al.*, 2005; Gilman *et al*., 2006; Levine *et al*., 2009). A high charge density of valence electrons supplied by the transition metal atom and p–d hybridized strong covalent bonds formed between B, C or N atom and transition metal atom can make borides, carbides and nitrides of transition metals potentially very hard materials. Borides of transition metals like Ru, Re, Os etc. have recently been found to be superhard materials (Levine *et al*., 2009). For example, microindentation measurements on rhenium diboride (ReB_2) indicated a hardness of about 48 GPa (Chung *et al*., 2007). Carbides and nitrides of 4d- and 5d-metals such as PtC, PtN_x, IrN_x and RuN (Gregoryanz *et al*., 2004; Ono *et al*., 2005; Crowhurst *et al*., 2006; Young *et al*., 2006) are recently synthesized, and high hardness is predicted for some of them (Ivanovskii, 2009). The study of Ruthenium Carbide from this latter class constitutes the other half of this work.

1.1. BORON CARBIDES

Boron Carbide is a fascinating material, both in terms of the variety of its technological and industrial applications based on its peculiar properties and the elusive nature of its structure over an unusually wide homogeneity range. It's very high hardness and low density have led to its use as an armour material and cutting tool material; high melting point, thermal stability and high degree of chemical inertness have made it suitable for refractory applications and wear resistant coatings; it is considered as a potential material for electronic and thermoelectric devices designed for high temperature applications; its large reaction cross-section for thermal neutron absorption has prompted its role as shielding material in nuclear reactors (Thevenot, 1990; Hosmane *et al.*, 2006; Vast *et al.*, 2009; Suri *et al.*, 2010; Shirai, 2010; Domnich *et al.*, 2011). It has been established that the stable phase of Boron Carbide extends over a range of 8–20 atomic percent of carbon though both limits of the range have not been conclusively fixed (Thevenot, 1990). Despite its early synthesis, investigation of properties and successful applications, the crystal structure of Boron Carbide across different stoichiometries is still being debated in the literature (Thevenot, 1990; Hosmane *et al.*, 2006; Vast *et al.*, 2009; Suri *et al.*, 2010; Shirai, 2010; Domnich *et al.*, 2011). Two of its stoichiometries studied most extensively are those corresponding to 20 at.% C, with a formula unit of $B_{12}C_3$ or B_4C, and 13.3 at.% C, with a formula unit of $B_{13}C_2$. This work will focus on these two stoichiometries of Boron Carbides.

1.1.1. $B_{12}C_3$ Stoichiometry

The basic structural unit of $B_{12}C_3$ has been identified as 12-atom icosahedra located at the vertices of a rhombohedral lattice of $R\bar{3}m$ (166) space group and the 3-atom linear chain linking the icosahedra along the (111) axis of the rhombohedral unit cell (Thevenot, 1990). $R\bar{3}m$ symmetry is preserved only if all the icosahedral atoms are identical. So the idealized structure is composed of icosahedral cage of 12 boron atoms and the chain of 3 carbon atoms, labeled as $B_{12}(CCC)$. Here we adopt the labeling of the formula unit such that the atoms constituting the 12-atom cage are specified outside the

brackets while those constituting the 3-atom chain are within the brackets. Two views of B_{12}(CCC) structure are shown in figure 1.1. The blue coloured boron atoms occupy the polar sites and the green coloured boron atoms occupy the equatorial sites within the icosahedron. Carbon atoms are shown in brown. All the figures of the structures are generated using the crystal visualization program VESTA (Momma and Izumi, 2011).
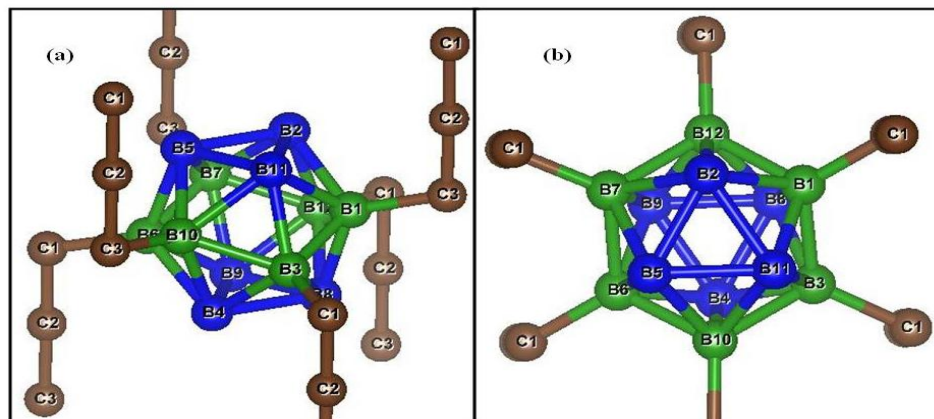
Fig.1.1 : The idealized B_{12}(CCC) structure (a) the icosahedral cage and the linear chain. (b) the projection on a plane perpendicular to the chain-axis.

Within the icosahedron, the atoms that are linked to other icosahedra directly, forming intericosahedral bonds, are called polar atoms. There are six polar atoms in an icosahedron, constituting the two triangular caps at the opposite ends of the icosahedral cage. (In figure 1.1, boron atoms shown in blue and labeled B2, B5, B11, B4, B8 and B9 are polar atoms.) The other six atoms of the icosahedron are linked to the end atoms of the 3-atom chain and they are called equatorial atoms. (In figure 1.1, boron atoms shown in green and labeled B7, B6, B10, B3, B1 and B12 are equatorial atoms.) They form a puckered hexagonal loop at the middle region of the icosahedron when viewed along the (111) rhombohedral axis or the chain-axis (figure1.1 (b)). Polar and equatorial atomic sites can be topographically distinguished by the projection perpendicular to the chain-axis (figure1.1 (b)). Polar atoms occupy the vertices of the two inner triangles while the equatorial atoms occupy the vertices of the two distorted outer triangles whose outlines form the puckered hexagonal loop. A comparison between figures 1.1(a) and 1.1(b) shows that this topographical marker is valid only for the projection perpendicular to the chain-axis. Each icosahedron is directly linked to six other icosahedra through

3

intericosahedral bonds between polar atoms and it is also linked to six 3-atom chains through bonds between the equatorial atoms and the chain end atoms. Thus each chain is linked to three icosahedra at one end and three at the other end. The 15 atoms in the unit cell occupy four distinct Wyckoff positions : polar (6h) sites, equatorial (6h) sites, chain end (2c) sites and chain center (1b).

The ground state structure of $B_{12}C_3$ has been widely accepted as $B_{11}C^p$(CBC), with one carbon atom occupying a polar site (C^p) in the icosahedral cage and one boron atom occupying the chain center. The structure $B_{11}C^p$(CBC) is supported by experimental evidence from nuclear magnetic resonance (NMR) data (Hynes and Alexander, 1971), X-ray diffraction data (Morosin *et al*., 1986), Raman spectrum measurement (Tallant *et al*., 1989), infrared (IR) spectrum measurement (Kuhlmann *et al*., 1992), neutron diffraction data (Kwei and Morosin, 1996), X-ray absorption measurement (Jiménez *et al*., 1998) and X-ray scattering measurement (Feng *et al*., 2004) and by theoretical modeling (Armstrong *et al*.,1983; Emin, 1988; Bylander *et al*.,1990; Lazzari *et al*., 1999; Mauri *et al*., 2001; Fanchini *et al*., 2006; Saal *et al*., 2007; Aydin and Simsek, 2009; Ivashchenko *et al*., 2009; Vast *et al*., 2009). Establishing this result has not been easy or straightforward. As boron and carbon atoms have nearby atomic and mass numbers, their electronic and nuclear scattering cross-sections are quite similar (Kwei and Morosin, 1996; Jiménez *et al*., 1998). Hence most characterization techniques cannot distinguish between these two atoms. For example, though some of the early evidences for $B_{11}C^p$(CBC) structure have been obtained from NMR studies, subsequent NMR measurements have proposed CCC chains and CBB chains, among other combinations. Starting from a few structural models, the density functional theory (DFT) based simulations of IR and Raman spectra (Lazzari *et al*., 1999) and NMR spectra (Mauri *et al*., 2001) and their good correspondence with experimental spectra have been decisive in establishing $B_{11}C^p$(CBC) as the ground state structure of $B_{12}C_3$ stoichiometry. Pinpointing the ground state structure of $B_{12}C_3$ from among the contrasting models suggested by experiments and theoretical works has led to another impasse with the experimental results.

In $B_{11}C^p$(CBC) structure the occupation of an icosahedral site by a carbon atom breaks the rhombohedral symmetry to base-centered monoclinic Cm (8). However a structure with monoclinic symmetry in $B_{12}C_3$ stoichiometry has never been detected in experimental measurements. On the one hand this has revived the proposals of other types of ground state structures preserving rhombohedral symmetry (Wang *et al*., 2014); on the other hand this has led to attempts to explain possible high temperature phase transitions of the structure from monoclinic symmetry to rhombohedral symmetry in terms of the random distribution of configurational disorder of the carbon atom within the icosahedra (Widom and Huhn, 2012; Ektarawong *et al*., 2014). The latter statistical models propose that a random occupation of all the six polar sites of the icosahedra in equal probability by a carbon atom can cause such phase transitions from monoclinic to rhombohedral symmetry. Some works (Fanchini *et al*., 2006) have proposed that at any given composition of Boron Carbide different structural entities with energies lying within a narrow band can coexist. This brings to focus the need to address the issue of the ground state structure of $B_{12}C_3$ stoichiometry in a conclusive way. It should be stressed that the structures proposed by early experimental works and their different variations constitute the initial structural models on which the majority of computational modeling works on $B_{12}C_3$ are based. Not many attempts have been made to study this system using structure searching techniques, instead of analyzing a few chosen structures. A recent effort using particle swarm optimization algorithm (Wang *et al*., 2014) has not yielded the $B_{11}C^p$(CBC) structure as a possible ground state structure. The present work proposes to address the problem of the ground state structure of $B_{12}C_3$ stoichiometry by an exhaustive structure search using evolutionary algorithm and by the subsequent study of the ground state properties using density functional theory.

1.1.2. $B_{13}C_2$ Stoichiometry

$B_{13}C_2$ corresponds to 13.3 at.% C in Boron Carbide. In the homogeneity range of Boron Carbide 20 at.% C is generally considered to be the carbon-rich stoichiometry. Though the boron-rich limit of Boron Carbide is generally accepted to be ~8 at.% C

$B_{13}C_2$ is the most interesting boron-rich stoichiometry for the still unsolved problems related to its crystal structure and electronic structure. Unlike $B_{12}C_3$ there is no consensus so far on the ground state crystal structure of $B_{13}C_2$. Two major candidate structures have been proposed : $B_{11}C(CBB)$ and $B_{12}(CBC)$. It has been discussed in chapter 3 that the most accepted structure of $B_{12}C_3$ stoichiometry is $B_{11}C^p(CBC)$. According to one group, when carbon concentration decreases from $B_{12}C_3$ carbon is substituted by boron in the chain, resulting in $B_{11}C(CBB)$ structure at 13.3 at.% C (Emin, 1988). When carbon concentration further decreases the substitution will be in the icosahedron, leading to $B_{12}(CBB)$ structure at 6.7 at.% C. This model explains the experimentally observed trends in structural and elastic properties, thermal and electrical transport properties, and IR and Raman spectra with the variation of carbon concentration (Wood *et al.*, 1985; Tallant *et al.*, 1989; Gieske *et al.*, 1991; Stein *et al.*, 1991; Aselage and Tissot, 1992; Aselage *et al.*, 2000). The other group interprets the available XRD data to propose that with the decrease in carbon concentration from 20 to 13.3 at.% C the substitution of carbon by boron takes place in the icosahedron, resulting in $B_{12}(CBC)$ structure at 13.3 at.% C (Kirfel *et al.*, 1979; Yakel, 1986).

DFT calculations have consistently supported the latter model. It has been computationally shown that $B_{12}(CBC)$ structure is energetically more stable than the $B_{11}C(CBB)$ and it has better agreement with experimental lattice parameters (Bylander and Kleinman, 1991; Saal *et al.*, 2007). However the DFT calculations have not been able to reproduce the semiconducting nature of $B_{13}C_2$. Boron carbide is observed to be a semiconductor over its entire homogeneity range (Werheit and de Groot, 1980; Wood and Emin, 1984; Samara *et al.*, 1993; Schmechel and Werheit, 1997). At 20 at.% C the DFT calculations agree with this observation because the unit cell of $B_{12}C_3$ contains 48 valence electrons, resulting in a filled valence band and empty conduction band. At 13.3 at.% C the unit cell of $B_{13}C_2$ contains only 47 valence electrons, equivalent to one hole per unit cell. As a consequence the DFT calculations predict metallic behaviour for $B_{13}C_2$, contrary to experimental observation of semiconducting nature. Though the valence band overlaps with the Fermi level in DFT calculations, indicating metallic

nature, there appears an apparent band gap between the valence band edge and the conduction band in the calculated band structure. Some have interpreted this as indicating the semiconducting nature and proposed that $B_{13}C_2$ is a Mott-Hubbard insulator (Bylander and Kleinman, 1991). Others have treated $B_{13}C_2$ as a metal and proposed that it has superconducting properties (Calandra *et al*., 2004). This long standing impasse between the DFT calculations and the experimental observations on the semiconducting nature of $B_{13}C_2$ has cast its shadow of doubt over the structural models supported by the DFT calculations.

On the part of experimentalists, attempts have been made to explain the observed dc conductivity of $B_{13}C_2$ based on different structural models. The bipolaron hopping mechanism (Aselage *et al*., 2000) depends on $B_{11}C(CBB)$ structure. Structural disorder leading to mid gap states has been proposed as an explanation for transforming the metallic nature of $B_{12}(CBC)$ structure into semiconducting nature (Schmechel and Werheit, 1997, 1999). Thus the problem of crystal structure of $B_{12}C_3$ is invariably linked to the problem of its electronic structure.

In a few recent efforts to explain these two problems deviation from stoichiometry and the presence of super lattices in $B_{13}C_2$ have been proposed as the possible approaches to the solution. Shirai *et al*. (2014) has proposed a nonstoichiometric supercell of $3[B_{11}C(CBC)] + 4[B_{12}(CBC)] + B_{12}(B_4)$, which corresponds to 14 at.% C, as a structural candidate. They propose that the presence of $B_{12}(B_4)$ units can reduce the hole density from 1 hole/unit cell to 0.25 hole/unit cell, signifying less metallic nature. However they have not obtained semiconducting nature in the electronic band structure. Ektarawong *et al*. (2015) has proposed a supercell of $B_{12}(CBC) + B_{11}C^e(BBC)$, formed by configurational disorder at higher temperatures. The splitting of valence states in $B_{11}C^e(BBC)$ units can compensate for the electron deficiency in $B_{12}(CBC)$ units, leading to semiconducting nature. They have also obtained semiconducting electronic structure for this supercell. However they maintain that the ground state structure of $B_{13}C_2$ is the metallic $B_{12}(CBC)$ and the semiconducting super lattice emerges only at sufficiently higher temperatures due to substitutional disorder. As an explanation for the absence of

experimental observation of the metallic structure of $B_{12}C_3$ even at low temperatures they have argued that the disordered semiconducting structure, though it can only be formed at higher temperatures, must have somehow been frozen into intermediate temperatures. The mechanism for this freezing has not been explained in their work.

The very fact that the experiments at different temperatures have recorded only the semiconducting nature of $B_{13}C_2$ suggests that $B_{13}C_2$ must be semiconducting even at 0 K. If there are disordered structures causing semiconducting nature they must show up not at high temperatures alone, but they must be intrinsically present in the composition at 0 K. Balakrishnarajan *et al.* (2007) have shown that configurational disorders can be intrinsically present in the ground state structure of Boron Carbide and are not exclusively by higher temperature entropic effects. What is needed is a structural solution that explains both the ground state crystal structure and the electronic structure of $B_{13}C_2$. These twin problems are addressed in the present work by performing the evolutionary algorithm based structure search to investigate the possible crystal structures and by the DFT based computation of the electronic structure and other ground state properties of $B_{13}C_2$ stoichiometry.

1.2. RUTHENIUM CARBIDES

Due to their high melting point, high hardness, good thermal conductivity and high resistance to wear and corrosion (Toth, 1971), transition metal carbides and nitrides have many industrial applications such as cutting and polishing tools, wear-resistant coatings *etc*. They are potential economically viable substitutes for diamond and cubic Boron Nitride in many applications. The wide ranging applications of these systems had led to various electronic structure studies to investigate their stability and structural properties (Guillermet and Grimvall, 1989; Haguland *et al*., 1991, 1993; Grossman *et al*., 1999; Hugosson *et al*., 2001; Zheng, 2005; X. Guo *et al*., 2008). Ruthenium Carbide shares many of the general properties of transition metal carbides and hence it is a potential candidate for a range of industrial applications.

Ruthenium Carbide has been synthesized in 1960 at ambient pressure and high temperature (Kempter and Nadler, 1960, Kempter, 1964). They have reported RuC stoichiometry in tungsten carbide (WC) type hexagonal structure with the space group $P\bar{6}m2$ (187). No further experimental study has been available since then. Recently in 2012, Ruthenium Carbide is synthesized in a high pressure–high temperature environment by laser–heated diamond anvil technique (Sanjay Kumar *et al.*, 2012). They have reported synthesis of Ru_2C stoichiometry in Fe_2N type hexagonal structure with the space group $P\bar{3}m1$ (164). As only a small amount of the sample is synthesized by this method, there are inherent difficulties in the estimation of the stoichiometry and structure and hence further confirmation of these results would be desirable.

The computational studies on Ruthenium Carbide have been concentrating mostly on RuC stoichiometry. Fan *et al.* (2006) have studied using DFT the rock salt structure of RuC and evaluated its elastic properties and electronic partial density of states. RuC in rock salt system is found to be mechanically stable and with the highest bulk modulus among the noble metal carbides (~347 GPa). In another DFT work E. Zhao *et al.* (2010), using the Perdew–Burke–Ernzerhof (PBE) generalized gradient approximation (GGA) to the exchange–correlation functional, have studied nine different structures of RuC including tungsten carbide structure, rock salt structure and zinc blende structure among others. Though they have obtained five distinct mechanically stable structures their dynamical stability has not been investigated in this work. Among these five structures zinc blende structure of RuC is energetically the most stable one. Abidri *et al.* (2010), using the local density approximation (LDA) to the exchange–correlation functional, have studied the mechanical stability of four structures of RuC, but they too have not attempted to check for dynamical stability. They have reported RuC–zinc blende system as energetically the most stable one with a hardness estimate of 36.94 GPa. Z. Zhao *et al.* (2010), using GGA–PBE functional, have studied ten different structures of RuC, investigating mechanical stability through elastic constants and dynamical stability through phonon dispersions. Only the zinc blende structure of RuC has been found to be dynamically as well as mechanically stable among the ten structures considered. Though

tungsten carbide structure and rock salt structure are mechanically stable, they lack dynamical stability. From the electronic energy band calculation, RuC–zinc blende system has been found to be a semiconductor and it has been estimated to have a Vickers hardness of 42.8 GPa. H. R. Soni *et al*. (2011), using GGA–PBE functional, have studied the dynamical stability of zinc blende structure and rock salt structure of RuC and found only the former to be dynamically stable. They too have noted the semiconducting nature of the RuC–Zinc blende system. From the phonon data, using the harmonic approximation, they have estimated the variation of different thermodynamic functions of RuC–Zinc blende system over a range of temperatures. Guang *et al.* (2012) have conducted a structure search for RuC stoichiometry using particle swarm optimization algorithm and they have reported $R\bar{3}m$ structure as the lowest energy one. Using GGA–PBE, they have found that the $R\bar{3}m$ structure has mechanical and dynamical stability and that it is metallic. Only a few computational studies have so far investigated stoichiometries other than RuC. A recent structure search using particle swarm optimization algorithm has yielded $P\bar{3}1m$ and $P63/mmc$ as two possible stable structures in Ru_2C stoichiometry in the pressure range 0-50 GPa (Lu *et al*., 2015). A study of the dynamical stability of $P\bar{3}m1$ structure in Ru_2C stoichiometry has been done in the pressure range 30-110 GPa (Sun *et al.,* 2013). The present work aims to arrive at a conclusive result among the varying opinions regarding the structure of Ruthenium Carbides over its different stoichiometries by performing a structure search using evolutionary algorithm and by computing the ground state properties of the emerging structures using DFT.

The fact that many of their industrial applications are in extreme conditions has motivated a growing body of computational work in recent years on the variation of properties of transition metal carbides at high pressures (Fu *et al*., 2009; Yin *et al*., 2010; Zaoui and Ferhat, 2011; Hao *et al*., 2011; P. Soni *et al*., 2011; Chauhan and Gupta, 2013; Varshney and Shriya, 2013; Mishra and Chaturvedi, 2013; Rathod *et al*., 2013; Li *et al*., 2014; Kavitha *et al*., 2015). Hao *et al.* (2014) has reported in RuC stoichiometry the phase transition of the Zinc blende structure to tetrahedral structure at ~9.3 GPa, which,

in turns, transforms to WC type hexagonal structure at ~26 GPa. After studying the ground state properties of Ruthenium Carbide systems we will be investigating the variation of their stability and properties with pressure, with the aim of providing helpful indicators for their experimental manipulation to effect new technological applications.

1.3. SCOPE AND OBJECTIVES

The problem of the ground state crystal structure has not been conclusively settled for Boron Carbide systems in $B_{12}C_3$ stoichiometry by means of an exhaustive structure search. For $B_{13}C_2$ stoichiometry the problem of crystal structure is intimately tied up with the unsolved problem of the discrepancy between theoretical models and experimental measurements of its electronic structure. The different reports of the structure of Ruthenium Carbides in its various stoichiometries have not resulted in a consensus on the specific systems to be pursued with the optimum utilization of experimental resources. The present work proposes to address these problems and aims to provide valuable indicators and benchmarks for the future theoretical and experimental works on these two systems. As crystal structure search has been performed only a few times in these two systems, a new structure search will have the potential for discovering quite interesting structural candidates. With this motivation the following specific objectives have been outlined for the present work :

1) Exhaustive structure search using evolutionary algorithm and density functional theory will be performed in the Boron Carbide stoichiometries $B_{12}C_3$ and $B_{13}C_2$ and in the Ruthenium Carbide stoichiometries RuC, Ru_2C and Ru_3C.

2) Using density functional theory the ground state properties of the lowest energy structures yielded by the structure search will be investigated. The mechanical stability of the structures will be studied by the computation of elastic constants and their dynamical stability, that of phonons. For the stable systems electronic structure will be generated and thermodynamic properties within the harmonic approximation will be calculated from phonons. The computed properties will be compared with the experimental results wherever possible.

3) For the stable semiconducting systems infrared spectra will be generated from Born effective charges and phonon polarizations, as easily verifiable experimental signatures of these systems.

4) Hardness of the stable systems will be estimated using different semi-empirical models.

5) The variation of the stability and properties of Ruthenium Carbide systems with pressure would be investigated, as many of their industrial applications are in extreme conditions.

1.4. ORGANIZATION OF THE THESIS

- Chapter one provides the introduction to the background and current status in the study of Boron Carbides and Ruthenium Carbides through the analysis of the literature. The problems related to these systems to be addressed in the present work are specified clearly.

- Chapter two presents in detail the computational methods being employed in this work. The evolutionary algorithm used for the structure search as well as the density functional theory used for the optimization of the structure and the calculation of the properties are discussed.

- Chapter three consists of the results of the structure search and the computation of the ground state properties of Boron Carbide systems in $B_{12}C_3$ stoichiometry.

- Chapter four contains the results of the structure search and the computation of the ground state properties of Boron Carbide systems in $B_{13}C_2$ stoichiometry.

- Chapter five furnishes the results of the structure search and the computation of the ground state properties of Ruthenium Carbide systems in RuC, Ru_2C and Ru_3C stoichiometries.

- Chapter six sets forth the study of the variation of the stability and properties of the Ruthenium Carbide systems with pressure.

- Chapter seven lists out the conclusions of this work and specifies the scope for the future work in the two areas being investigated here.

Chapter 2

COMPUTATIONAL DETAILS

2.1. INTRODUCTION

This work employs crystal structure search to address the unsolved problems related to the crystal structure in the different stoichiometries of Boron Carbides and Ruthenium Carbides. Evolutionary algorithm based code Universal Structure Predictor: Evolutionary Xtallography (USPEX) is used for this. For the energy calculation and structure optimization during the structure search density functional theory (DFT) is employed. DFT is subsequently used to calculate the different properties of the lowest energy structures yielded by the structure search. DFT code Vienna Ab initio Simulation Package (VASP) is used as part of the structure search as well as for the computation of the properties. The hardness of the stable systems are estimated by three different semi-empirical models.

2.2. CRYSTAL STRUCTURE PREDICTION

As the crystal structure of a material determines all of its properties, identifying the correct structure has central role in the study of materials. Out of the infinitely large number of possible atomic configurations there can, in principle, be a finite number of distinct structures at each set of thermodynamic conditions. These correspond to the extremum value of a specific property like energy, hardness, transition temperature etc. The most general approaches to the prediction of such structures are based on computational optimization. In the case of the determination of the ground state, it involves calculation of the free energy of the system, and the unbiased exploration of its energy landscape for identifying the most stable atomic configuration corresponding to

the global minimum of energy. The number of distinct points on the landscape can be estimated (Oganov, 2010) in terms of the binomial coefficients as, :

$$C = \binom{V/\delta^3}{N} \Pi_i \binom{N}{n_i} \tag{2.1}$$

where N is the number of atoms in the unit cell of volume V, δ is a discretization parameter and n_i is the number of atoms of ith type in the unit cell. For even a small system (N ~ 10-20 atoms), C ~10^N for $\delta = 1$ Å and V = 10 Å^3.

The dimensionality of the energy landscape is:

$$d = 3N + 3 \tag{2.2}$$

where 3N-3 degrees of freedom correspond to the atomic positions, and the remaining six, to the lattice parameters. Then, Eq.(2.1) can be expressed as:

$$C \sim \exp(\alpha d) \tag{2.3}$$

where α is a system-specific constant. It is clear that the number of possible structural combinations increases exponentially with the system size or landscape dimensionality. As the scaling of the number of combinations with the system size is faster than any polynomial, this is an NP-hard problem (non-deterministic polynomial-time hard). If intermediate structure relaxation is performed, this problem can be simplified. The relaxation process results in realistic correlations being evolved between atomic positions and the intrinsic dimensionality is reduced :

$$d^* = 3N + 3 - \kappa \tag{2.4}$$

where κ is the (non-integer) number of correlated degrees of freedom. This reformulates Eq.(2.3):

$$C^* \sim \exp(\beta d^*) \tag{2.5}$$

This analysis shows that any structure search method, when incorporated with structure relaxation or local optimization, becomes effective in the prediction of possible structural candidates. Evolutionary algorithm is one such structure search method which is robust enough for predicting structures of complex systems. In the present work, evolutionary algorithm is used for the crystal structure prediction of Boron Carbides and Ruthenium Carbides. The complexity of the structure of Boron Carbide has been the motivation for

choosing this method.

2.2.1. Universal Structure Predictor: Evolutionary Xtallography (USPEX)

A recently developed evolutionary algorithm based code, Universal Structure Predictor: Evolutionary Xtallography (USPEX) (Glass *et al*., 2006; Oganov and Glass, 2006) is used in this work for the crystal structure search. Evolutionary algorithm emulates biological evolution in its basic mechanisms : reproduction, mutation, recombination and selection. The candidate structures are individuals in a population that undergo evolution under the cyclic application of these mechanisms. The survival of specific structures is determined by a fitness function. The following diagram (figure 2.1) represents the evolutionary algorithm (Lyakhov, 2011):
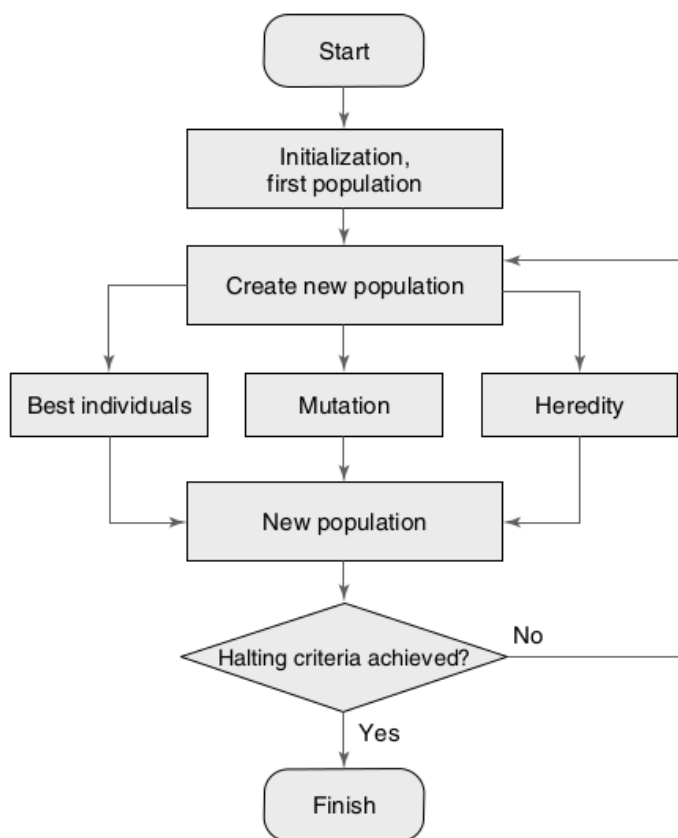
Fig.2.1: Scheme of evolutionary algorithm

In USPEX, the structures are represented by floating-point numbers, with the fractional coordinates for the atoms and the matrix of lattice vectors for the lattice. The first generation is populated by random structures. Each structure is relaxed and the negative of its enthalpy, which acts as the fitness parameter, is evaluated. A few lowest–enthalpy structures are selected as parent structures. Three variation operators are employed in USPEX that mediate between the parent and offspring structures :

(i) Heredity operator : It combines spatially coherent slabs of two parent structures in terms of fractional coordinates with the matrices of lattice translation vectors as weighted averages of the lattice vectors matrices of the two parent structures.

(ii) Mutation operator : It changes the cell shape by random deformation.

(iii) Permutation operator : It interchanges chemical identities of randomly selected atom pairs in the case of systems containing more than one chemical species.

A new candidate structure is generated from the parent structures by applying one of the three variation operators. At least one structure in the new generation will be the lowest enthalpy structure of the parent generation, called the best individual (figure 2.1), without the variation operators acting on it. Through these steps it is ensured that the best structure obtained in any generation is better than or equal to the best structure obtained in the previous generations.

The search for the ground state of the energy landscape is a complex problem and proper constraints have to be introduced for directing the search towards physically meaningful candidate structures and for optimizing the computational resources. Three constraints are imposed on the generated candidate structures for this :

(i) All interatomic distances must be above the specified sum of the covalent radii of the corresponding atom pair.

(ii) All cell lengths must be larger than the specified diameter of the largest atom.

(iii) The angle between any two lattice vectors must be in the 60^0–120^0 range.

As these constraints remove only the redundant regions of configuration space, the search for new structures remains unconstrained. If any of these constraints is violated, the candidate structure is discarded; otherwise, it is relaxed. The locally optimal structure is

recorded and used for producing structures for the next generation. This procedure continues until all the specified generations are exhausted or a particular structure turns up repeatedly as the fittest one over a given number of generations.

USPEX also provides the option of doing a more guided structure search using seed structures. If the user is certain that the structure search can be focused on a specific region of the energy landscape where the probability of finding the candidate structures is large. The coordinates of the user-specified structures can be provided for the code to refer to during the implementation stage. This feature of USPEX is utilized in this work during the second phase of the structure search in Boron Carbide stoichiometries.

In USPEX external DFT codes or molecular dynamics (MD) codes are used for the local optimization and energy calculation. In the present work Vienna Ab initio Simulation Package (VASP) which implements electronic density functional theory, is used for this link with USPEX. Four advancing stages of energy calculations and relaxations are done with increasing plane-wave energy cutoff and finer k-grid resolution of 0.14, 0.10, 0.08 and 0.06. The significance of these parameters will be discussed in section 2.3.4 of this chapter. USPEX automatically generates k-grid for the structures and the inputs for the calculation of the fitness parameter. For the fittest structures obtained from USPEX the atomic coordinates are slightly varied using PHONOPY code (Togo *et al*., 2008) within a tolerance of 5% to identify the highest symmetry structure in the structural vicinity of the original one, the procedure yielding the corresponding Bravais cells. Further relaxation and properties calculation are done using these Bravais cells.

2.3. DENSITY FUNCTIONAL THEORY

2.3.1. Many-body Problem

To calculate the properties of a many-body system like a solid, in terms of its quantum mechanical description in the non-relativistic approximation, the many-body Schrödinger equation should be solved. The corresponding wave function will involve the electron coordinates as well as the nuclear coordinates. In the case of solids the nuclear motion is sluggish compared to the electron motion by virtue of the large

disparity of their masses. This motivates the idealization in which electrons follow the instantaneous position of the ions. Thus in this approximation, called the Born-Oppenheimer approximation, the nuclei are treated as immobile compared to the electrons. Then, the kinetic energy of the nuclei can be neglected and the Coulomb repulsion between them can be treated as constant depending only on the ionic configuration. This allows the many-body Schrödinger equation to be formulated in terms of only the coordinates of electrons. In Hartree atomic units, for a system containing N electrons, the 3N-dimensional many-electron Schrödinger equation is :

$$\left[-\sum_i \frac{\nabla_i^2}{2} + \sum_i V_n(\mathbf{r}_i) + \frac{1}{2}\sum_{i \neq j} \frac{1}{|\mathbf{r}_i - \mathbf{r}_j|} \right] \Psi = E\Psi \qquad (2.5)$$

where $V_n(r)$ is the Coulomb potential of the nuclei as experienced by the electrons :

$$V_n(r) = -\sum_I \frac{Z_I}{|\mathbf{r} - \mathbf{R}_I|} \qquad (2.6)$$

Because of the presence of the coupled coordinates in the third term, representing Coulomb interaction between the electrons, Eq.(2.5) cannot be exactly solved even for a two-particle system and it cannot be numerically solved accurately when the total number of electrons is ~20 or more. The question is whether we can have an approximate description of the many-body problem based on wavefunction approach. Different approximation techniques were developed subsequently.

The first and simplest approximation in this perspective is the Hartree approximation. This is motivated by the fact that the effective Coulomb interaction experienced by any electron due to the consolidated effect of all the other electrons is very small compared to the Coulomb interaction between any pair of electrons, especially when the number of electrons is large. It is then plausible that each electron moves independent of the others, and the residual interaction with all the other electrons can be incorporated in terms of a mean potential. In this independent particle approximation, each particle resides in a different orbital, so that we can write the wavefunction in a product form: $\Psi = \prod_i \varphi_i$. In this mean-field approximation, the electrons are assumed to move in a mean electrostatic potential created by the whole system of electrons. With the help of this electrostatic potential called the Hartree potential energy $V_H(\mathbf{r})$, the

interaction term can be reinstated in an average manner while maintaining the single-particle description. In the mean-field approximation the set of N three-dimensional single-particle equations corresponding to Eq.(2.5) are :

$$\left[-\frac{\nabla^2}{2} + V_n(\mathbf{r}) + V_H(\mathbf{r})\right]\varphi_i(\mathbf{r}) = \varepsilon_i\varphi_i(\mathbf{r}) \tag{2.7}$$

$$\text{where} \quad V_H(\mathbf{r}) = \int d\mathbf{r}' \frac{n(\mathbf{r}')}{|\mathbf{r}-\mathbf{r}'|} \tag{2.8}$$

$$\text{and} \quad n(\mathbf{r}) = \sum_i^{occ.}|\varphi_i(\mathbf{r})|^2 \tag{2.9}$$

$V_H(\mathbf{r})$ satisfies the Poisson's equation :

$$\nabla^2 V_H(\mathbf{r}) = -4\pi n(\mathbf{r}) \tag{2.10}$$

Eqns.(2.7), (2.9) and (2.10) need to be solved together by iterative method called the self-consistent field method and the set of single-particle equations (2.7) are called Hartree equations (Hartree, 1928).

However, the Hartree approximation is not an acceptable wavefunction for Fermions since it lacks the anti-symmetry property of Fermions. In the Hartree-Fock approximation, the consequences of the Pauli exclusion principle are incorporated by ensuring the antisymmetric nature of the many-electron wavefunction by expressing it as a Slater determinant of the single-particle wavefunctions. This gives rise to a nonlocal Fock exchange interaction potential $\widehat{V}_x(\mathbf{r}, \mathbf{r}')$ in Eq.(2.7) :

$$\left[-\frac{\nabla^2}{2} + V_n(\mathbf{r}) + V_H(\mathbf{r})\right]\varphi_i(\mathbf{r}) + \left[\widehat{V}_x(\mathbf{r}, \mathbf{r}')\varphi_i\right](\mathbf{r}) = \varepsilon_i\varphi_i(\mathbf{r}) \tag{2.11}$$

$$\text{where} \quad [\widehat{V}_x(\mathbf{r}, \mathbf{r}')\varphi_i](\mathbf{r}) \text{ stands for} \quad -\int d\mathbf{r}' \sum_j \frac{\varphi_j^*(\mathbf{r}')\varphi_i(\mathbf{r}')}{|\mathbf{r}-\mathbf{r}'|}\varphi_j(\mathbf{r}) \tag{2.12}$$

The set of single-particle equations (2.11) are called Hartree-Fock equations (Fock, 1930).

In the configuration interaction method the quantum correlation effect between the electrons, arising from their Coulomb interaction, is incorporated. This is done by expressing the many-electron wavefunction as a linear combination of a finite number of Slater determinant wavefunctions, called configuration state functions, each one resulting from a different way of occupying the vacant single particle states by the electrons. It gives rise to, in Eq.(2.11), a nonlocal correlation interaction term $\widehat{V}_c(\mathbf{r}, \mathbf{r}')$ in addition to

the exchange interaction $\widehat{V}_x(\mathbf{r}, \mathbf{r}')$ that arises due to correlation between the electrons demanded by Pauli principle. These two nonlocal potentials are clubbed together into a nonlocal exchange-correlation potential $\widehat{V}_{xc}(\mathbf{r}, \mathbf{r}')$. The corresponding set of single-particle equations can be expressed as :

$$\left[-\frac{\nabla^2}{2} + V_n(\mathbf{r}) + V_H(\mathbf{r}) + \widehat{V}_{xc}(\mathbf{r}, \mathbf{r}') \right] \varphi_i(\mathbf{r}) = \varepsilon_i \varphi_i(\mathbf{r}) \tag{2.13}$$

Some of the other wavefunction based post Hartree-Fock methods are Møller–Plesset perturbation method, Coupled Cluster method etc. Even when the insurmountable problem of solving the many-electron Schrodinger equation (2.5) is now greatly simplified, the computational complexity of solving single-particle equations of the type (2.13) still remains large. Solving the Slater determinant of the single-particle wavefunctions demands huge computational cost. If N represents the number of electrons, which is a measure of the system size, the computational cost scales as N^4 for Hartree-Fock method, N^6 for configuration interaction method, N^4 or N^5 for second order Møller–Plesset perturbation method, N^6 for Coupled Cluster method and so on. What is required is an approach that retains the single-particle description, incorporates the exchange and correlation effects and strikes a balance between the computational cost and accuracy of the calculation.

2.3.2. Hohenberg-Kohn Theorems

In Density Functional Theory the many-body problem is reformulated in terms of the ground state electron density, instead of the wavefunction. The simplification of this approach is that the total wavefunction $\Psi(\mathbf{r_1,....r_n})$ depends on 3N spatial coordinates whereas the electron density n($\mathbf{r}$) depends only on three spatial coordinates. Going back to the many-electron equation (2.5), the total energy of the system is :

$$E = \langle \Psi | \widehat{H} | \Psi \rangle = \int dr_1 \ldots \ldots dr_n \Psi^*(r_1 \ldots \ldots r_n) \widehat{H} \; \Psi(r_1 \ldots \ldots r_n) \tag{2.14}$$

where the Hamiltonian $\qquad \widehat{H} = -\sum_i \frac{\nabla_i^2}{2} + \sum_i V_n(r_i) + \frac{1}{2} \sum_{i \neq j} \frac{1}{|r_i - r_j|} \tag{2.15}$

The sum of the kinetic energy and the exchange-correlation resulting from the electron-electron interaction term is universal. Hence the Hamiltonian $\widehat{H}$ depends on the system

via the so called external potential $V_n(\mathbf{r})$ which depends upon the ionic coordinates. This means that $V_n(\mathbf{r})$ uniquely determines the ground state wavefunction Ψ and, through it, the ground state electron density $n(\mathbf{r})$. Conversely, it can be proved that every $n(\mathbf{r})$ corresponds to a unique $V_n(\mathbf{r})$ up to a constant, if the ground state is nondegenerate. If this is so, the Hamiltonian, and hence the ground state wavefunction and ground state energy, can be determined from the ground state electron density $n(\mathbf{r})$.

The first Hohenberg-Kohn theorem (Hohenberg and Kohn, 1964) states that if E is the ground state energy of the system, which is the lowest possible energy, the external potential $V_n(\mathbf{r})$, and hence E is a functional of the electron density $n(\mathbf{r})$ only.

$$E = E[n(\mathbf{r})] \tag{2.16}$$

Since $n(\mathbf{r})$ uniquely determines $V_n(\mathbf{r})$ and hence the Hamiltonian, all the properties of the ground state and the excited states can be determined, in principle, in terms of $n(\mathbf{r})$. This theorem greatly simplifies the problem of finding the ground state energy : While the energy of any general state depends on 3N spatial coordinates through the total wavefunction $\Psi(\mathbf{r_1,....r_n})$, the ground sate energy depends only on three spatial coordinates through the electron density $n(\mathbf{r})$.

Dependence of of the kinetic energy and exchange-correlation energy functionals on n(r) is also unknown. The exact functional form of E[n(r)] of a general many-electron system is unknown.   Hence various approximation methods are evolved to estimate it. Though the first Hohenberg-Kohn theorem states the existence of this functional, it does not give a prescription to determine it. This is provided by the second Hohenberg-Kohn theorem (Hohenberg and Kohn, 1964). It states that the ground state electron density (n_0)

is exactly the function that minimizes the total energy E :

$$\left.\frac{\delta E[n]}{\delta n}\right|_{n_0} = 0 \tag{2.17}$$

In the Kohn-Sham method, under the independent electron approximation, the problem of N interacting electrons is mapped into one of N noninteracting electrons moving in an effective potential. If we go back to Eq.(2.13), the presence of the coupled coordinates in the nonlocal potential term $\widehat{V}_{xc}(\mathbf{r}, \mathbf{r'})$ make it difficult for the set of equations to be solved. In the Kohn-Sham method the nonlocal exchange-correlation

potential is replaced by a local potential $V_{xc}(\mathbf{r})$ depending on only one space coordinate and yet supposed to make the same effect. The noninteracting electrons are supposed to occupy certain pseudo orbitals called Kohn-Sham orbitals $\varphi_{KS}(\mathbf{r})$. The ground state electron density is $n(\boldsymbol{r}) = \sum |\varphi_{KS}(\mathbf{r})|^2$ where the summation is over the occupied KS orbitals.

The total energy can be expressed using (2.14) and (2.15) as :

$$E = -\sum_i \int d\mathbf{r}\ \varphi_i^*(\mathbf{r}) \frac{\nabla^2}{2} \varphi_i(\mathbf{r}) + \int d\mathbf{r}\ n(\mathbf{r}) V_n(\mathbf{r}) + \frac{1}{2} \iint d\mathbf{r}\ d\mathbf{r}' \frac{n(r)\ n(r\prime)}{|\mathbf{r}-\mathbf{r}\prime|} + E_{xc}[n(\mathbf{r})]\ (2.18)$$

where $E_{xc}[n(\mathbf{r})]$ is called the exchange-correlation energy. Minimizing the energy using Eq.(2.17) leads from Eq.(2.18) to a set of single-particle equations :

$$\left[-\frac{\nabla^2}{2} + V_n[n(\mathbf{r})] + V_H[n(\mathbf{r})] + V_{xc}[n(\mathbf{r})] \right] \varphi_{KS}(\mathbf{r}) = \mathcal{E}_i \varphi_{KS}(\mathbf{r}) \qquad (2.19a)$$

The set of equations (2.19a) are called Kohn-Sham equations (Kohn and Sham, 1965). These are the fundamental equations of density functional theory. The exchange-correlation potential is given by, $V_{xc}(\mathbf{r}) = \left. \frac{\delta E_{xc}[n]}{\delta n} \right|_{n_r}$. The ground state energy is,

$$E = \sum_i^{occ} \mathcal{E}_i - \int d^3r \left[\frac{1}{2} V_H(\mathbf{r}) + V_{xc}(\mathbf{r}) \right] n(r) + E_{xc}. \qquad (2.19b)$$

As in the case of Hartree equations, the Kohn-Sham equations (2.19a) need to be solved self-consistently. For this $V_{xc}(\mathbf{r})$ should be calculated from $E_{xc}[n(\mathbf{r})]$. The two main approximation methods to estimate $E_{xc}[n(\mathbf{r})]$ are local density approximation (LDA) and generalized gradient approximation (GGA). In LDA, the exchange-correlation energy of a real system due to the electron density $n(\mathbf{r})$ is approximated to that of a homogeneous electron gas having the same electron density, provided $n(\mathbf{r})$ is varying sufficiently slowly for the real system (Ceperley and Alder, 1980; Perdew and Zunger, 1981). In the case of the homogeneous electron gas the exact functional form of the exchange energy in terms of the electron density is known and standard parametrization schemes are available for its correlation energy (Ceperley and Alder, 1980; Perdew and Zunger, 1981). In GGA, in addition to $n(\mathbf{r})$, $E_{xc}[n(\mathbf{r})]$ depends on grad($n(\mathbf{r})$) also.

$$E_{xc}^{LDA}(\mathbf{r}) = \int n(\mathbf{r})\ \varepsilon[n(r)]\ d\mathbf{r} \qquad (2.20)$$

$$E_{xc}^{GGA}(\mathbf{r}) = \int n(\mathbf{r})\ \varepsilon[n(r), \nabla(n(r))]\ d\mathbf{r} \qquad (2.21)$$

where $\varepsilon[n(r)]$ represents the exchange-correlation energy per unit volume.

2.3.3. Self-consistent Cycle

To summarize, the set of equations to be solved together in density functional theory are :

Kohn-Sham equations :
$$\left[-\frac{\hbar^2}{2m}\nabla^2 + V_{KS}(\mathbf{r})\right]\varphi_i(\mathbf{r}) = \varepsilon_i\varphi_i(\mathbf{r}) \qquad (2.22)$$

Kohn-Sham effective potential :
$$V_{KS}(\mathbf{r}) = V_n(\mathbf{r}) + V_H(\mathbf{r}) + V_{xc}(\mathbf{r}) \qquad (2.23)$$

$$V_n(r) = -\sum_I \frac{Z_I}{|\mathbf{r}-\mathbf{R}_I|} \qquad (2.24)$$

$$\nabla^2 V_H(\mathbf{r}) = -4\pi n(\boldsymbol{r}) \qquad (2.25)$$

$$V_{xc}(\mathbf{r}) = \frac{\delta E_{xc}[n(r)]}{\delta n(r)} \qquad (2.26)$$

$$n(\mathbf{r}) = \sum_i |\varphi_i(r)|^2 \qquad (2.27)$$

The self-consistent calculations involve the following steps :

(i) Assume an initial value for the electron density $n(\mathbf{r})$

(ii) Substitute $n(\mathbf{r})$ in the Poisson's equation (2.25) and solve it to get the Hartree energy $V_H(\mathbf{r})$. Using LDA or GGA scheme, evaluate the exchange-correlation energy from $n(\mathbf{r})$, and then use Eq.(2.26) to get the exchange-correlation potential $V_{xc}(\mathbf{r})$.

(iii) Substitute $V_n(r)$, $V_H(\mathbf{r})$ and $V_{xc}(\mathbf{r})$ in the single-particle Kohn-Sham equation (2.22) and solve it to get $\varphi_i(\mathbf{r})$.

(iv) Substitute $\varphi_i(\mathbf{r})$ in (2.27) to get the new value of $n(\mathbf{r})$

(v) The new value of $n(\mathbf{r})$ is mixed with the old value to get a modified $n(\mathbf{r})$ and the cycle is repeated until the difference between the new and old values of $n(\mathbf{r})$ reaches the specified accuracy.

2.3.4. Pseudopotentials and Computational Parameters

In the present work, DFT as implemented in Vienna Ab initio Simulation Package (VASP) (Kresse, and Hafner, 1993; Kresse, and Furthmüller, 1996) is used. To solve the

Kohn-Sham equations, the Kohn-Sham wavefunctions $\varphi_i(\mathbf{r})$ are expanded in terms of a basis set which transforms problem of solving the differential equation (2.22) into an eigenvalue problem. For a periodic solid, the Kohn- Sham orbital is expanded in terms of plane waves. As the ground state electron density n($\mathbf{r}$) is expressed in terms of the Kohn-Sham orbitals (Eq.2.27), n($\mathbf{r}$) is expanded in terms of plane wave basis and the number of basis functions can be increased by using higher values of the plane wave energy cut off, ENCUT. Charge density and other quantities are evaluated by integrating over the Brillouin Zone (BZ) and the integrals are approximated by sums over a suitable discrete k–grid.

As the core electrons of the atoms are hardly affected when the atoms are brought together to form a solid, it can be assumed that only the valence electrons take part in atomic interactions. This provides the motivation for dividing the electrons in an atom into core electrons and valence electrons, in terms of their contribution in atomic interactions, and removing the nucleus and core electrons together from the calculations. This is called frozen core approximation. The remaining valence electron wavefunctions are replaced by a pseudo wavefunction, designed to reproduce the effects of the actual wavefunctions (Heine, 1970). Reduction in the number of electrons to be incorporated for the calculation saves computational cost. Employing a smoothly varying pseudo wavefunction helps to avoid the problem of the rapid oscillations of the valence electron wavefunctions as they approach the core region of highly localized electrons. Pseudopotential is the potential generated from the pseudo wavefunctions and the valence electron density. In this approach the number of plane waves needed for the expansion of a pseudo wavefunction is significantly reduced, resulting in faster computations. In the present work Projector augmented wave (PAW) pseudopotentials (Blochl, 1994; Kresse and Joubert, 1999) as supplied with VASP are used, with 4p, 4d and 5s as the valence states for Ruthenium, and 2s and 2p for both boron and carbon. Solution of Kohn-Sham equations result in the pseudo energies ε_i for the ith Kohn-Sham orbital. The total energy of the system is obtained by Eq.(2.19b). Usually the KS equations are solved in the reciprocal space and hence total energy is to be determined by integrating the energy

eigenvalues in the first Brillouin zone. The integration is usually replaced by discrete sum. Thus it is important have an efficient way of discretizing the Brillouin zone. We have used Monkhorst-Pack k-meshes (Monkhorst and Pack, 1976) for our calculations except for hexagonal systems for which Gamma centered k-meshes are used.

For Boron Carbides local density approximation (LDA) scheme is used for the exchange–correlation functional while for Ruthenium Carbides Perdew–Burke–Ernzerhof (PBE) (Perdew *et al.*, 1996, 1997) generalized gradient approximation (GGA) is used. The states are smeared using Methfessel–Paxton scheme (Methfessel and Paxton, 1989) with a smearing parameter of 0.1 eV. The convergence of plane wave energy cutoff and that of k–points are achieved to a precision of 0.1 meV/atom. Both the lattice parameters and the atomic coordinates of all the structures are relaxed until energies converge to a precision of less than 10^{-10} eV/atom and Hellmann–Feynman forces to less than 10^{-5} eV/A^0.

2.3.5. Elastic Properties and Mechanical Stability

Elastic properties provide the measure of the resistance of a system to elastic deformation and hence the validation of its structural stability. The more the resistance to elastic deformation, the more would be the magnitude of the elastic constant. To study the mechanical stability of Boron Carbides and Ruthenium Carbides emerging from the structure search, the elastic stiffness constants C_{ij} at the equilibrium lattice parameters are calculated. Stress and strain tensors are related by the elastic stiffness constants (Page and Saxe, 2001, 2002). In generalized form, the elastic stiffness constants C_{ijkl} and stress tensor σ_{ij} can be defined as

$$C_{ijkl} = \frac{1}{V_0} \frac{\partial^2 E}{\partial \epsilon_{ij} \, \partial \epsilon_{kl}} \tag{2.28}$$

$$\text{and} \qquad \sigma_{ij} = \frac{1}{V_0} \frac{\partial E}{\partial \epsilon_{ij}} \tag{2.29}$$

where V_0 is the volume of the unstrained crystal, ϵ_{ij} are elements of the strain tensor and E is the energy of a deformed crystal. Using these expressions, the energy can be expanded s a Taylor series (Wallace, 1972):

$$E(V, \epsilon) = E(V_0, 0) + V_0 \sum_{i,j=1}^{3} \sigma_{ij}\epsilon_{ij} + \frac{V_0}{2} \sum_{i,j,k,l=1}^{3} C_{ijkl}\epsilon_{ij}\epsilon_{kl} + \cdots \qquad (2.30)$$

where $E(V_0, 0)$ is the corresponding ground state energy. In Voigt notation scheme (Nye, 1985) the subscripts (ij,kl) of strain tensors are expressed as : $11 \rightarrow 1, 22 \rightarrow 2, 33 \rightarrow 3, 23 \rightarrow 4, 13 \rightarrow 5$ and $12 \rightarrow 6$. Then Eq.(2.30) becomes :

$$E(V, \epsilon) = E(V_0, 0) + V_0 \sum_{\alpha=1}^{6} \sigma_\alpha \tilde{\epsilon}_\alpha + \frac{V_0}{2} \sum_{\alpha,\beta=1}^{6} C_{\alpha\beta}\tilde{\epsilon}_\alpha\tilde{\epsilon}_\beta + \cdots \qquad (2.31)$$

In (3), $\tilde{\epsilon}_\alpha = \epsilon_\alpha$ for $\alpha = 1, 2$ and 3 and $2\epsilon_\alpha$ for $\alpha = 4, 5$ and 6. As the elastic constants tensor is symmetric, there are at most 21 independent elements for the 6 x 6 matrix $C_{\alpha\beta}$, for the triclinic crystal. As the symmetry of the crystal increases, some of the matrix elements would be connected by symmetry relations and the number of independent matrix elements would be further reduced. Thus, monoclinic system has 13 independent elements, rhombohedral has 6 elements, hexagonal has 5 and cubic has only 3. By applying small specific elastic strains $\epsilon_\alpha (\alpha = 1-6)$ to the equilibrium unit cell, a set of elastic constants $C_{\alpha\beta}$ can be obtained from the corresponding change in energy. VASP uses a finite difference scheme for generating the force constants matrix – Hessian matrix – employed in the computation of elastic constants. An illustration of the calculation of elastic constants of a cubic crystal is described here. From Eq.(2.31), the change in energy per unit volume due to small deformations from the equilibrium configuration is,

$$\Delta E = \frac{1}{2} (\tilde{\epsilon}_1 \ \tilde{\epsilon}_2 \ \tilde{\epsilon}_3 \ \tilde{\epsilon}_4 \ \tilde{\epsilon}_5 \ \tilde{\epsilon}_6) \begin{pmatrix} C_{11} & C_{12} & C_{13} & C_{14} & C_{15} & C_{16} \\ C_{21} & C_{22} & C_{23} & C_{24} & C_{25} & C_{26} \\ C_{31} & C_{32} & C_{33} & C_{34} & C_{35} & C_{36} \\ C_{41} & C_{42} & C_{43} & C_{44} & C_{45} & C_{46} \\ C_{51} & C_{52} & C_{53} & C_{54} & C_{55} & C_{56} \\ C_{61} & C_{62} & C_{63} & C_{64} & C_{65} & C_{66} \end{pmatrix} \begin{pmatrix} \tilde{\epsilon}_1 \\ \tilde{\epsilon}_2 \\ \tilde{\epsilon}_3 \\ \tilde{\epsilon}_4 \\ \tilde{\epsilon}_5 \\ \tilde{\epsilon}_6 \end{pmatrix} \qquad (2.31a)$$

For cubic geometry, there are only 3 independent elastic constants C_{11}, C_{12} and C_{44}. $C_{11} = C_{22} = C_{33}$, $C_{12} = C_{13} = C_{23}$, $C_{44} = C_{55} = C_{66}$ and $C_{\alpha\beta} = 0$ for all other α and β. Also, incorporating the symmetric nature of the elastic constants tensor, Eq.(2.31a) becomes,

$$\Delta E = \frac{1}{2}(\tilde{\epsilon}_1 \; \tilde{\epsilon}_2 \; \tilde{\epsilon}_3 \; \tilde{\epsilon}_4 \; \tilde{\epsilon}_5 \; \tilde{\epsilon}_6) \begin{pmatrix} C_{11} & C_{12} & C_{12} & 0 & 0 & 0 \\ C_{12} & C_{11} & C_{12} & 0 & 0 & 0 \\ C_{12} & C_{12} & C_{11} & 0 & 0 & 0 \\ 0 & 0 & 0 & C_{44} & 0 & 0 \\ 0 & 0 & 0 & 0 & C_{44} & 0 \\ 0 & 0 & 0 & 0 & 0 & C_{44} \end{pmatrix} \begin{pmatrix} \tilde{\epsilon}_1 \\ \tilde{\epsilon}_2 \\ \tilde{\epsilon}_3 \\ \tilde{\epsilon}_4 \\ \tilde{\epsilon}_5 \\ \tilde{\epsilon}_6 \end{pmatrix} \tag{2.31b}$$

If a small longitudinal elastic strain $\tilde{\epsilon}_1 = \epsilon$ is applied, the equation can be reduced to

$$\Delta E = \frac{1}{2}(\epsilon \; 0 \; 0 \; 0 \; 0 \; 0) \begin{pmatrix} C_{11} & C_{12} & C_{12} & 0 & 0 & 0 \\ C_{12} & C_{11} & C_{12} & 0 & 0 & 0 \\ C_{12} & C_{12} & C_{11} & 0 & 0 & 0 \\ 0 & 0 & 0 & C_{44} & 0 & 0 \\ 0 & 0 & 0 & 0 & C_{44} & 0 \\ 0 & 0 & 0 & 0 & 0 & C_{44} \end{pmatrix} \begin{pmatrix} \epsilon \\ 0 \\ 0 \\ 0 \\ 0 \\ 0 \end{pmatrix} \tag{2.31c}$$

$$\Delta E = \frac{1}{2}(\epsilon \; 0 \; 0 \; 0 \; 0 \; 0) \begin{pmatrix} C_{11}\epsilon \\ C_{12}\epsilon \\ C_{12}\epsilon \\ 0 \\ 0 \\ 0 \end{pmatrix} = \frac{1}{2}C_{11}\epsilon^2 \tag{2.31d}$$

Plotting the values of ΔE against the applied strain ϵ, the graph will be parabolic near the equilibrium point of $\epsilon = 0$. The curvature of the curve near the equilibrium gives the value of C_{11}. More precisely, the strain energy can be fitted to a polynomial in ϵ, and twice the coefficient of ϵ^2 gives C_{11}. Other elastic constants can be determined in similar way.

Calculation of elastic constants of a crystal pre-strained by subjecting it to large applied stresses τ_{ij} is more involved. The usual linear strain in Eq.(2.30) is,

$$\epsilon_{ij} = \left(\frac{1}{2}\right)\left(\frac{\partial u_i}{\partial x_j} + \frac{\partial u_j}{\partial x_i}\right) \tag{2.32}$$

where $u_i(\bar{r})$ is the displacement of the material point at $\bar{r}$ in the ith direction. This has to be replaced by the Lagrangian strain,

$$\gamma_{ij} = \left(\frac{1}{2}\right)\left(\frac{\partial u_i}{\partial x_j} + \frac{\partial u_j}{\partial x_i} + \sum_{k=1}^{3}\frac{\partial u_k}{\partial x_j}\frac{\partial u_k}{\partial x_i}\right) \tag{2.33}$$

When a uniform pressure P is applied to the crystal ($\tau_{ij} = -P\delta_{ij}$), the energy of the strained crystal will have additional terms and the total energy can be expressed in the form of Eq.(2.30) in terms of modified elastic constants $\tilde{C}_{ijkl}$ in place of C_{ijkl} (Wallace,

27

1972; Sin'ko and Smirnov, 2002). The relationships between the modified elastic constants and the conventional ones are (in Voigt notation) :

$$\tilde{C}_{\alpha\alpha} = C_{\alpha\alpha} - P \qquad \text{for } \alpha = 1,6 \tag{2.34}$$

$$\tilde{C}_{12} = C_{12} + P, \qquad \tilde{C}_{13} = C_{13} + P, \qquad \tilde{C}_{23} = C_{23} + P \tag{2.35}$$

$$\tilde{C}_{\alpha\beta} = C_{\alpha\beta} \qquad \text{for all other values of } \alpha \text{ and } \beta \tag{2.36}$$

These modified elastic constants are used in the case of the analysis of the pressure-induced variation of the elastic constants of Ruthenium Carbides (section 6.2.2).

For mechanical stability the elastic energy should always be positive. This is equivalent to the Born stability criterion (Born and Huang, 1956; Wallace, 1972; Nye, 1985; Mouhat and Coudert, 2014) that all the eigenvalues of the matrix **C** of elastic stiffness constants should be positive. For symmetric systems, the condition of positive elastic energy can be expressed in terms of closed form relationships between different elastic constants. For the relevant crystal classes of Ruthenium Carbides these relationships are given below :

Cubic :

$$C_{11} > 0, \quad C_{44} > 0, \quad (C_{11} + 2C_{12}) > 0, \quad (C_{11} - C_{12}) > 0 \tag{2.37}$$

Rhombohedral I :

$$C_{11} > |C_{12}|, \quad C_{44} > 0, \quad (C_{11} + C_{12})C_{33} > 2C_{13}^2, \quad (C_{11} - C_{12})C_{44} > 2C_{14}^2 \tag{2.38}$$

Hexagonal :

$$C_{11} > |C_{12}|, \quad C_{44} > 0, \quad (C_{11} + C_{12})C_{33} > 2C_{13}^2 \tag{2.39}$$

The monoclinic and triclinic systems of Boron Carbides have, respectively, 13 and 21 independent elastic constants and such simple closed form expressions are not possible for them. For such less symmetric systems the easier formulation of the stability criterion is by verifying that all the eigenvalues of the matrix of elastic constants are positive.

From the independent elastic constants of a system, bulk modulus (B) and shear modulus (G) are calculated. Two approximation methods are used for the calculation of the polycrystalline elastic moduli — the Voigt method (Voigt, 1928) and the Reuss (Reuss, 1929) method. Using the standard formulae for the relevant crystal classes (Watt, 1980; Watt and Peselnick, 1980; Dieter, 1988; Mehl *et al.*, 1994; Golesorkhtabar *et al.*,

2013), bulk and shear moduli are calculated in Voigt and Reuss approximations. The required formulae are :

Cubic [Independent elastic constants : C_{11}, C_{12}, C_{44}] :

$$B_V = B_R = (C_{11} + 2C_{12})/3 \tag{2.40}$$

$$G_V = (C_{11} - C_{12} + 3C_{44})/5 \tag{2.41}$$

$$G_R = \frac{5(C_{11}-C_{12})C_{44}}{4C_{44}+3(C_{11}-C_{12})} \tag{2.42}$$

Hexagonal [Independent elastic constants : C_{11}, C_{12}, C_{13}, C_{33}, C_{44}] :

$$B_V = [2(C_{11} + C_{12}) + 4C_{13} + C_{33}]/9 \tag{2.43}$$

$$G_V = [C_{11} + C_{12} + 2C_{33} - 4C_{13} + 12C_{44} + 12C_{66}]/30 \tag{2.44}$$

$$C_{66} = (C_{11} - C_{12})/2 \tag{2.45}$$

$$B_R = \frac{[(C_{11}+C_{12})C_{33}-2C_{13}^2]}{[C_{11}+C_{12}+2C_{33}-4C_{13}]} \tag{2.46}$$

$$G_R = \frac{\frac{5}{2}\{[(C_{11}+C_{12})C_{33}-2C_{13}^2]C_{44}C_{66}\}}{3B_VC_{44}C_{66}+[(C_{11}+C_{12})C_{33}-2C_{13}^2](C_{44}+C_{66})} \tag{2.47}$$

Trigonal/ Rhombohedral [Independent elastic constants : C_{11}, C_{12}, C_{13}, C_{14}, C_{33}, C_{44}] : B_V, G_V and B_R are the same as those of Hexagonal symmetry.

$$G_R = \frac{\frac{5}{2}\{[(C_{11}+C_{12})C_{33}-2C_{13}^2](C_{44}C_{66}-C_{14}^2)\}}{3B_V(C_{44}C_{66}-C_{14}^2)+[(C_{11}+C_{12})C_{33}-2C_{13}^2](C_{44}+C_{66})} \tag{2.48}$$

where B_V is given by Eq.(2.43) and C_{66}, by Eq.(2.45).

Monoclinic [Independent elastic constants : C_{11}, C_{22}, C_{33}, C_{44}, C_{55}, C_{66}, C_{12}, C_{13}, C_{23}, C_{15}, C_{25}, C_{35} and C_{46}] :

$$B_v = [C_{11}+C_{22}+C_{33}+2(C_{12}+C_{13}+C_{23})]/9 \tag{2.49}$$

$$G_v = [C_{11}+C_{22}+C_{33}+3(C_{44}+C_{55}+C_{66}) - (C_{12}+C_{13}+C_{23})]/15 \tag{2.50}$$

$$B_R = \Omega / [a(C_{11}+C_{22}-2C_{12})+b(2C_{12}-2C_{11}-C_{23})+c(C_{15}-2C_{25})+$$
$$d(2C_{12}+2C_{23}-C_{13}-2C_{22})+2e(C_{25}-C_{15})+f] \tag{2.51}$$

$$G_R = 15\{4[a(C_{11}+C_{22}+C_{12})+b(C_{11}-C_{12}-C_{23})+c(C_{15}+C_{25})+d(C_{22}-C_{12}-C_{13}-C_{23})$$

$$+e(C_{15}-C_{25})+f]/\Omega +3[g/\Omega +(C_{44}+C_{66})/(C_{44}C_{66}-C_{46}{}^2)]\}^{-1} \tag{2.52}$$

where $\quad a = C_{33}C_{55}-C_{35}{}^2 \tag{2.53}$

$\quad\quad b = C_{23}C_{55}-C_{25}C_{35} \tag{2.54}$

$\quad\quad c = C_{13}C_{35}-C_{15}C_{33} \tag{2.55}$

$\quad\quad d = C_{13}C_{55}-C_{15}C_{35} \tag{2.56}$

$\quad\quad e = C_{13}C_{25}-C_{15}C_{23} \tag{2.57}$

$\quad\quad f = C_{11}(C_{22}C_{55}-C_{25}{}^2)-C_{12}(C_{12}C_{55}-C_{15}C_{25})+C_{15}(C_{12}C_{25}-C_{15}C_{22})$

$\quad\quad\quad +C_{25}(C_{23}C_{35}-C_{25}C_{33}) \tag{2.58}$

$\quad\quad g = C_{11}C_{22}C_{33}-C_{11}C_{23}{}^2-C_{22}C_{13}{}^2-C_{33}C_{12}{}^2+2C_{12}C_{13}C_{23} \tag{2.59}$

and $\quad \Omega = 2[C_{15}C_{25}(C_{33}C_{12}-C_{13}C_{23})+C_{15}C_{35}(C_{22}C_{13}-C_{12}C_{23})+C_{25}C_{35}(C_{11}C_{23}-C_{12}C_{13})]$

$\quad\quad\quad - [C_{15}{}^2(C_{22}C_{33}-C_{23}{}^2)+C_{25}{}^2(C_{11}C_{33}-C_{13}{}^2)+C_{35}{}^2(C_{11}C_{22}-C_{12}{}^2)]+C_{55}g \tag{2.60}$

Triclinic [all 21 elastic constants are independent] :

B_V and G_V are the same as those of Monoclinic symmetry.

$$B_R = [(S_{11}+S_{22}+S_{33}) + 2(S_{12}+S_{13}+S_{23})]^{-1} \tag{2.61}$$

$$G_R = 15[4(S_{11}+S_{22}+S_{33}) - (S_{12}+S_{13}+S_{23}) + 3(S_{44}+S_{55}+S_{66})]^{-1} \tag{2.62}$$

Voigt approximation corresponds to the upper bound and Reuss approximation corresponds to the lower bound of the elastic modulus. Hill approximation (Hill, 1952) gives the average of the two :

$$B_H = (B_V + B_R)/2 \text{ and } G_H = (G_V + G_R)/2 \tag{2.63}$$

From B and G values, Young's modulus Y and Poisson's ratio ν are calculated (Hill, 1952) :

$$Y = 9BG/(3B + G) \tag{2.64}$$

$$\nu = (3B - 2G)/[2(3B + G)] \tag{2.65}$$

2.3.6. Density Functional Perturbation Theory

In density functional perturbation theory (DFPT), perturbation theory is applied to calculate various response functions of condensed matter system from first-principles. A

response function of a system is studied by subjecting the system to an appropriate small perturbation and measuring the consequent change in system. Suppose the system is perturbed by applying an external force. Then the external potential $V_n(\mathbf{r})$ gets modified to $V_n(\mathbf{r},\lambda)$, where λ is a parameter that describes the strength of the perturbation. Then the energy of the perturbed system can be expanded as a power series in lambda, the strength of perturbation.

$$E_\lambda \cong E + \lambda \frac{\partial E}{\partial \lambda} + \frac{1}{2}\lambda^2 \frac{\partial^2 E}{\partial \lambda^2} + \cdots \qquad (2.66)$$

According to Hellmann-Feynman theorem, the first order derivative $\frac{\partial E}{\partial \lambda}$ does not depend on any derivative of electron density $n(\mathbf{r})$.

$$\frac{\partial E}{\partial \lambda} = \int n(\mathbf{r}) \frac{\partial V(\mathbf{r})}{\partial \lambda} d\mathbf{r} \qquad (2.67)$$

This leads to the remarkable result that to calculate the second order change in energy, it is sufficient to know the first order change in the electron density due to the perturbation.

$$\frac{\partial^2 E}{\partial \lambda^2} = \int \frac{\partial V(\mathbf{r})}{\partial \lambda} \frac{\partial n(\mathbf{r})}{\partial \lambda} d\mathbf{r} + \int n(\mathbf{r}) \frac{\partial^2 V(\mathbf{r})}{\partial \lambda^2} d\mathbf{r} \qquad (2.68)$$

Continuing the analysis of the various orders of change in the energy it can be shown that it is sufficient to know nth order change in the electron density to calculate (2n+1)st order change in energy. This is known as the (2n+1) theorem which is extremely useful for calculating nonlinear response of materials.

Interatomic force constants are calculated using DFPT. By diagonalizing the dynamical matrix obtained from the interatomic force constant the phonon frequencies can be determined. Dynamical stability of the systems is determined by calculating the phonons for which force constants are generated on supercells using density functional perturbation theory (Baroni *et al*., 1987, 2001**).** The phonon dispersion curves for the relevant systems are calculated by using PHONOPY code (Togo *et al*., 2008), which is an interface for setting up phonon calculations and then using the generated data to calculate thermodynamic properties. Only linear response is studied in the present thesis., which can be calculated by knowing the electron density, and its first derivative with respect to the perturbation. In density functional perturbation theory, Kohn-Sham equations are supplemented with equation for the first derivative of the electron density

with respect to the perturbation. These equations are simultaneously solved in a self-consistent manner.

2.3.7. Thermodynamic Properties

From the phonon data, through the harmonic approximation, thermal properties due to phonons, such as internal energy, constant–volume heat capacity, Helmholtz free energy and entropy, are evaluated over a range of temperatures from the standard equations of statistical mechanics using the PHONOPY code.

Partition Function,

$$Z = \exp(-\varphi/kT) \prod_i \frac{\exp(-\hbar\omega_i/2kT)}{[1-\exp(-\hbar\omega_i/kT)]} \tag{2.69}$$

Helmholtz Free Energy,

$$F = -kT \ln Z = \varphi + \frac{1}{2}\sum_i \hbar\omega_i + kT\sum_i \ln[1 - \exp(-\hbar\omega_i/kT)] \tag{2.70}$$

Entropy,

$$S = -\left(\frac{\partial F}{\partial T}\right)_V = \frac{1}{2T}\sum_i \hbar\omega_i \coth(\hbar\omega_i/2kT) - k\sum_i \ln[2\sinh(\hbar\omega_i/2kT)] \tag{2.71}$$

Internal energy,

$$E = kT^2 \frac{\partial \ln Z}{\partial T} = \varphi + \frac{1}{2}\sum_i \hbar\omega_i + \sum_i \frac{\hbar\omega_i}{\exp(\hbar\omega_i/kT)-1} \tag{2.72}$$

Heat Capacity,

$$C_V = \left(\frac{\partial E}{\partial T}\right)_V = k\sum_i \left(\frac{\hbar\omega_i}{kT}\right)^2 \frac{\exp(\hbar\omega_i/kT)}{[\exp(\hbar\omega_i/kT)-1]^2} \tag{2.73}$$

where k is Boltzmann constant, $\hbar$ is Planck's constant divided by 2π, T is the temperature and ω_i is the ith phonon frequency. The term φ represents the non-vibrational contributions to the Helmholtz free energy. It can be electronic contribution, if the system is metal; magnetic contribution, if the system is magnetic, and so on. It consists of two parts : φ = U− TS where U is internal energy and S is the entropy due to all the nonvibrational excitations. U is negative for a bound system and, at T = 0K, U is the cohesive energy of the system. As its both parts are negative, φ is negative and larger in magnitude than the total zero–point energy $\frac{1}{2}\sum_i \hbar\omega_i$, and together they form the binding energy of the crystal lattice.

2.3.8. Infrared Spectrum

Born effective charge (BEC) describes the effect of the long range Coulomb part of the force constants. For this reason it is of fundamental importance in the discussion of lattice dynamics. For insulators and semiconductors, the Born effective charge $Z_{\alpha\beta}^*(l)$ of the atom l can be defined in one of the following ways (Baroni *et al.*, 2001) :

(i) The change in induced macroscopic polarization P_α along the direction α caused by the periodic displacement $u_\beta(l)$ of the atom l along the direction β under the condition of zero macroscopic electric field :

$$Z_{\alpha\beta}^*(l) = V \left.\frac{\partial P_\alpha}{\partial u_\beta(l)}\right|_{\mathcal{E}=0} \tag{2.74}$$

where V is the volume of the unit cell.

(ii) The change in induced force on the atom l along the direction β caused by the electric field $\mathcal{E}_\alpha$ along the direction α under the condition of no atomic displacement :

$$Z_{\alpha\beta}^*(l) = \left.\frac{\partial F_\beta(l)}{\partial \mathcal{E}_\alpha}\right|_{u(l)=0} \tag{2.75}$$

(iii) The second partial derivative of the total energy with respect to the applied electric field along the direction α and to the displacement of the atom l along the direction β during a vibrational distortion :

$$Z_{\alpha\beta}^*(l) = -\frac{\partial^2 E}{\partial \mathcal{E}_\alpha \, \partial u_\beta(l)} \tag{2.76}$$

The intensity of the infrared (IR) active modes are calculated in terms of the BECs and the phonon polarization vectors (Baroni *et al.*, 2001) :

$$I(\omega) = \sum_{\alpha=1}^{3}\left|\sum_l \sum_{\beta=1}^{3} Z_{\alpha\beta}^*(l) u_\beta(l)\right|^2 \tag{2.77}$$

where $u_\beta(l)$ is the normalized eigenvector of the dynamical matrix with frequency ω, α and β are Cartesian directions, l represent atoms of the system and $Z_{\alpha\beta}^*(l)$ is the BEC tensor of the l-th atom.

2.3.9. Hardness

In order to estimate the hardness of the stable systems of Boron Carbides and Ruthenium Carbides three different semi-empirical models of hardness are used : (1) the model based on bond strength by Šimůnek and Vackář (2006) and Šimůnek (2007, 2009), (2) the model based on elastic constants by Chen *et al.* (2011) and Tian *et al.* (2012) and (3) the model based on Debye temperature by Abrahams and Hsu (1975) and Deus and Schneider (1983).

2.3.9.1. Model Based on Bond Strength

According to the hardness model based on the strength of different bonds in the system, proposed by Šimůnek and Vackář (2006) and Šimůnek (2007, 2009), the hardness H of the multi-bond ideal single crystal, neglecting the anisotropy effect, has the form (Šimůnek, 2009):

$$H = \frac{C}{\Omega}[b(ij)s(ij) + b(kl)s(kl) + \ldots\ldots\ldots\ldots + b(mn)s(mn)] \qquad (2.78)$$

where *b(ij)* is the number of bonds between atoms *i* and *j* in the unit cell of volume Ω and *s(ij)* is their bond strength given by,

$$s(ij) = \frac{\sqrt{(e_i e_j)}}{n_i n_j d_{ij}} e^{-\sigma f_{ij}} \qquad (2.79)$$

$$\text{and} \qquad f_{ij} = \left(\frac{e_i - e_j}{e_i + e_j}\right)^2 \qquad (2.80)$$

Here n_i and n_j are coordination numbers, respectively, of atoms *i* and *j* and d_{ij} is their interatomic distance. $e_i = Z_i/R_i$ is the reference potential of atom *i* where Z_i is its valence electron number and R_i, its atomic radius. In the semi–empirical model (Šimůnek, 2009), the parameters chosen to fit known data are $C = 1450$ and $\sigma = 2.8$. Substituting the atomic radii and distances in Å, the above formula gives the hardness in GPa.

2.3.9.2. Model Based on Elastic Constants

Using the Pugh's ratio (k = G/B) and the shear modulus (G), Chen *et al.* (2011) have derived a semi-empirical formula of hardness,

$$H = 2(k^2G)^{0.585} - 3 \tag{2.81}$$

However, as this formula sometimes yields negative values of hardness, Tian *et al.* (2012) have modified it with new fitting parameters:

$$H = 0.92k^{1.137}G^{0.708} \tag{2.82}$$

Substituting G in GPa yields the hardness in GPa from this formula. The relative effectiveness of these two models for different systems is studied extensively (table 2 in Chen *et al.* (2011) and table 1 in Tian *et al.* (2012)). In general, the two models give the same order of hardness for different systems.

2.3.9.3. Model based on Debye temperature

The Madelung–Einstein formula for Debye temperature has been modified by incorporating hardness by Abrahams and Hsu (1975) and further improved for fitting with the data by Deus and Schneider (1983) into the form :

$$\Theta_D = aH^{1/2}\rho^{-1/6}M^{-1/3} + b \tag{2.83}$$

where Θ_D is Debye temperature in K, H is Vickers hardness in GPa, ρ is the density of the system in kg/m^3, M is the molar mass of the system in g and a and b are the fitting parameters. The parameter b should be of the order of Θ_D. The fitting parameters a = 2500 and b = 200 are used in the case of Ruthenium Carbides. The Debye temperature can be calculated from the average sound velocity v_m (Anderson, 1963), which, in turn, is obtained from the elastic constant data.

$$\Theta_D = \frac{h}{k_B}\left(\frac{3N_0}{4\pi V_0}\right)^{1/3} v_m \tag{2.84}$$

where h is Planck's constant, k_B is Boltzmann constant, V_0 is the unit cell volume and N_0 is the number of atoms in the unit cell. The average wave velocity v_m in the polycrystalline material is given by Anderson (1963),

$$v_m = \left[\frac{1}{3}\left(\frac{2}{v_t^3} + \frac{1}{v_l^3}\right)\right]^{-1/3} \tag{2.85}$$

where v_t and v_l are the mean transverse and longitudinal elastic wave velocities in the material, respectively. They can be deduced from the Navier's equations in terms of the

Voigt-Reuss-Hill-averaged values of polycrystalline bulk and shear moduli as follows (Anderson, 1963; Schreiber *et al*., 1973) :

$$v_t = (G/\rho)^{1/2} \tag{2.86}$$

$$v_l = [(3B + 4G)/3\rho]^{1/2} \tag{2.87}$$

GROUND STATE STRUCTURE AND PROPERTIES OF B$_{12}$C$_3$

3.1. INTRODUCTION

The ground state structure of Boron Carbide in B$_{12}$C$_3$ stoichiometry has been an active problem because of the absence of experimental detection of monoclinic symmetry as predicted by calculations based on density functional theory. This has called into question the structural models deduced from different experiments and theoretical calculations. The difficulty in determining the structure of Boron Carbide from X-ray or neutron diffraction experiments because of the nearly identical form factors of boron and carbon has further complicated the prospects. The present work tries to address the problem of the ground state structure of Boron Carbide in B$_{12}$C$_3$ stoichiometry. In this work an exhaustive structure search has been performed in B$_{12}$C$_3$ stoichiometry using evolutionary algorithm and density functional theory. We have successfully obtained B$_{11}$C^p(CBC) as the ground state structure of this stoichiometry. To our knowledge, this is the first independent confirmation of this structure using a structure searching technique, with no preconceived notions about the possible outcomes. In addition, the structure search has yielded a hierarchy of possible structures at different higher energies, one of them not previously reported in the literature. We have also investigated the possibility of the existence of structures with larger unit cells in B$_{12}$C$_3$ stoichiometry by performing a second series of guided structure search using supercells of the basic B$_{12}$C$_3$ unit cell. This has yielded an interesting 30-atom supercell in B$_{12}$C$_3$ which has not been reported before. We have subsequently studied using density functional theory the mechanical and dynamical stability of the structures obtained from the structure search, their electronic structure, hardness and thermodynamic properties. We have also computationally generated their IR spectra and contrasted them against the experimental measurements. It

is hoped that this exhaustive analysis will provide independent corroboration of the results of many of the previous experimental and theoretical works and also put forward some new possible structural models for the ground state of $B_{12}C_3$, in an effort to extend the prior studies.

3.2. RESULTS AND DISCUSSION

3.2.1. Structures

The various input variables in USPEX have been studied in detail with reference to simple systems of known structures like Cu, NaCl etc. and then with systems of more complex structures like the perovskites $BaTiO_3$ and $SrTiO_3$. Having achieved the optimal tuning of the variables to accurately reproduce these known structures, we have attempted the structure search of $B_{12}C_3$ stoichiometry using USPEX input cell consisting of 12 boron atoms and 3 carbon atoms. A list of input variables used in USPEX is given in Appendix I. DFT as implemented in VASP is used in combination with USPEX for the structure relaxation and energy calculation required in the structure search. The local density approximation (LDA) to the exchange–correlation functional is used here. In each trial the number of generations is fixed as 25. In USPEX the default choice for the population per generation is twice the number of atoms per input cell, rounded off to nearest multiple of 10. We have chosen the corresponding USPEX variable *populationSize* as 30 and the also the variable *initialPopSize*, representing the number of individuals in the first generation, as 30. A total number of 12 such trials are done by changing the input variables slightly in each successive trial. The lowest energy structure obtained is $B_{11}C^p(CBC)$, shown in figure 3.1, independently confirming a significant body of experimental measurements and theoretical modeling. The next higher energy structure emerging from the structure search is $B_{11}C^e(CBC)$ (figure 3.2), which has been reported in the literature, where one carbon atom occupies an equatorial site in the icosahedral cage. We have obtained a previously unreported structure, named 14-atom-cage (figure 3.3), having the next higher energy. Instead of the icosahedron and 3-atom

chain, this structure consists of a cage of 14 atoms and one interstitial carbon atom connecting four such cages. The cages are also directly bonded together.
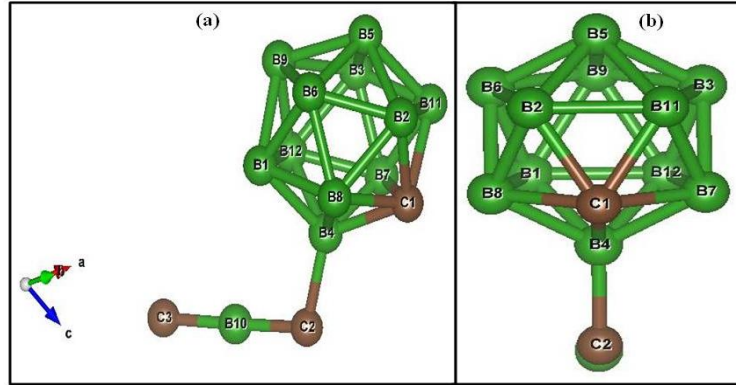
Fig.3.1: $B_{11}C^p$(CBC) structure. Panel (a) gives the view of the cage and the chain. Panel (b) gives the projection on a plane perpendicular to the chain-axis
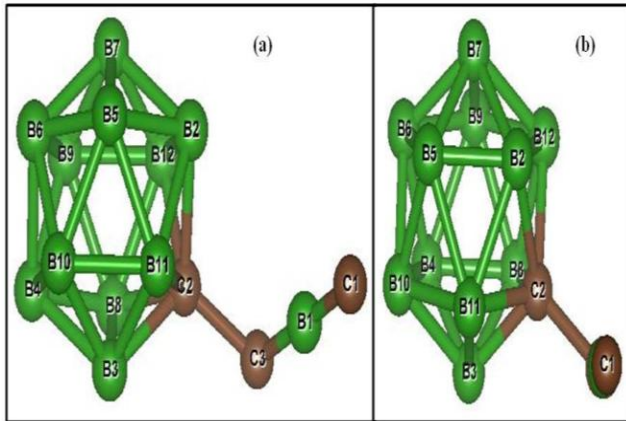
Fig 3.2: $B_{11}C^e$(CBC) structure.
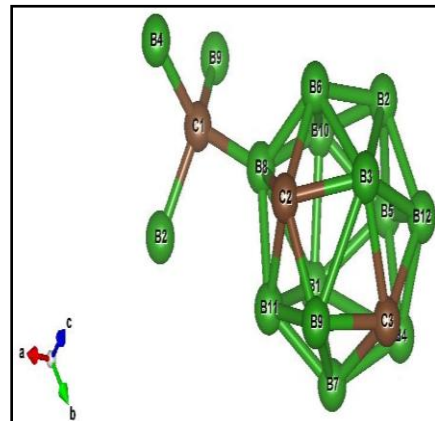
Fig.3.3: 14-atom-cage structure.

The next two higher energy structures are $B_{10}C^{pe}_2$(CBB) (figure3.4), where one carbon occupies the polar site and another carbon occupies the equatorial site in the icosahedron, and $B_{11}C^e$(BCC) (figure3.5), where the chain center is occupied by a carbon instead of boron.

All these five lowest energy structures yielded by the structure search have base-centered monoclinic symmetry Cm. The 30-atom Bravais cells of these five structures are further relaxed using a plane wave energy cutoff of 900 eV which is 2.82 times the default value as per the POTCAR file of boron and 2.25 times the default value for
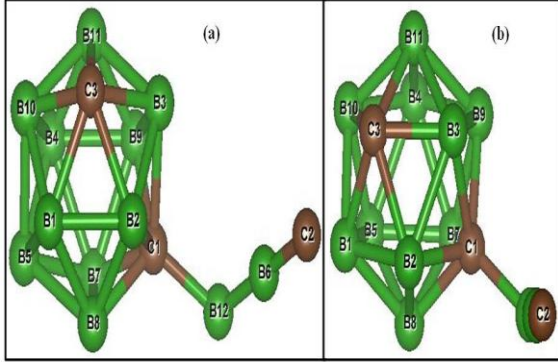
Fig.3.4: $B_{10}C^{pe}{}_{2}$(CBB) structure.
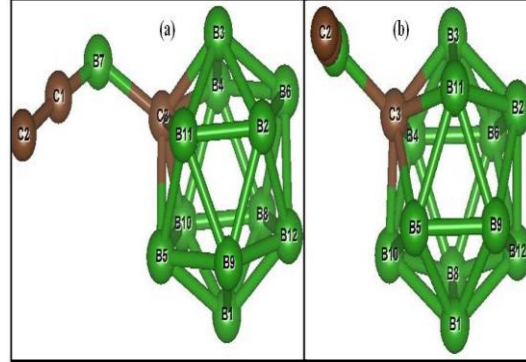
Fig.3.5: $B_{11}C^{e}$(BCC) structure.

carbon. A finer k-grid of 3x5x5 is used for relaxing the Bravais cells of the structures with chain and 3x4x5 for the Bravais cell of the 14-atom-cage structure. The energy values and lattice parameters of the primitive cells are presented in table 3.1 with the results from other works quoted in square brackets. In VASP the total energy is computed with respect to the energies of the constituent atoms and hence the total energy reported here is the negative of the cohesive energy. The total energy is negative for these five systems, implying energetically stable nature. To determine the thermodynamical stability of these Boron Carbide systems their formation energy values are calculated with reference to Alpha-boron and Graphite, which are the ground states of elemental boron and carbon, respectively. Convergence of k-grid is done for both Alpha-boron and Graphite using plane wave energy cutoff of 900 eV and the structures are fully relaxed. For Alpha-boron, using a k-grid of 6x6x6, a total energy/atom of -7.4723 eV is obtained. For Graphite, using a k-grid of 19x19x7, a total energy/atom of -10.1263 eV is obtained. The formation energy E_f is calculated as :

$$E_f = \text{Total energy of } B_{12}C_3 - 12 \times \text{Total energy per atom of Alpha-Boron} - 3 \times \text{Total energy per atom of Graphite} \quad (3.1)$$

The energy values and lattice parameters obtained in this work for $B_{11}C^{p}$(CBC) and $B_{11}C^{e}$(CBC) systems have good agreement with the ones reported in previous computational and experimental works. The difference in total energy between these two systems is 0.5352 eV/f.u.=35.7 meV/atom, which is exactly the value previously reported in the literature (Vast, 2009). These two systems have negative formation energy,

Table 3.1: Structural data of Boron Carbide systems. Lengths are in Å and angles are in degrees.

	$B_{11}C^p$(CBC)	$B_{11}C^e$ (CBC)	14-atom-cage	$B_{10}C^{pe}_2$ (CBB)	$B_{11}C^e$ (BCC)
Total energy/f.u.(eV)	-121.7026 [-108.885[i]]	-121.1674	-119.6473	-119.3652	-119.2185
Formation energy/atom (meV)	-110.41 [-111.73[ii], -121.33[iii], -109.00[iv], -117.40[v], -119.00[vi]]	-74.73 [-84.00[iii], -74.00[iv]]	26.61	45.42	55.20
a	4.9905 [5.01[vii], 5.10[viii], 5.155[ix]]	5.1040 [5.13[viii]]	4.9765	4.9389	5.0399
b = c	5.1476 [5.143[vii]]	5.1448	5.1655	5.1672	5.1542
α	65.13 [65.57[vii], 65.8[viii], 65.68[ix]]	64.72 [64.9[viii]]	78.89	64.91	65.04
β = γ	66.12 [66.39[vii]]	64.91	62.56	66.84	66.94

[i]Bylander *et al.*, 1990(LDA) [ii]Saal *et al.*, 2007(GGA) [iii]Vast *et al.*, 2009(LDA; E_f with respect to alpha-boron and diamond) [iv]Widom and Mihalkovič, 2009(GGA; E_f with respect to alpha-boron and diamond) [v]Widom and Huhn, 2012(GGA; E_f with respect to beta-boron and graphite) [vi]Smith *et al.*,1955(Expt.) [vii]Ivashchenko *et al.*, 2009(LDA)   [viii]Lazzari *et al.*, 1999(LDA) [ix]Morosin *et al.*,1995(Neutron Diffraction)

which implies that they can be synthesized if sufficient energy can be supplied to overcome the reaction barrier. For the other three systems also the synthesis can be achieved at sufficiently high temperature. Thermal energy kT corresponding to formation energy per atom gives an estimate of the order of the temperature of synthesis. For the 14-atom-cage system E_f/atom is 26.61 meV, which corresponds to the temperature of 319K. Once the synthesis of this system is achieved by providing sufficient energy to cross the reaction barrier, it can be maintained in thermodynamical stability at approximately room temperature. For $B_{10}C^{pe}$(CBB) and $B_{11}C^e$(BCC), the temperatures corresponding to E_f/atom are, respectively, 545 K and 662 K. Once their synthesis is achieved by overcoming the reaction barrier, they can be thermodynamically stable around these temperatures. Formation energies of the five systems presented in table 3.1 lie within a band of 166 meV/atom, so they can be formed together in any optimal high temperature synthesis of $B_{12}C_3$. There has been a recent proposal (Huhn and Widom, 2013) of a new phase diagram of Boron Carbide where $B_{12}C_3$ exists in monoclinic structure up to 600K. The results of our work support this finding. It has been established here that structures with monoclinic symmetry can be thermodynamically stable up to 660 K. The values of the lattice parameters clearly show the distortion from

rhombohedral symmetry to base-centered monoclinic symmetry due to the occupation of icosahedral sites by one or two carbon atoms.

The atomic positions of these systems are given in table A II.1 in Appendix II. The atoms occupying specific sites are indicated against each Wyckoff position. For the systems with chain in table A II.1 the last three positions represent the chain sites with the middle one corresponding to the chain center. In Cm symmetry the Wyckoff positions of the lattice are modified to four 2b sites of the icosahedra and seven 1a sites. Four of the seven 1a sites belong to the icosahedra and the remaining three belong to the 3-atom chain (table A II.1). In the 14-atom-cage system, there are five 2b sites and four 1a sites in the cage, the carbon atom attached to the cage occupies 1a site (table A II.1).

Modifying the scheme given in Lazzari *et al.*(1999) and Ivashchenko *et al.* (2009), the 41 different bonds in each of the structures with chain can be classified into six types of generally increasing bond lengths : intrachain bond ($b^{(1)}$), chain-icosahedron bond ($b^{(2)}$), intericosahedron bond ($b^{(3)}$), equatorial hexagon bond ($b^{(4)}$), polar-equatorial bond ($b^{(5)}$) and polar triangle bond ($b^{(6)}$). The last three together constitute 30 intraicosahedral bonds. Among the 45 bonds in the 14-atom-cage structure 36 are intracage bonds. Ten atoms in the 14-atom-cage are directly bonded to atoms in the neighbouring cages, forming 5 intercage bonds ($b^{(3)}$ type). The remaining four atoms in the cage are bonded to other cages through the carbon atom attached to the cage ($b^{(2)}$ type). In the case of the five Boron Carbide systems under study the average bond lengths of these six types of bonds are presented in table 3.2. Bonds between different atomic species are considered separately. Values from other works, treating the bonds of different atomic species together, are quoted in square brackets. The bond lengths obtained in this work for $B_{11}C^p$(CBC) and $B_{11}C^e$(CBC) systems are in excellent agreement with the previously reported values from computational and experimental works. This lends validity to the computational data on the other systems considered in this work. There is, in general, a significant reduction in bond lengths when atoms forming the bond occupy the 1a site in the icosahedra. This implies that charge density

concentration may be higher in the icosahedral a-sites resulting in the formation of stronger bonds.

Table 3.2: Average bond lengths in Å for the Boron Carbide systems

		$b^{(1)}$	$b^{(2)}$	$b^{(3)}$	$b^{(4)}$	$b^{(5)}$	$b^{(6)}$
$B_{11}C^p$ (CBC)	B-C	1.4239 [1.42[i, ii], 1.438[iii], 1.434[iv]]	1.5896 [1.58[i],1.59[ii], 1.669[iii], 1.675[iv]]	1.6392 [1.66[i],1.71[ii], 1.699[iii],1.716[iv]]		1.7328 [1.72[i]]	1.7398 [1.74[i]]
	B-B			1.7228	1.7366 [1.73[i, ii], 1.687[iii], 1.693[iv]]	1.7800 [1.77[i, ii], 1.76[iii, iv]]	1.8007 [1.80[i], 1.78[ii], 1.81[iii, iv]]
$B_{11}C^e$ (CBC)	C-C		1.5385				
	B-C	1.4361 [1.43[ii]]	1.5966 [1.59[ii]]		1.6942	1.7457	
	B-B			1.7122 [1.69[ii]]	1.7362 [1.72[ii]]	1.7804 [1.78[ii]]	1.7769 [1.78[ii]]
14-atom cage	B-C		1.5565	1.6159	1.7142 (1.6176 - 1.8349)		
	B-B			1.6957	1.8171 (1.6779 - 2.1598)		
$B_{10}C^{pe}{}_{2}$ (CBB)	B-C	1.4373	1.5869	1.6248	1.6764	1.7251	1.7242
	B-B	1.5092	1.6756	1.7348	1.7409	1.7851	1.8025
$B_{11}C^e$ (BCC)	C-C	1.3548					
	B-C	1.3922	1.6245		1.6777	1.7147	
	B-B		1.7350	1.7037	1.7443	1.7686	1.7981

[i]Ivashchenko *et al*., 2009(LDA)   [ii]Lazzari *et al*.,1999(LDA)   [iii]Morosin *et al*.,1995(Neutron Diffraction) [iv]Morosin *et al*.,1987(X-ray Diffraction)

As boron has the tendency to form structures with larger unit cells (Hoard and Hughes, 1967; Shirai, 2010), We have also considered the possibility of the existence of structures with larger unit cells in $B_{12}C_3$ stoichiometry by performing a guided structure search. Here we have used USPEX input cells of 24 boron atoms and 6 carbon atoms. We have also used seed structures to confine the structure search within certain regions of the energy landscape where there is an increased probability of finding the potential structures with larger unit cells. The seed structures used are the different combinations of the 15-atom unit cells of $B_{12}C_3$ stoichiometry. We have used some of the structures with chains obtained in our structure search and also their variants with substitutional disorder. The number of generations is fixed as 50 and both *populationSize* and *initialPopSize* are chosen as 60. Increasing the number of generations is quite important in an evolutionary algorithm based structure search, as new candidate structures may

emerge after fairly large number of generations. It also ensures that the repeated appearance of the same offspring structure over many generations is due to the occurrence of the ground state and not due to the search getting stuck in a plateau in the energy landscape. The lowest energy structure obtained is composed of $(B_{11}C^p)$ and $(B_{10}C^{pe}_2)$ icosahedra and (CBC) and (CBB) chains (figure3.6). Its symmetry is triclinic (space group: P1) and each atom of the unit cell occupies a Wyckoff 1a site. The structure is further relaxed using the plane wave energy cutoff of 900 eV and a finer k-grid of 6x6x4. The structural data are given in table 3.3 and the atomic positions in table A II.2 in Appendix II. The bond lengths are comparable to those of the individual units. The labeling used for this 30-atom unit cell is such that each distinct structural unit is given in separate brackets.
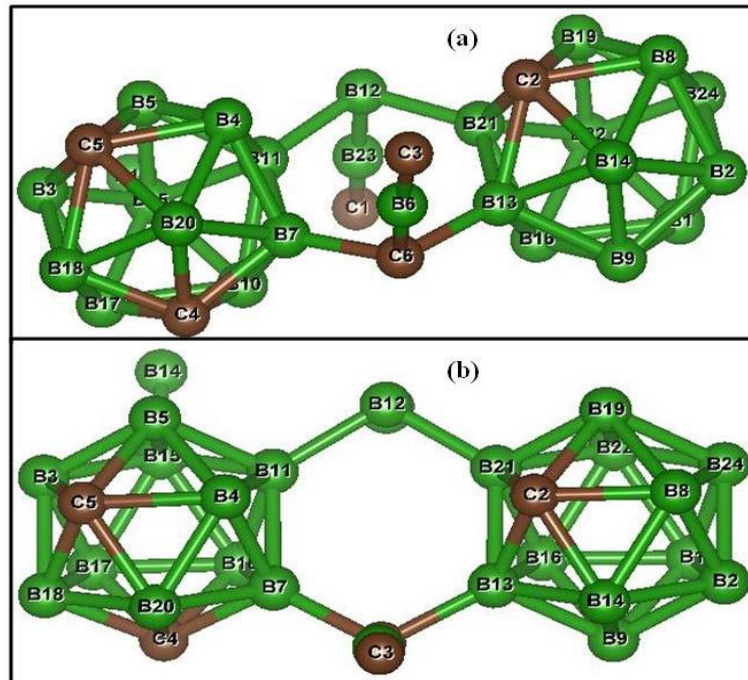
Fig.3.6: $(B_{11}C^p)(B_{10}C^{pe}_2)(CBC)(CBB)$ structure

Table 3.3: Structural data of $(B_{11}C^p)(B_{10}C^{pe}_2)(CBC)(CBB)$. Lengths are in Å and angles are in degrees.

a	b	c	α	β	γ	Total energy/f.u. (eV)	Formation energy/atom (meV)
4.9929	5.5600	7.6581	90.25	96.43	90.62	-120.3716	-21.67

The remarkable feature about this structure is that its formation energy is negative and within 89 meV/atom of that of the ground state structure $B_{11}C^p$(CBC). This implies that within the normal synthesis condition of Boron Carbide, this 30-atom structure is likely to be formed along with the two lower energy structures $B_{11}C^p$(CBC) and $B_{11}C^e$(CBC). The possibility of structures with the configuration of supercells acting as disorders in the homogeneous composition of $B_{12}C_3$ stoichiometry has been discussed in the literature (Vast *et al.*, 2009; Ektarawong *et al.*, 2014). Our structure search using 30-atom supercells confirm that supercells of this type have a potential presence in $B_{12}C_3$ stoichiometry. The structure search has yielded a structure of larger unit cell which cannot be reduced to representation in terms of smaller unit cells.

3.2.2. Elastic constants

The elastic constants are crucial for the determination of the mechanical properties of materials, providing important information on their stability, stiffness and brittle/ductile character. In order to analyze the mechanical stability of the six Boron Carbide systems we have computed their elastic stiffness constants C_{ij} at the equilibrium lattice parameters. From the independent elastic constants of a system, bulk modulus (B) and shear modulus (G) are calculated using the standard formulae for monoclinic lattice, as given by Eqns.(2.49)–(2.60) (Watt,1980; Dieter,1988) and triclinic lattice, as given by Eqns.(2.49)–(2.50) and (2.60)–(2.61) (Golesorkhtabar *et al.*, 2013) in Voigt (Voigt, 1928) and Reuss (Reuss, 1929) approximation schemes. Voigt approximation corresponds to the upper bound and Reuss approximation corresponds to the lower bound of the elastic modulus. Hill approximation (Hill, 1952) gives the average of the two. From B and G values, Young's modulus Y and Poisson's ratio ν are calculated using Eqns.(2.64)–(2.65). The elastic constants and the average values of B, G, Y (in GPa) and ν are tabulated in table 3.4 with the experimental data from other works given in square brackets.

The calculated values of elastic moduli are in excellent agreement with the experimental data. The remarkable correspondence between the elastic moduli of the 30-atom supercell with the experimental data is to be emphasized. There are 13 independent

Table 3.4: Elastic Properties of Boron Carbides

	$B_{11}C^p$ (CBC)	$B_{11}C^e$ (CBC)	14-atom cage	$B_{10}C^{pe}_2$ (CBB)	$B_{11}C^e$ (BCC)	$(B_{11}C^p)(B_{10}C^{pe}_2)$ (CBC)(CBB)		
C_{11}	481.455	482.011	531.368	515.685	487.898	563.244		
C_{12}	158.166	152.150	163.682	154.915	162.087	52.609		
C_{13}	154.638	166.801	116.878	154.193	190.419	157.555	C_{14}	26.699
C_{15}	17.408	18.448	4.836	17.295	-5.424	-0.6710	C_{16}	1.549
C_{22}	565.310	550.471	550.973	520.249	447.154	495.891		
C_{23}	55.645	65.271	98.971	45.598	38.555	158.698	C_{24}	10.612
C_{25}	26.769	18.832	-0.605	34.685	36.110	-2.555	C_{26}	7.793
C_{33}	512.124	497.142	468.310	485.980	418.462	451.380	C_{34}	18.726
C_{35}	9.498	12.489	-3.684	19.079	16.306	6.134	C_{36}	17.995
C_{44}	170.526	165.548	254.663	178.517	172.019	241.487	C_{45}	3.995
C_{46}	26.988	28.555	-9.109	32.996	31.277	1.865		
C_{55}	246.506	244.990	268.264	244.193	225.636	218.324	C_{56}	28.736
C_{66}	224.715	231.027	233.107	221.410	198.501	155.532		
B	254.036	254.344	255.114	244.917	230.703	248.487	[247[i], 235[ii], 199[iii]]	
G	203.015	199.684	226.779	202.254	176.477	198.339	[200[i], 197[ii], 188[iv]]	
Y	480.932	474.799	524.826	475.791	421.863	469.975	[472[i], 462[ii], 448[v]]	
ν	0.1845	0.1899	0.1571	0.1762	0.1952	0.1848	[0.18[i], 0.17[ii], 0.21[v]]	
B/G	1.2513	1.2737	1.1249	1.2109	1.3073	1.253		

[i]Gieske *et al*.,1991   [ii]Manghnani *et al*., 2000   [iii]Nelmes *et al*., 1995
[iv]Schwetz and Grellner, 1981   [v]Murthy, 1985

elastic constants for monoclinic geometry and 21 for triclinic geometry. For mechanical stability the elastic energy should always be positive. This is equivalent to the Born stability criterion (Mouhat and Coudert, 2014) that all the eigenvalues of the matrix **C** of elastic stiffness constants should be positive. For the six systems presented here this stability condition has been verified and all of them are found to be mechanically stable. The high value of Bulk modulus (~ 250 GPa) indicates high hardness for these systems. The calculated values of B/G ratio for the given systems (table 3.4) are smaller than 1.75, the critical value to separate brittleness and ductility, according to Pugh's criterion (Pugh, 1954). This indicates that these systems are all brittle.

3.2.3. Phonons

A system is dynamically stable only if all the phonon modes of the system have real frequencies for all the wave vectors. Phonon dispersions can be used to compute many dynamical properties of materials. Quantities like free energy, entropy, internal energy, specific heat and electron–phonon interaction can be calculated from phonon data within harmonic approximation. Using the self consistent density functional perturbation theory (DFPT) the phonon modes of Boron Carbide systems are calculated with 1x2x2 supercells (120 atoms) of the Bravais cells. PHONOPY code is used for the post-processing. The ACONVASP online utility (Setyawan and Curtarolo, 2010) is used for selecting the high symmetry points in the Brillouin zone for each system. The phonon dispersion curves and density of states (DOS) of these systems are presented in figures 3.7–3.12. The DOS values are normalized to formula units. The absence of imaginary frequencies at all wave vectors confirms that these systems are dynamically stable. The higher the maximum frequency of acoustic phonon modes higher is the stability of the material against elastic deformation. The maximum frequency of acoustic phonon modes of these six systems are above 30 THz, indicating high stability against elastic deformation.
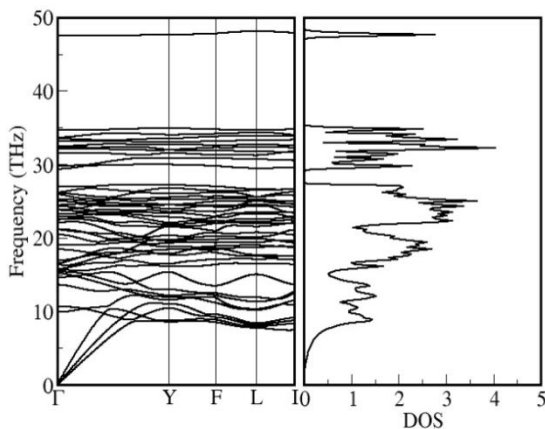
Fig.3.7: Phonon dispersions & density of states of $B_{11}C^p$(CBC)
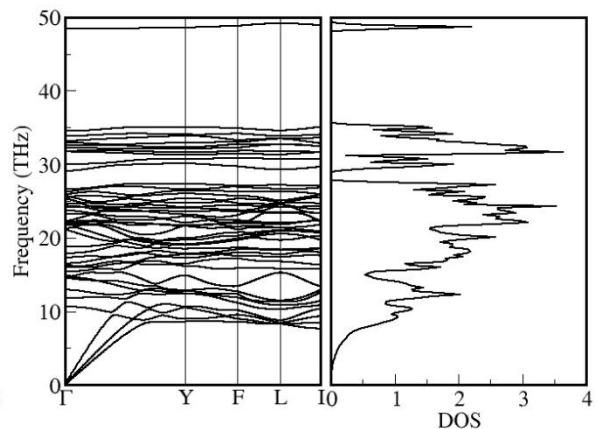
Fig.3.8: Phonon dispersions & density of states of $B_{11}C^e$(CBC)
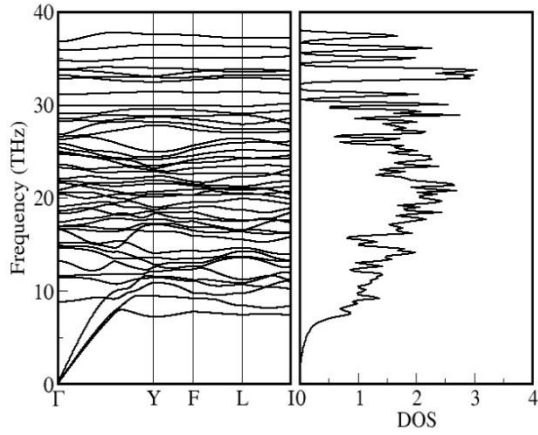
Fig.3.9: Phonon dispersions & density of states of 14-atom-cage
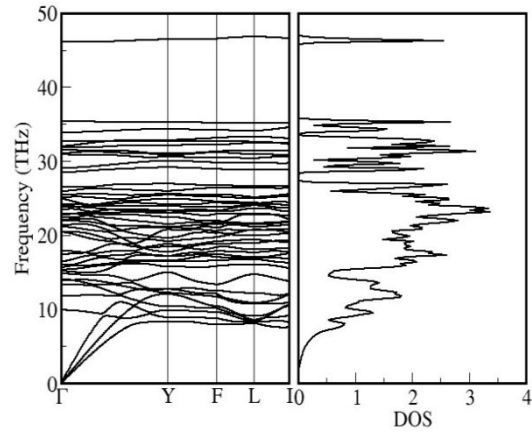
Fig.3.10: Phonon dispersions & density of states of $B_{10}C^{pe}_2$(CBB)
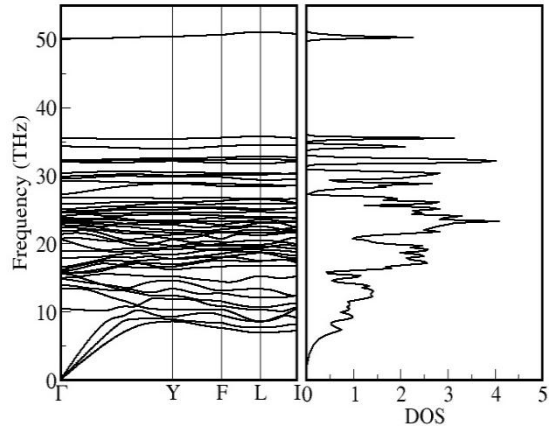
Fig.3.11: Phonon dispersions & density of states of $B_{11}C^e$(BCC)
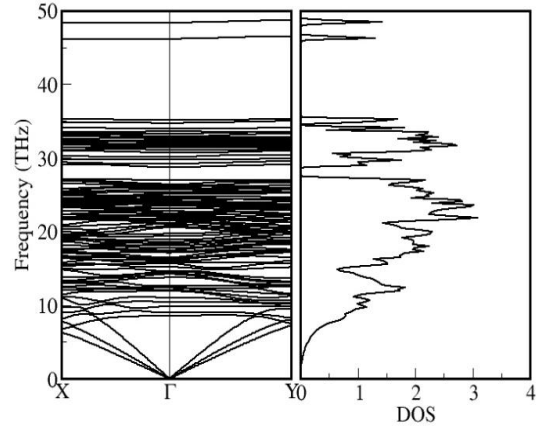
Fig.3.12: Phonon dispersions & density of states of $(B_{11}C^p)(B_{10}C^{pe}_2)$(CBC)(CBB)

3.2.4. Electronic Structure

The electronic energy bands along the high symmetry directions of the Brillouin zone and the partial density of states are presented in figures 3.13–3.18 for Boron Carbide systems. The Fermi level is set to 0 eV. All the six Boron Carbide systems studied here are found to be semiconductors with indirect band gaps. The calculated energy band gap values of Boron Carbide systems are presented in table 3.5.
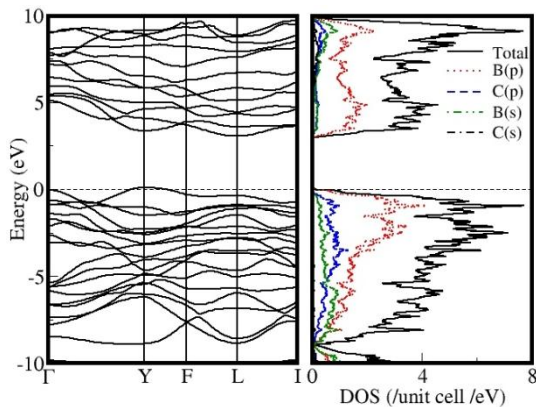
Fig.3.13: Electronic bands & partial density of states of $B_{11}C^p$(CBC)
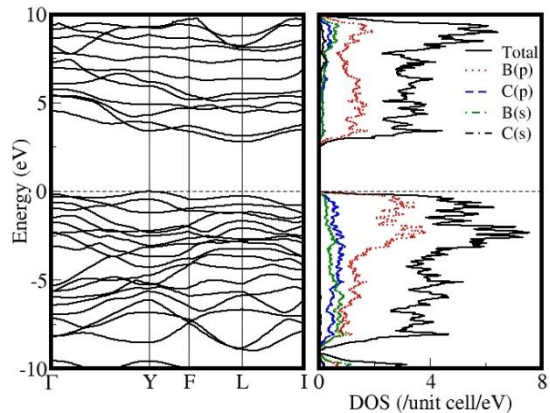
Fig.3.14: Electronic bands & partial density of states of $B_{11}C^e$(CBC)
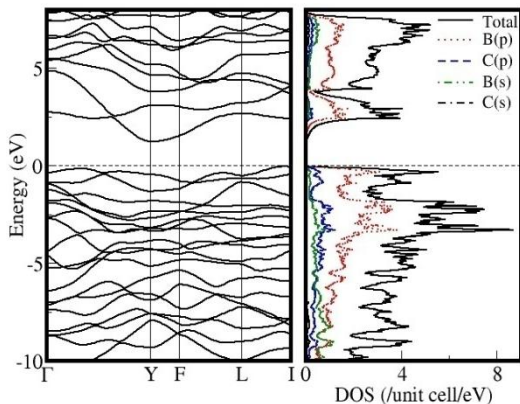
Fig.3.15: Electronic bands & partial density of states of 14-atom-cage
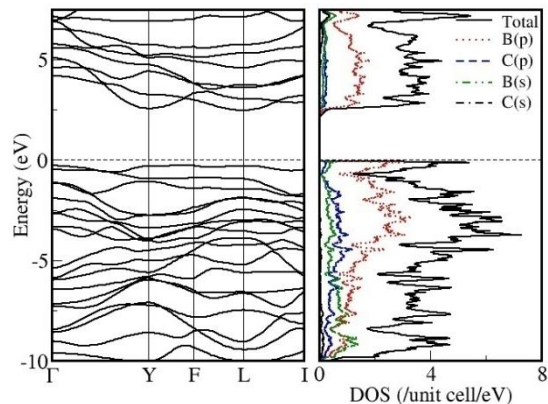
Fig.3.16: Electronic bands & partial density of states of $B_{10}C^{pe}_2$(CBB)
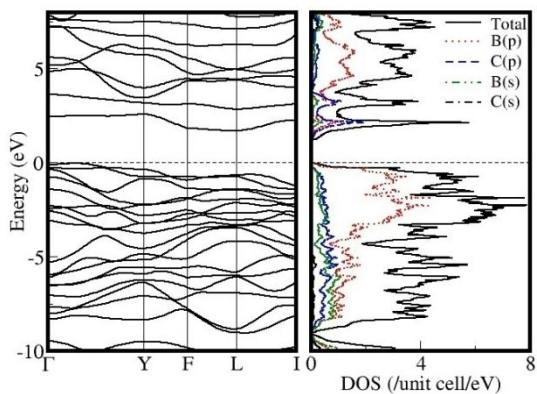
Fig3.17: Electronic bands & partial density of states of $B_{11}C^e$(BCC)
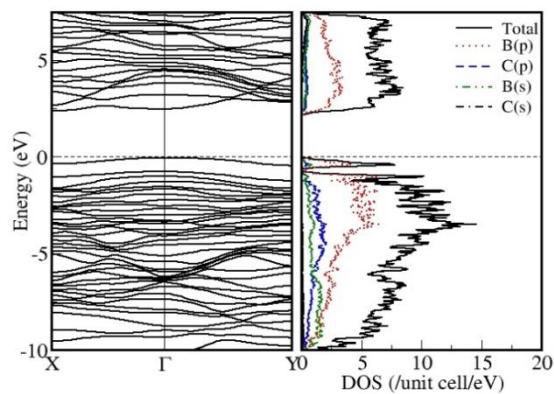
Fig.3.18: Electronic bands & partial density of states of $(B_{11}C^p)(B_{10}C^{pe}_2)$(CBC)(CBB)

Table 3.5: Energy band gaps (in eV) of Boron Carbides

$B_{11}C^p$(CBC)	$B_{11}C^e$ (CBC)	14-atom cage	$B_{10}C^{pe}_2$ (CBB)	$B_{11}C^e$ (BCC)	$(B_{11}C^p)(B_{10}C^{pe}_2)$ (CBC)(CBB)
2.885 [2.781[i], 2.95[ii], 3.00[iii], 2.09[iv]]	2.547	1.283	2.220	1.248	2.186

[i]Bylander *et al.*, 1990(LDA)   [ii]Ivashchenko *et al.*, 2009 (LDA)
[iii]Ektarawong *et al.*, 2014(GGA)   [iv]Werheit, 2006(Expt.)

The electronic bands and dos are calculated using the primitive cell of 15 atoms except for the larger system whose primitive cell contains 30 atoms. All the experimental and computational works confirm that Boron Carbide in $B_{12}C_3$ stoichiometry is a semiconductor. The band gap obtained here for $B_{11}C^p$(CBC) is in fair agreement with the results from other computational works. The band gap values could be larger than these, as DFT based calculations generally underestimate the energy band gap. It is to be noted that the correspondence with the experimental estimate of 2.09 eV is the best for the system with 30-atom unit cell. There is a significant reduction in the band gap when the structure does not contain the (CBC) chain (Ivashchenko *et al.*, 2009). In the case of 14-atom-cage system and $B_{11}C^e$(BCC) the band gap is reduced to less than half of the lowest energy system, $B_{11}C^p$(CBC). The possibility of tuning the band gap by controlling the structural unit may have significance in electrical, electronic and optical applications of Boron Carbides. The band gaps deduced by different experimental measurements vary over a range of values. If the composition of $B_{12}C_3$ stoichiometry consists of different structural entities or polytypes, a correspondence between computational and experimental values can be attempted by considering the relative contribution of different polytypes. In this context it is significant that two of the systems under investigation in this work have relatively lower values of band gap. The predominant contribution to the partial density of states is from the 2p orbital of boron.

3.2.5. Infrared Spectra

As form factors of boron and carbon atoms are nearly identical, it is rather difficult to get unique signatures of the Boron Carbide systems from X-ray diffraction pattern. Infrared spectra, on the other hand, provide a convenient signature for

experimental verification. We have computationally generated the infrared spectra of the six Boron Carbide systems considered here. For insulators and semiconductors the intensity of the infrared (IR) active modes are calculated in terms of the Born effective charges and the phonon polarization vectors using Eq.(2.77) (Baroni *et al*., 2001). The computed IR spectra of Boron Carbide systems are presented in figures 3.19–3.24. A measurement of IR spectra (Kuhlmann *et al*., 1992), quoted in many of the previous works (Lazzari *et al*., 1999; Vast *et al*., 2009; Shirai, 2010), is given against each for comparison. A broadening of 10 cm^{-1} is applied to the computed peaks. The background is not accounted for in these individual computed spectra.
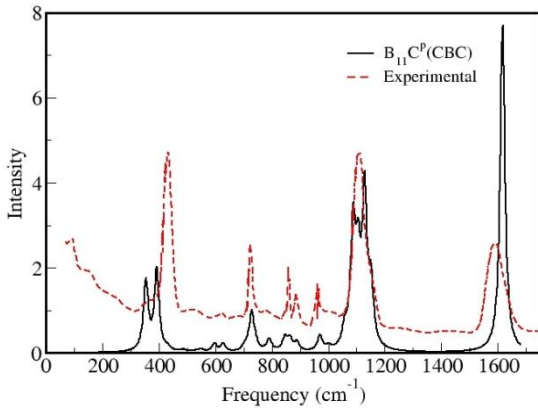
Fig.3.19: IR spectra of $B_{11}C^p$(CBC)
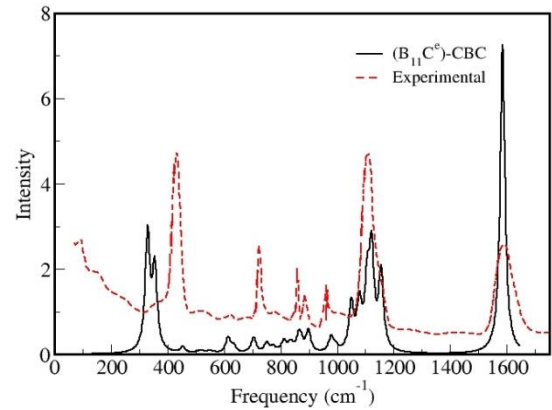
Fig.3.20: IR spectra of $B_{11}C^e$(CBC)
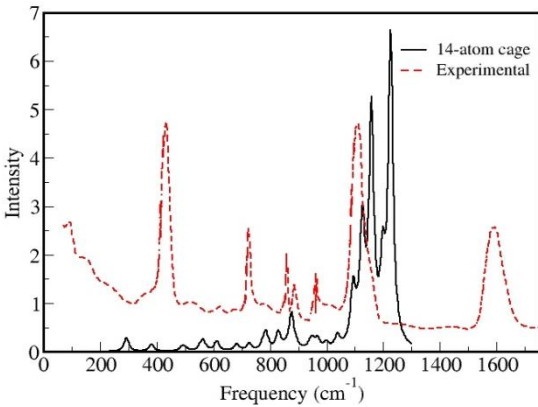
Fig.3.21: IR spectra of 14-atom-cage
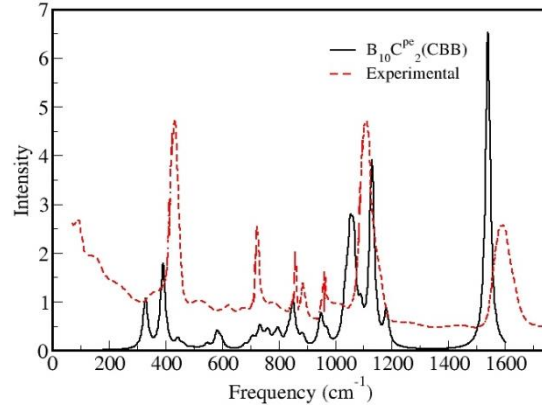
Fig.3.22: IR spectra of $B_{10}C^{pe}_2$(CBB)
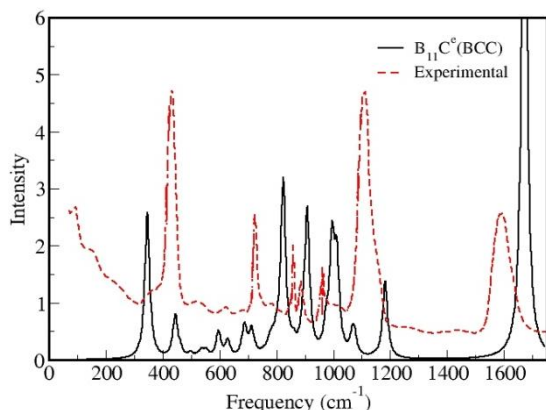
Fig.3.23: IR spectra of $B_{11}C^e$(BCC)
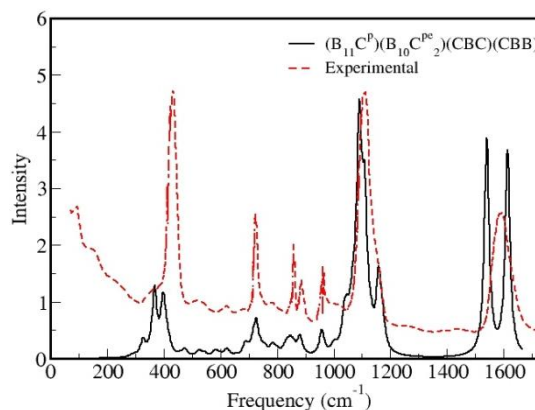
Fig.3.24: IR spectra of $(B_{11}C^p)(B_{10}C^{pe}{}_2)$(CBC)(CBB)

Except for the 14-atom-cage and $B_{11}C^e$(BCC) systems IR spectra of the Boron Carbide systems exhibit most of the features of the experimental spectrum. The frequencies of IR active modes of the four systems exhibiting good correlation to the seven major peaks in the experimental spectrum are tabulated in table 3.6.

Table. 3.6: Frequencies (in cm^{-1}) of the major peaks
in the IR spectra of Boron Carbides

Experimental peaks	$B_{11}C^p$ (CBC)	$B_{11}C^e$ (CBC)	$B_{10}C^{pe}{}_2$ (CBB)	$(B_{11}C^p)(B_{10}C^{pe}{}_2)$ (CBC)(CBB)
1590	1616.93	1585.03	1539.72	1613.63
1110	1128.89	1122.50	1130.05	1109.93
964	970.84	979.36	949.79	958.28
890	889.32	898.84	884.68	882.66
860	846.20	865.40	851.20	846.96
730	729.29	704.77	733.64	727.57
430	393.04	355.47	392.06	396.87
% weighting factor in the fitted spectrum	11.09	46.55	27.37	15.00

In the case of more than one computed peak in the vicinity the one with more resemblance to the experimental peak in terms of both frequency and intensity is

52

specified. Using the computed spectra of these four systems we have done a curve fitting by minimizing the mean square errors with the experimental spectrum and assuming a linear background. The result of the curve fitting is given in figure 3.25. The relative weighting factors of the four systems in the fitted spectrum are given in table 3.6. The lowest weighting factor of 11.09% in the case of $B_{11}C^p(CBC)$ is a surprising result as this is generally considered to be the predominant structure in the composition of $B_{12}C_3$.
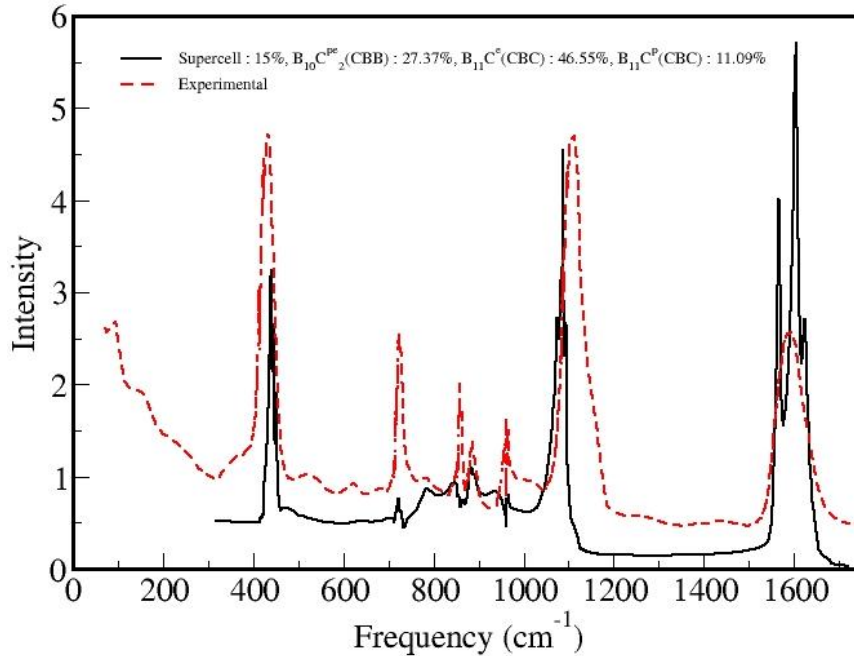
Fig.3.25: The fitted IR spectrum of Boron Carbides

We have also done a fitting using the spectra of $B_{11}C^p(CBC)$, $B_{11}C^e(CBC)$ and the supercell $(B_{11}C^p)(B_{10}C^{pe}_2)(CBC)(CBB)$ and then the relative weighting factor is only 1.25% for $B_{11}C^p(CBC)$ while it is 53.22% for $B_{11}C^e(CBC)$ and 45.53% for the 30-atom unit cell. $B_{11}C^p(CBC)$ forms part of the 30-atom unit cell $(B_{11}C^p)(B_{10}C^{pe}_2)(CBC)(CBB)$. This raises the possibility that the presence of $B_{11}C^p(CBC)$ in the composition of $B_{12}C_3$ could mostly be as part of structures with larger unit cells rather than as independent 15-atom structural units. In the pioneering work of Lazzari *et al*. (1999) the comparison between computational and experimental IR spectra has shown maximum correspondence in the case of $B_{11}C^p(CBC)$. They have considered only three different structures in that work and two of them are included in the present work. If we compare

the spectra of $B_{11}C^p$(CBC) and $B_{11}C^e$(CBC) against experimental spectrum it is clear that the spectrum of the former shows more correspondence with the experimental spectrum (figure 3.19, table 3.6). However, if we consider the possibility that the composition of $B_{12}C_3$ may consist of different structural entities whose energies are accessible within the normal synthesis conditions of Boron Carbide, the experimental IR spectrum could be due to the relative contribution from all these entities. The approach of considering the cumulative spectrum of potential structural entities may be more realistic when comparing with the experimental spectrum.

3.2.6. Hardness

The semi-empirical model based on the bond strength, proposed by Šimůnek and Vackář (2006) and Šimůnek (2007, 2009), is considered here to calculate the hardness of Boron Carbide systems. According to this model, the hardness H of the multi-bond ideal single crystal can be evaluated using Eqns.(2.78)–(2.80). For boron $Z_1 = 3$ and $R_1 = 0.98$ Å (Kittel, 1996), so e_1=3.0612; for carbon $Z_2 = 4$ and $R_2 = 0.92$ Å (Kittel, 1996), so $e_2 = 4.3478$.

The bond strength depends on both the number of atoms to which a given atom is bonded and the bond length (Eq.3.2). In Boron Carbides the coordination number depends on the specific atomic site occupied by boron or carbon. For an atom occupying polar or equatorial site the coordination number is 6, for an atom at the chain-end it is 4 and for one at the chain-center it is 2. Bond length varies for the six types of bonds as listed in table 3.2 and it further varies among B-B, B-C and C-C bonds. Thus, the bond strength in Boron Carbides changes with the atomic site, the type of the bond and the pair of bonding atoms. To classify the bonds based on these three factors we use the following labeling scheme: subscript 1 is for boron and 2 is for carbon; superscript in brackets represents the type of the bond as classified in table 3.2. In this labeling $b_{11}^{(1)}$ represents intrachain B-B bond, $b_{12}^{(3)}$ represents intericosahedron B-C bond, and so on. Each bond of the type $b_{ij}^{(\alpha)}$ has a distinct bond strength and hence its contribution should be considered separately while determining the hardness. All the 41 bonds in each of the four systems with chain are classified according to this scheme and their calculated bond

strengths are listed in table A III.1 in Appendix III. In order to avoid counting the bonds twice, we have grouped bonds of the type 3-6 while accounting the bonds formed by boron or carbon atom occupying a polar or equatorial site. Among them only B-B bonds are grouped in the account of B atoms occupying polar and equatorial sites and only B-C bonds in the account of C atoms occupying these sites. Bonds of the type 1 and 2 are grouped while accounting the bonds formed by boron or carbon atom occupying the chain-end site. There is no need to separately count the bonds formed by the chain-center atoms as these bonds are accounted for while considering the bonds formed by the chain-end atoms. The average bond lengths for each type of the bonds 1-6 are taken from table 3.2 except in the case of the chain-icosahedron B-C bonds formed by the chain-end atoms in $B_{10}C^{pe}_2$(CBB) and $B_{11}C^e$(BCC). For these the contributions of boron atom and carbon atom at the chain-end are computed separately, instead of taking the average B-C bond lengths, and the bond lengths are specified in table A III.1 against the corresponding bond types. Among the 45 bonds in 14-atom-cage the 36 intracage bonds take up the place of bonds of type 4-6 in the other four structures. In table A III.1 they are given against type 4 bonds for convenience. The 5 intercage bonds are given against type 3 bonds. A single carbon atom takes up the place of the chain and the 4 carbon-cage bonds are given against type 2 bonds. In this structure each of the twelve cage atoms are bonded to six atoms and each of the other two cage atoms are bonded seven atoms. Since 12 out of 14 cage atoms have the same number of neighbours the coordination number of each cage atom is taken as 6. The coordination number of the external carbon atom is 4, like that of the chain-end atom in the other four structures. The values of hardness (H_b) calculated using these parameters are also given in table 3.7. $(B_{11}C^p)(B_{10}C^{pe}_2)$(CBC)(CBB) is not considered for this analysis. It can be reasonably argued that its hardness value can be of the order of that of the two 15-atom systems constituting it. The experimental reports of the Vickers hardness (HV) and Knoop hardness (HK) values of Boron Carbides vary over a wide range. Some relatively recent experimental data are given in table 3.7. There is excellent agreement between the hardness values calculated using the model based on

bond strength and the experimental values. The four structures with chain have hardness values close to the superhard regime (> 40 GPa).

Table 3.7: Hardness values (in GPa) of Boron Carbides from models based on bond strength (H_b) and Pugh's ratio (H_P)

	H_b	H_P	Experimental Values
$B_{11}C^p$(CBC)	37.74	30.68	
$B_{11}C^e$(CBC)	37.84	29.71	HV = 32±2[i]
14-atom cage	33.07	31.76	HK = 33.8–36.7[ii]
$B_{10}C^{pe}_2$(CBB)	37.10	26.43	HV = 31.31±0.79–38.86±2.13[iii]
$B_{11}C^e$(BCC)	38.00	37.45	HV = 40.5[iv]
$(B_{11}C^p)(B_{10}C^{pe}_2)$ (CBC)(CBB)		30.13	

[i]Hayun *et al*., 2009   [ii]Werheit *et al*., 2004   [iii]Grasso *et al*., 2011   [iv]Domnich *et al*., 2002

Some of the semi-empirical models of hardness attempt to correlate hardness with different combinations of elastic properties. Using the Chen-Tian modified formula (Eq.2.82) and the values of elastic moduli from table 3.4, the hardness of the Boron Carbide systems are estimated and the values (H_P) are given in table 3.7. The hardness values from the two models are of the same order. For $(B_{11}C^p)(B_{10}C^{pe}_2)$(CBC)(CBB) the model based on Pugh's ratio gives a hardness value of 30.13 GPa which is close to that of $B_{11}C^p$(CBC).

3.2.7. Thermodynamic Properties

From the phonon data, through the harmonic approximation, thermal properties due to phonons, such as internal energy (E), constant–volume heat capacity (C_v), Helmholtz free energy (F) and entropy (S), are evaluated over a range of temperatures from the standard equations of statistical mechanics (Eqns.(2.69)–(2.73)) using the PHONOPY code. The results of the calculations are presented in figures 3.26–3.31. The values are normalized to formula units. The six systems exhibit almost identical variations of F, S, E and C_v. The entropy S and the constant–volume heat capacity C_v show the expected pattern in their temperature variation. C_v obeys Dulong–Petit law at very high temperatures and Debye–T^3 law at very low temperatures.
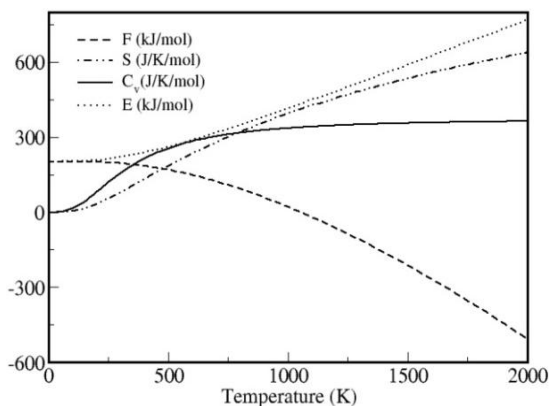
Fig.3.26: Thermal properties of
$B_{11}C^p$(CBC)
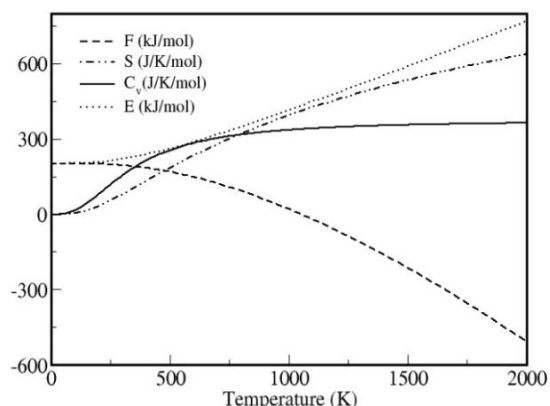
Fig.3.27: Thermal properties of
$B_{11}C^e$(CBC)
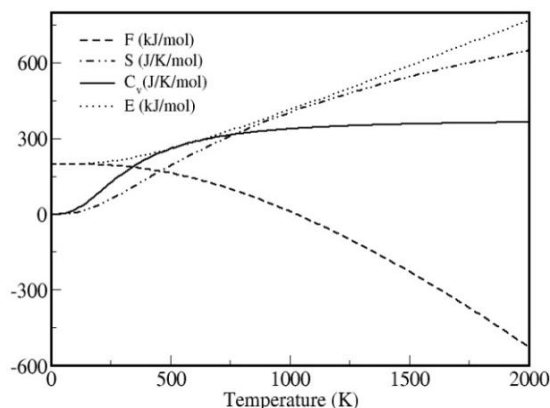
Fig.3.28: Thermal properties of
14-atom cage
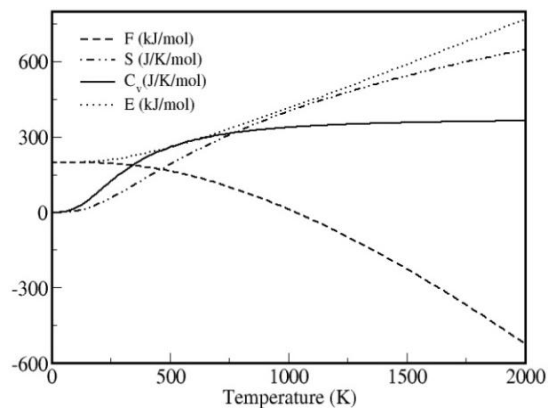
Fig.3.29: Thermal properties of
$B_{10}C^{pe}_2$(CBB)
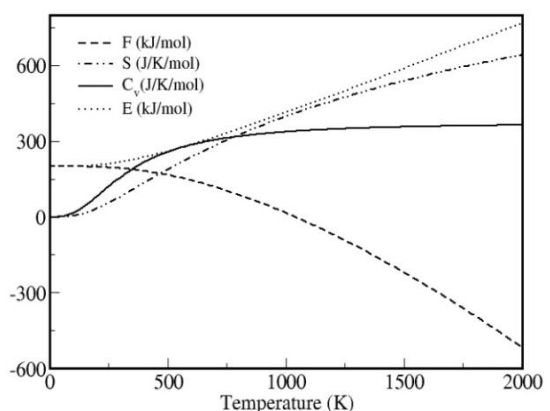
Fig.3.30: Thermal properties of
$B_{11}C^e$(BCC)
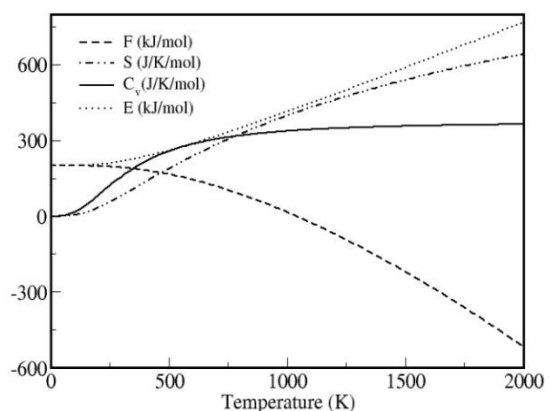
Fig.3.31: Thermal properties of
$(B_{11}C^p)(B_{10}C^{pe}_2)$(CBC)(CBB)

57

3.3. SUMMARY

Exhaustive structure search based on evolutionary algorithm is carried out for Boron Carbides in $B_{12}C_3$ stoichiometry. Six unique structures are obtained whose energies are accessible in the normal synthesis conditions of Boron Carbides. The structure obtained with lowest energy is $B_{11}C^p$(CBC), which has been widely reported in experimental and theoretical studies. Some new structures like 14-atom-cage have also emerged in the structure search. Five structures have base-centered monoclinic symmetry and the structure with 30-ato unit cell has triclinic symmetry. Three of these structures have negative formation energies. One such structure is $(B_{11}C^p)(B_{10}C^{pe}_2)$(CBC)(CBB) consisting of 30 atoms, indicating that structures with larger unit cells can be part of $B_{12}C_3$ composition. For each of these six systems the matrix of elastic stiffness constants has only positive eigenvalues, confirming that these systems have mechanical stability. The calculated elastic moduli are in excellent agreement with the experimentally measured values. The high value of Bulk modulus (~ 250 GPa) indicates high hardness for these systems and the B/G ratio shows that all of them are brittle. As all the phonon modes of each of these systems have real frequencies for all the wave vectors, these systems are dynamically stable. The electronic structures of these systems show that they are semiconductors. There is a significant reduction in the band gap when the structure does not contain the (CBC) chain. The computed IR spectra of the systems are compared against experimental spectrum. For four of the systems whose individual spectra exhibit maximum correspondence with the experimental spectrum a curve fitting of the cumulative spectrum is done. The relative weighting factors of the contribution of different systems imply that the presence of $B_{11}C^p$(CBC) in the ground state composition could mostly be through structures of larger unit cells. Two semi-empirical models, one based on bond strength and the other on elastic moduli, are used to estimate the hardness of these Boron Carbide systems. In the case of the model based on bond strength there is excellent agreement between the calculated and experimental values of hardness. For the four structures with chain the hardness values are close to the superhard regime (> 40

GPa). The variation of thermodynamic properties with temperature is deduced from the phonon data and it is found to be identical for the six systems.

Chapter 4

GROUND STATE STRUCTURE AND PROPERTIES OF $B_{13}C_2$

4.1. INTRODUCTION

$B_{13}C_2$ stoichiometry of Boron Carbide has been plagued by the lack of consensus on the ground state structure as well as the contradictory results of its metallic nature predicted by the DFT calculations and the semiconducting nature recorded by the experiments. Since the computation of the electronic structure of any system depends on its crystal structure, these two problems are invariably connected. The present work tries to address these two problems in $B_{13}C_2$ stoichiometry. The work done in $B_{12}C_3$ stoichiometry using larger unit cells has indicated that structures with larger unit cells could be the key to solving these twin problems. The structure search employing evolutionary algorithm and density functional theory under local density approximation is performed in $B_{13}C_2$ stoichiometry using 30-atom unit cells to investigate the possible crystal structures. A unique 30-atom unit cell has emerged as the lowest energy structure in the structure search. Its mechanical stability is investigated by DFT based calculation of the elastic constants and dynamical stability by the DFPT based calculation of the phonon dispersions. Once it is established that the structure is mechanically and dynamically stable, its electronic structure is generated. Born effective charges (BEC) are calculated using DFPT and using the BEC tensor and the phonon data, IR spectrum is generated and contrasted with the experimental measurement. Two semi-empirical hardness models, one based on bond strength and the other on elastic constants, are employed in this work for the estimation of hardness of the $B_{13}C_2$ system. Within the harmonic approximation, thermal properties over a range of temperatures are calculated from the phonon data. With the exhaustive structure search and the calculation of a range

of properties this work aims to solve the fundamental problems related to the crystal structure and electronic structure of $B_{13}C_2$.

4.2. RESULTS AND DISCUSSION

4.2.1. Structure

At first different trials of the structure search have been done using the 15-atom unit cells of $B_{13}C_2$. In these trials the USPEX input cells consisting of 13 boron atoms and 2 carbon atoms are used. None of the lowest energy structures obtained has exhibited dynamical stability. At the next stage the seeded structure search using 30-atom unit cells of $B_{13}C_2$ is performed. The different combinations of 15-atom unit cells are given as seeds, including some configurationally disordered variants, by maintaining the stoichiometry. The previous experience with the seeded structure search performed on the 30-atom unit cells of $B_{12}C_3$ has shown that the final structures that emerge out of the structure search can be distinctly different from the seeds provided. The sole purpose of the seeding is to perform a guided structure search where the search is confined to certain regions of the energy landscape that have potential for hosting the lowest energy structures. This also ensures computational economy. In the second stage we have used USPEX input cells of 26 boron atoms and 4 carbon atoms. The number of generations is fixed as 50 and both *populationSize* and *initialPopSize* are chosen as 60.

The lowest energy structure obtained is composed of B_{12} and $B_{11}C^p$ icosahedral units, CBC chain, and one carbon and two boron atoms as interstitial atoms that serve as the links connecting different icosahedra. The structure is shown in figures 4.1 and 4.2. From figure 4.2, using the topographical marker scheme described in section 1.1, the polar and equatorial atoms of the $(B_{11}C^p)$ cage (panel (a)) and B_{12} cage (panel (b)) can be identified. A scheme of $(B_{12})(B_{11}C^p)(CBC)$-C-B-B is used to label this structure, the atoms within the brackets representing single units and the three atoms outside the brackets as three separate units, with no chain between them. The 30-atom primitive cell has triclinic symmetry, but the 60-atom Bravais cell formed from the primitive cell has base-centered monoclinic symmetry Cm. The Bravais cell is further relaxed using a plane
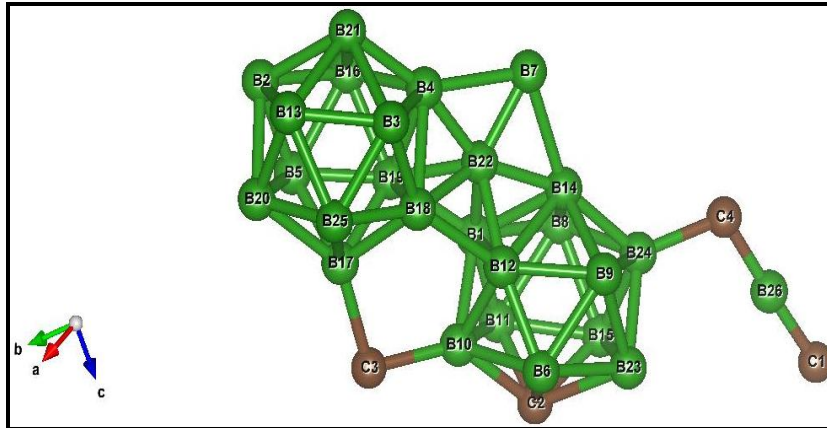
Fig.4.1: The structure of $(B_{12})(B_{11}C^p)(CBC)$-C-B-B
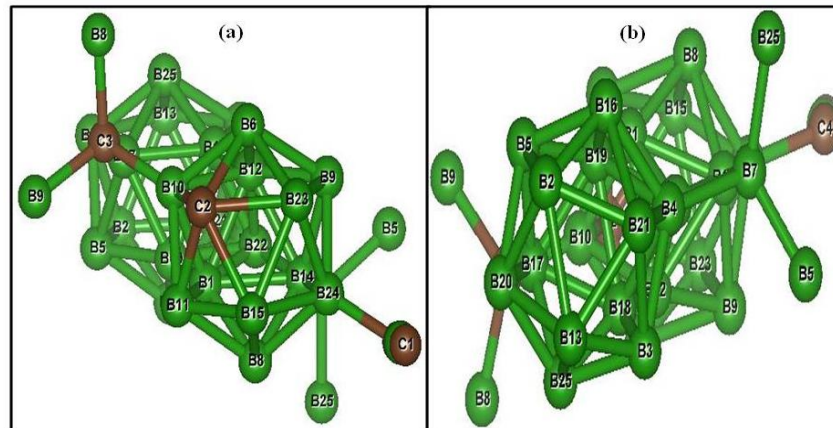
Fig.4.2: Two projections on a plane perpendicular to the chain

wave energy cutoff of 900 eV and a Gamma centered finer k-grid of 3x6x4. The lattice parameters of the primitive cell and energy values are presented in table 4.1. The atomic positions of the 60-atom Bravais cell having Cm symmetry, with the atoms occupying 4b sites and 2a sites, are given in table A II.3 in Appendix II. The total energy reported here is the negative of the cohesive energy. The total energy is negative for this system, implying energetically stable nature. To determine the thermodynamical stability of the system its formation energy value is calculated with reference to Alpha-boron and Graphite, which are the ground states of elemental boron and carbon, respectively. Convergence of k-grid is done for both Alpha-boron and Graphite using plane wave energy cutoff of 900 eV and the structures are fully relaxed. For Alpha-boron, using a k-

grid of 6x6x6, a total energy/atom of -7.4723 eV is obtained. For Graphite, using a k-grid of 19x19x7, a total energy/atom of -10.1263 eV is obtained. The formation energy E_f is calculated as :

$$E_f = \text{Total energy of } B_{13}C_2 - 13 \times \text{Total energy per atom of Alpha-Boron}$$
$$- 2 \times \text{Total energy per atom of Graphite} \qquad (4.1)$$

Table 4.1: Structural data of $(B_{12})(B_{11}C^p)(CBC)$-C-B-B.
Lengths are in Å and angles are in degrees.

a = b	c	α = β	γ	Total energy/f.u. (eV)	Formation energy/atom (meV)
5.61357	8.11073	83.70	60.25	-117.1007	19.45

Saal *et al.* (2007) using DFT-GGA has reported -81 meV/atom and 45 meV/atom for the formation energies of $B_{12}(CBC)$ and $B_{11}C(CBB)$ respectively, with reference to Alpha-born and Graphite. The formation energy of the structure with larger unit cell obtained here is in between the two. Though it is positive the formation energy per atom corresponds to a temperature of only 233 K, which means that the system can be formed under the normal synthesis conditions of Boron Carbides.
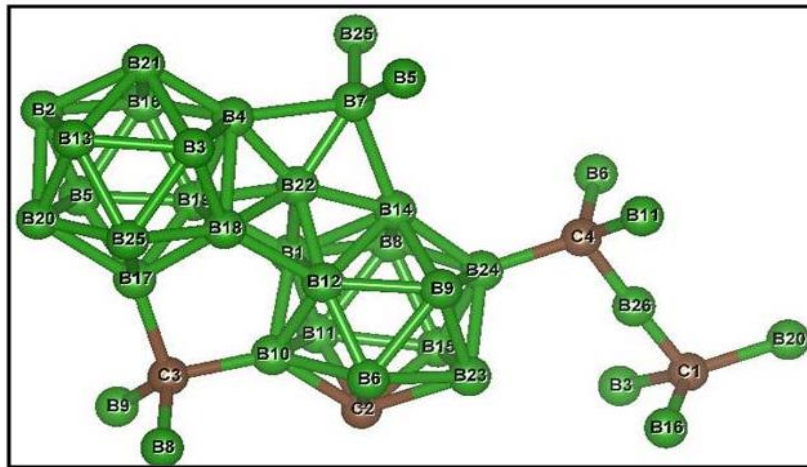
Fig.4.3: The structure of $(B_{12})(B_{11}C^p)(CBC)$-C-B-B with additional atoms belonging to other unit cells (as specified by the repeated numerals) to indicate the bonding pattern of chain-end and interstitial atoms.

There are 88 bonds in the 30-atom unit cell of $(B_{12})(B_{11}C^p)(CBC)$-C-B-B. Each icosahedron has 30 bonds as described in chapter 3 in the case of $B_{12}C_3$ systems. The CBC chain and the three interstitial atoms form different bonds between B_{12} cage and $B_{11}C^p$ cage as shown in fig.4.3. One end of the CBC chain (C1 in fig.4.3) is bonded to three different B_{12} cages (B3, B16 and B20 atoms) and the other end (C4 in fig.4.3) is bonded to three different $B_{11}C^p$ cages (B6, B11 and B24 atoms), forming 6 chain-icosahedron bonds. The interstitial atoms B7 and C3 have complementary bonding pattern between the two types of icosahedra. B7 is bonded to three different B_{12} cages (B4, B5 and B25 atoms; all equatorial) and one $B_{11}C^p$ cage (B14 atom; polar), as shown in fig.4.3. C3 is bonded to three different $B_{11}C^p$ cages (B8, B9 and B10 atoms; all equatorial) and one B_{12} cage (B17 atom; polar). B22 forms a mesh between B_{12} and $B_{11}C^p$ cages. It is bonded to the three atoms in a polar cap of a $B_{11}C^p$ cage (B1, B12 and B14 atoms) and to three atoms in a B_{12} cage (B18 and B19 are polar; B4 is equatorial). In addition to these 14 interstitial-icosahedron bonds, B7 and B22 are bonded to each other, making a total of 15 bonds involving interstitial atoms. There are 5 intericosahedron direct bonds between B_{12} and $B_{11}C^p$ cages (B2-B23, B13-B15, B18-B12, B19-B1 and B21-C2). Considering the two intrachain bonds the total number of bonds in the unit cell adds up to 88. The average bond lengths are given in table 4.2 in the generally increasing order with the experimental values given in square brackets. A classification scheme based on the lengths of the bonds is adopted here, with the type of the bond indicated by a superscript in brackets. The difference between the bonds in the $B_{12}C_3$ systems (table 3.2) is that equatorial hexagon bonds are, on the average, longer than polar-equatorial bonds. The intrachain bond length is almost the same for $B_{11}C^p$(CBC) system of $B_{12}C_3$ stoichiometry (table 3.2) and the system obtained here for $B_{13}C_2$ stoichiometry. The bond lengths are in fair agreement with the experimental data from X-ray diffraction and neutron diffraction.

Table 4.2: Average bond lengths in Å in $(B_{12})(B_{11}C^p)(CBC)$-C-B-B.

Type of Bond			B-B	B-C
intrachain		$b^{(1)}$		1.42412 [1.431[i], 1.436[ii]]
chain-icosahedron		$b^{(2)}$		1.60482 [1.617[i], 1.610[ii]]
interstitial (B22)-icosahedron		$b^{(3)}$	1.62391	
interstitial (C3)- icosahedron		$b^{(4)}$		1.63848
interstitial (B7)-icosahedron		$b^{(5)}$	1.76531	
intericosahedron		$b^{(6)}$	1.77516 [1.735[i], 1.721[ii]]	1.61909
polar-equatorial	B_{12} cage	$b^{(7a)}$	1.78746 [1.793[i], 1.795[ii]]	
	$B_{11}C^p$ cage	$b^{(7b)}$	1.76752	1.72658
equatorial hexagon	B_{12} cage	$b^{(8a)}$	1.75615 [1.773[i], 1.767[ii]]	
	$B_{11}C^p$ cage	$b^{(8b)}$	1.81632	
polar triangle	B_{12} cage	$b^{(9a)}$	1.81050 [1.824[i], 1.814[ii]]	
	$B_{11}C^p$ cage	$b^{(9b)}$	1.84846	1.82788

[i]Kirfel *et al*., 1979 (XRD)   [ii]Morosin *et al*.,1986 (Neutron Diffraction)

4.2.2. Elastic Constants

In order to analyze the mechanical stability of $(B_{12})(B_{11}C^p)(CBC)$-C-B-B its elastic stiffness constants C_{ij} at the equilibrium lattice parameters are computed from the change in energy caused by small specific elastic strains applied to the to the equilibrium unit cell. As the 30-atom cell has only triclinic symmetry it has 21 independent elastic constants. From the independent elastic constants of the system, bulk modulus (B) and shear modulus (G) are calculated using the standard formulae for triclinic lattice (Eqns.(2.49)–(2.50) and (2.60)–(2.61)) in Voigt and Reuss approximation schemes and Hill approximation gives the average of the two. The elastic constants and the average values of B, G, Young's modulus (Y) (in GPa) and Poisson's ratio ν are tabulated in table 4.3 with the experimental data from other works given in square brackets. The computed elastic moduli of this structure are in excellent agreement with the experimental data. The values of elastic moduli are found to decrease from $B_{12}C_3$ stoichiometry to $B_{13}C_2$ stoichiometry (tables 3.4 and 4.3) in accordance with

Table 4.3: Elastic Properties of $(B_{12})(B_{11}C^p)(CBC)$-C-B-B.

Elastic Constants and Elastic Moduli (in GPa)						
C11	495.651	C23	63.720	C36	12.465	B	223.21 [231[i]]
C12	104.320	C24	4.642	C44	152.812	G	186.73 [189[i]]
C13	77.991	C25	-9.372	C45	19.604	Y	438.04 [446[i]]
C14	-7.798	C26	16.513	C46	6.626	ν	0.1729 [0.18[i]]
C15	3.932	C33	549.160	C55	175.254	B/G	1.195
C16	-3.594	C34	-20.596	C56	1.479		
C22	480.862	C35	-35.523	C66	180.158		

[i]Gieske *et al*., 1991(Expt.)

the experimental measurements (Gieske *et al*., 1991). For mechanical stability the elastic energy should always be positive. This is equivalent to the Born stability criterion that all the eigenvalues of the matrix **C** of elastic stiffness constants should be positive. This stability condition has been verified for the matrix of elastic constants and this shows that $(B_{12})(B_{11}C^p)(CBC)$-C-B-B is mechanically stable. The calculated value of B/G ratio for this systems is smaller than 1.75, the critical value to separate brittleness and ductility, according to Pugh's criterion. This indicates that the system is brittle.

4.2.3. Phonons

In order to determine the dynamical stability of $(B_{12})(B_{11}C^p)(CBC)$-C-B-B its phonon modes of are calculated using the self consistent DFPT method and with 1x2x1 supercells (120 atoms) of Bravais cell. PHONOPY code is used for the post-processing. The ACONVASP online utility (Setyawan and Curtarolo, 2010) is used for selecting the high symmetry points in the Brillouin zone for each system. The phonon dispersion curves and density of states (DOS) are presented in figure 4.4. The DOS values are normalized to primitive unit cell. A system is dynamically stable only if all the phonon modes of the system have positive frequencies for all the wave vectors. The absence of imaginary frequencies at all wave vectors confirms that this system is dynamically stable.
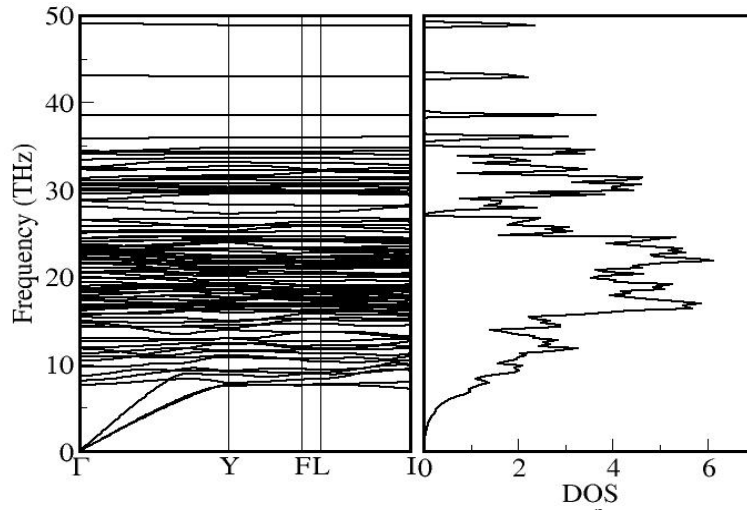
Fig.4.4: Phonon bands and dos of $(B_{12})(B_{11}C^p)(CBC)$-C-B-B.

4.2.4. Electronic Structure

The electronic energy bands along the high symmetry directions of the Brillouin zone and the partial density of states of $(B_{12})(B_{11}C^p)(CBC)$-C-B-B are presented in figure 4.5. The Fermi level is set to 0 eV.
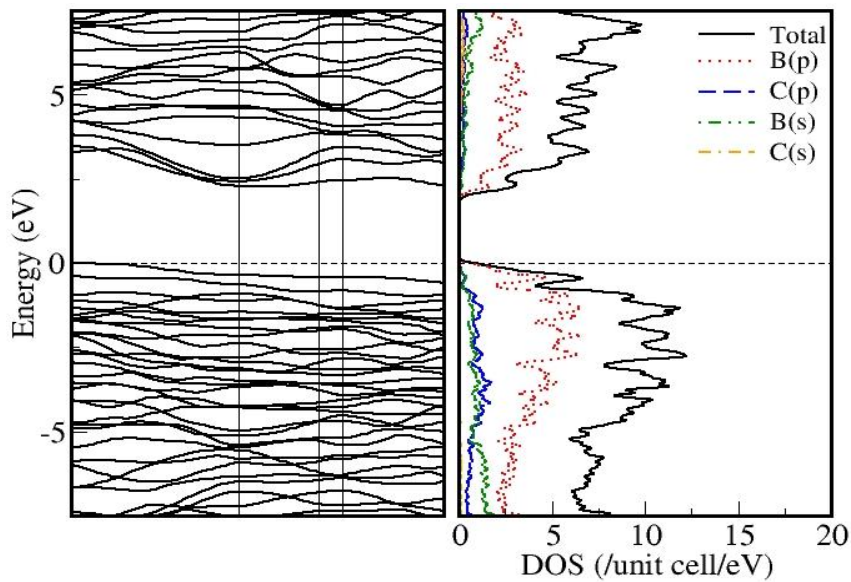
Fig.4.5: Electronic bands and dos of $(B_{12})(B_{11}C^p)(CBC)$-C-B-B.

The system is a semiconductor, as there is a clear separation between valence band and conduction band with no overlaps over the Fermi level. The indirect band gap is 1.964eV. The predominant contribution to the density of states is from B(p) orbital. But, unlike in the case of $B_{12}C_3$ systems, the contribution of B(s) orbital is slightly greater than that of C(p) nearer to the Fermi level. The result of a semiconducting system with larger unit cell is similar to the one reported by Ektarawong *et al.* (2015) for the supercell of $B_{12}(CBC)$ + $B_{11}C^e(BBC)$. Using GGA-PBE96 functional they have got a band gap of 1.36 eV and using MBJ-GGA functional, a value of 2.09 eV. But, there are two significant differences between the two results. Firstly, the supercell structure they have proposed can be formed only at higher temperatures due to substitutional disorder among the ordered unit cells of $B_{12}(CBC)$; it is not a ground state structure to be formed at the normal synthesis conditions of $B_{13}C_2$. The structure proposed here, on the other hand, can be thermodynamically stable at around 233 K. Secondly, there are both CBC and BBC chains in their supercell structure whereas in the structure proposed in this work there are only CBC chains. It must be emphasized that the comparisons between the bond lengths from DFT calculations and the experimental data have consistently supported $B_{12}(CBC)$ structure over $B_{11}C(BBC)$ structure (Bylander and Kleinman, 1991; Saal *et al.*, 2007; Vast *et al.*, 2009) as the experimental data have not given any conclusive evidence for (BBC) chains in $B_{13}C_2$ stoichiometry. In the same work Ektarawong *et al.* (2015) have reported that according to their calculations using MBJ-GGA functional a supercell of $B_{12}(CBC)$ + $(B_{11}C^p)CBB$ is also semiconducting, with a band gap of 1.8 eV. The structural unit proposed in our work is distinctly different from this latter supercell in their work in the absence of the (CBB) chain and in the way the two icosahedra are bonded through CBC chain and interstitial atoms. However the closeness of the two band gap values suggests an independent validation of our approach.

The experimental data on the exact band gap in $B_{13}C_2$ stoichiometry widely vary. But the dc conductivity measurements over the entire homogeneity range of Boron Carbide (Werheit and de Groot, 1980; Wood and Emin, 1984; Samara *et al.*, 1993; Schmechel and Werheit, 1997) clearly record that the conductivity is maximum at 13.3

at.% C. This means that the band gap of $B_{13}C_2$ must be smaller than that in $B_{12}C_3$. For $B_{11}C^p$(CBC) system of $B_{12}C_3$ stoichiometry our DFT calculations have estimated a band gap of 2.885 eV which is in fair agreement with other DFT calculations (table 3.5). Werheit *et al.* (1991) and Werheit (2006) have experimentally estimated a band gap of 2.09 eV for $B_{12}C_3$. These results clearly show that the band gap calculated in this work for the $B_{13}C_2$ system corresponds to the experimental data. Here we have conclusively demonstrated that the given 30-atom structure with larger unit cell can solve the long standing problem of the discrepancy between the DFT models and the experimental observations over the semiconducting nature of $B_{13}C_2$.

4.2.5. Infrared Spectrum

The Born effective charges of $(B_{12})(B_{11}C^p)$(CBC)-C-B-B are computed using DFPT (Eq.(2.76)) and infrared spectrum is generated using BEC tensors and phonon polarization (Eq.(2.77)). The computed spectrum is compared with the experimental measurement by Werheit *et al.* (1999) on $^{11}B_{6.5}C$ sample in figure 4.6. The frequencies of the main peaks are given in table 4.4. The experimental values of frequencies are from Werheit *et al.* (1999). A broadening of 15 cm^{-1} is applied to the computed peaks. The background is not accounted for and no fitting is done.
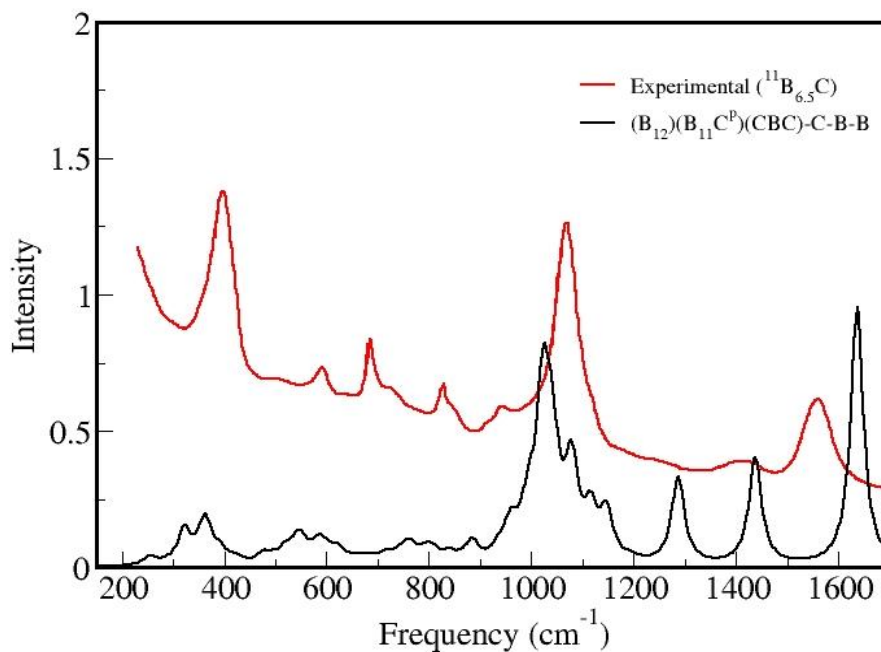
Fig.4.6: IR spectrum of $(B_{12})(B_{11}C^p)(CBC)$-C-B-B.

Table 4.4: Frequencies (in cm^{-1}) of the major peaks in the IR spectra of $(B_{12})(B_{11}C^p)(CBC)$-C-B-B.

Experimental Values	Calculated Values
1558	1636.50
1411	1437.55
1074	1025.98
947	961.72
834	884.37
739[*]	803.67
692	760.69
600	585.74
508[*]	475.92
407	362.90

The starred values are the frequencies corresponding to small humps appearing in the experimental spectrum. The computed peak at 1286.90 cm^{-1} is not present in the measured spectrum. In all other major features the computed IR spectrum is in agreement

with the experimental spectrum. This implies that $(B_{12})(B_{11}C^p)(CBC)$-C-B-B is a good structural candidate for $B_{13}C_2$ stoichiometry.

4.2.6. Hardness

The hardness model based on bond strength, described in detail in section 2.3.9, is used here to estimate the hardness of $(B_{12})(B_{11}C^p)(CBC)$-C-B-B. Compared to the $B_{12}C_3$ systems discussed in chapter 3, $(B_{12})(B_{11}C^p)(CBC)$-C-B-B has more types of bonds with varying bond lengths as listed in table 4.2. The bond length further varies for B-B and B-C bonds. The labeling scheme used to represent a bond is the same as discussed in section 3.2.6, with only one variation. As the three types of intraicosahedral bonds differ in bond lengths between B_{12} and $B_{11}C^p$ cages, an additional superscript is used to distinguish between them, with superscript 'a' for B_{12} cage and 'b' for $B_{11}C^p$ cage. The numeral assigned to each type of bond differs between $B_{12}C_3$ systems and the $B_{13}C_2$ system because of the increase in the number of bonds and the variation in bond lengths. In the labeling scheme adopted here $b_{11}^{(7a)}$ represents polar-equatorial B-B bond in B_{12} cage, $b_{12}^{(9b)}$ represents polar triangle B-C bond in $B_{11}C^p$ cage, and so on. There are 15 bonds of the type $b_{ij}^{(\alpha)}$ listed in table 4.2. Each of them has a distinct bond strength and hence its contribution should be considered separately while determining the hardness. All the 88 bonds in $(B_{12})(B_{11}C^p)(CBC)$-C-B-B are classified according to this scheme and their calculated bond strengths are listed in table A III.2. The grouping of the bonds for the purpose of counting are as discussed in section 3.2.6. All the average bond lengths are taken from table 4.2. The calculated hardness from the model based on bond strength (H_b) is given in table 4.5. Hardness of $(B_{12})(B_{11}C^p)(CBC)$-C-B-B is also estimated using

Table 4.5: Hardness values of $(B_{12})(B_{11}C^p)(CBC)$-C-B-B

H_b	H_P	Experimental values
33.76	30.46	HV = 43.8[i], 45[ii]

[i]Werheit *et al.*, 1999   [ii]Amberger and Stumpf, 1981

Chen's model based on elastic constants and Pugh's ratio and the value (H_P) is given in table 4.5. The experimental reports of the hardness of $B_{13}C_2$ are also given. The calculated values are less than the experimental values though both are of the same order. Instead of taking merely the average bond lengths if all the variations within the same types of bonds are taken into account and the contributions of these deviant bonds are separately evaluated, the model based on bond strength can give an improved estimate of the hardness.

4.2.7. Thermodynamic Properties

From the phonon data, within the harmonic approximation, thermal properties due to phonons, such as internal energy (E), constant-volume heat capacity (C_v), Helmholtz free energy (F) and entropy (S) are evaluated over a range of temperatures (Eqns.(2.69)-(2.73)). The variations of these quantities with temperature are plotted in figure 4.7. The values are normalized to the primitive unit cell.
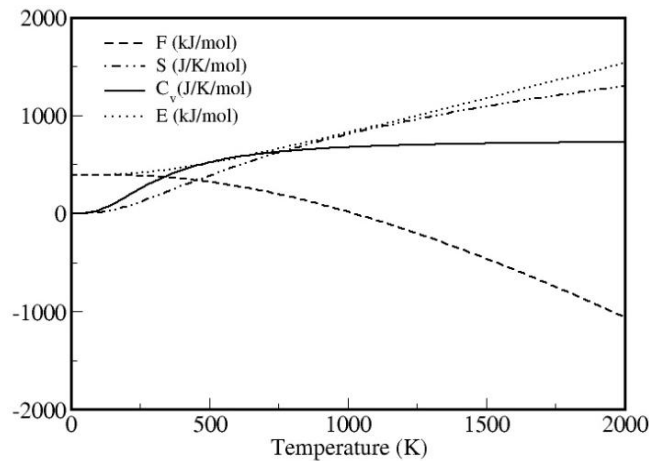
Fig.4.7: Thermal properties of $(B_{12})(B_{11}C^p)(CBC)$-C-B-B.

The entropy S and the constant–volume heat capacity C_v show the expected pattern in their temperature variation. C_v obeys Dulong–Petit law at very high temperatures and Debye–T^3 law at very low temperatures.

4.3. SUMMARY

Exhaustive structure search based on evolutionary algorithm and density functional theory is carried out for the Boron Carbide in $B_{13}C_2$ stoichiometry using 30-atom unit cells. A structure consisting of B_{12} cage, $B_{11}C^p$ cage, CBC chain and three interstitial atoms emerges as the lowest energy structure. The formation energy of $(B_{12})(B_{11}C^p)(CBC)$-C-B-B is 19.45 meV/atom which is accessible within the synthesis conditions of $B_{13}C_2$. The 30-atom cell has triclinic symmetry, but its 60-atom Bravais cell exhibits base-centered monoclinic symmetry. The bond lengths of the system are in good agreement with the results from X-ray diffraction and neutron diffraction measurements. The matrix of elastic constants of the system has only positive eigenvalues, confirming mechanical stability of the system. The computed elastic moduli are in excellent agreement with the experimental measurements. The phonon dispersions have no imaginary frequencies, establishing the dynamical stability. The electronic bands and dos exhibit a clearly defined indirect band gap of 1.964 eV, solving the problem of the discrepancy between the DFT calculations and the experimental observations over the semiconducting nature of $B_{13}C_2$. The computed band gap is in accordance with the trends in the measurements of dc conductivity of Boron Carbide over its entire homogeneity range and the optical measurements of band gap. The IR spectrum generated from BEC tensor and phonon polarizations corresponds to the experimental spectrum in all the major features. A hardness of 33.76 GPa is estimated for this system using the semi-empirical model based on bond strength and the value is of the same order of the experimental measurements.

Chapter 5

GROUND STATE STRUCTURE AND PROPERTIES OF
RUTHENIUM CARBIDES

5.1. INTRODUCTION

The first experimental synthesis of Ruthenium Carbide has reported hexagonal structure ($P\bar{6}m2$) in RuC stoichiometry. Most of the computational works in this stoichiometry have been focusing on zinc blende structure whereas the only structure search performed in this stoichiometry has yielded neither zinc blende structure nor hexagonal structure, but only rhombohedral structure. In Ru_2C stoichiometry also the only structure search carried out has not addressed the absence of the reported hexagonal structure ($P\bar{3}m1$) from the experimental synthesis of Ruthenium Carbide in this stoichiometry. The two experimental reports indicate high pressure and/or high temperature for the synthesis of Ruthenium Carbide and hence a proper knowledge of its ground state structure and properties would be necessary for planning the optimum utilization of the experimental resources. The present work aims to address the problem of the ground state structure of Ruthenium Carbides. In this work an exhaustive structure search of Ruthenium Carbides has been undertaken using evolutionary algorithm with no assumptions about the possible outcomes. We have investigated the possible structures of three stoichiometries, RuC, Ru_2C and Ru_3C. The mechanical stability is analyzed through the computation of elastic constants and the dynamical stability through the phonon spectra for the five distinct Ruthenium Carbide systems yielded by this structure search. For the three dynamically stable systems electronic band structure, hardness and thermodynamic properties are also computed. Infrared spectrum is generated for the semiconducting system as a convenient signature for experimental verification.

5.2. RESULTS AND DISCUSSION

5.2.1. Structures

The optimal tuning of the various input variables in USPEX has been achieved by accurately reproducing known structures of simple systems like Cu, NaCl etc. and then more complex structures of perovskites like $BaTiO_3$ and $SrTiO_3$. Having completed the structure search for Boron Carbides, the study of the structures of Ruthenium Carbides is attempted, starting with the simplest stoichiometry RuC. DFT as implemented in VASP is used in combination with USPEX for the structure relaxation and energy calculation required in the structure search. The Perdew–Burke–Ernzerhof (PBE) generalized gradient approximation (GGA) to the exchange–correlation functional is used here. Projector augmented wave (PAW) pseudopotentials as supplied with VASP are used, with 4p, 4d and 5s as the valence states for Ru, and 2s and 2p for C. The number of atoms in the input cell in USPEX is systematically increased in each trial from 2 to 8 with the expectation that the evolutionary mechanism involving more atoms will result in the emergence of structures of increasing complexity. In each case the number of generations is fixed as 25. The default choice for the population per generation in USPEX is twice the number of atoms per input cell, rounded to closest multiple of 10. For the choices of 2 atoms per USPEX input cell (one Ru atom and one C atom) and 4 atoms per input cell (two Ru atoms and two C atoms) the variable *populationSize* is taken as 12. As the number of atoms in the input cell is raised in subsequent trials, *populationSize* is also increased to 24. For RuC stoichiometry, for 2 atoms per USPEX input cell, zinc blende structure ($F\bar{4}3m$) is obtained as the fittest structure. For 4 atoms per input cell, rhombohedral structure ($R\bar{3}m$) and for 8 atoms per input cell, trigonal structure ($P\bar{3}m1$) emerge as two additional fittest structures for RuC stoichiometry. Trigonal systems (space group : 143–167) can be of P-centered types and R-centered types. Following the convention in the literature, the two R-centered trigonal structures obtained here are named with the tag "rhombohedral" and the P-centered one, with "trigonal". Cartesian components of the conventional lattice vectors are specified identically for P-centered trigonal systems and hexagonal systems : (a, 0, 0), (-a/2, √3a/2, 0), (0, 0, c) while they are

different for R-centered trigonal (rhombohedral) systems : (ã, -ã/√3, h), (0, 2ã/√3, h), (-ã, -ã/√3, h). Trials with up to 10 atoms per input cell are attempted, but, beyond 8 atoms per input cell, an increase in the number of atoms per input cell yields as fittest structures only those that have previously emerged with lower number of atoms per input cell. The procedure is repeated for the stoichiometries Ru_2C and Ru_3C. Only the rhombohedral structure $(R3m)$ emerges as the fittest structure for Ru_2C stoichiometry and only the hexagonal structure $(P\bar{6}m2)$ for Ru_3C stoichiometry.

Each structure is further relaxed using an ENCUT of 900 eV, which is 2.25 times the default value as per the POTCAR files of Ru and C, and the improved k-grid. The structures are tabulated in table 5.1 along with their lattice parameters and formation energies. Lattice parameter of RuC-Zinc blende structure from other computational works is given in brackets. VASP gives total energy with respect to the free atom energy and its value is negative for these five structures, implying energetically stable nature. However, thermodynamical stability has to be determined with respect to the formation energy. If it is negative, it means that the system can be spontaneously formed from its constituent elements. The formation energies of these Ruthenium Carbide systems are calculated with reference to crystalline Ruthenium and Graphite. To get the total energy per atom of Ruthenium and Graphite, convergence of k–grid is done for both using ENCUT of 900 eV and the structures are fully relaxed. For Ruthenium, using a k–grid of 31x31x20, a total energy/atom of -9.2751 eV is obtained. For Graphite, using a k–grid of 19x19x7, a total energy/atom of -9.2320 eV is obtained. For a structure with unit cell stoichiometry of Ru_aC_b, the formation energy E_f is calculated by the following formula :

$$E_f = Total\ energy\ of\ Ru_aC_b - a \times Total\ energy\ per\ atom\ of\ Ru\ in\ its\ stable\ form$$
$$- b \times Total\ energy\ per\ atom\ of\ Graphite \qquad (5.1)$$

For RuC stoichiometry, different structures have been computationally modeled in previous studies (Abidri *et al.*, 2010; E. Zhao *et al.*, 2010; Z. Zhao *et al.*, 2010; H.R. Soni *et al.*, 2011). The present structure search has yielded zinc blende structure, considered in these previous works, thus confirming its status as a stable structure of this stoichiometry. The lattice parameter obtained for zinc blende structure in the present work is in very

good agreement with the values from the previous studies (table 5.1). It must be emphasized that no exhaustive structure search was employed in these earlier studies (Abidri *et al*., 2010; E. Zhao *et al*., 2010; Z. Zhao *et al*., 2010; H.R. Soni *et al*., 2011), only certain specific structures were proposed and their properties calculated.

<div align="center">Table 5.1: Structural Data of Ruthenium Carbides.</div>

Stoichio-metry	Structure (space group)	k-grid	Lattice parameters (lengths in Å)	Atomic positions	Formation energy/ f.u. (eV)
RuC	Zinc blende ($F\bar{4}3m$ /216)	9x9x9	a = 4.565 (4.566[a],4.59[b], 4.545[c],4.608[d])	Ru: 4a (0, 0, 0) C : 4d (3/4, 3/4, 3/4)	0.9127 (0.91[a])
RuC	Rhombohedral ($R\bar{3}m$ /166)	11x11x11	a = 6.499, α = 24.75°	Ru: 2c (z, z, z) (-z, -z, -z) z = 0.270863 C : 2c (z, z, z) (-z, -z, -z) z = 0.462960	0.7239
RuC	Trigonal ($P\bar{3}m1$ /164)	11x11x4	a = b = 2.774, c = 6.385	Ru: 2d (1/3,2/3,z)(2/3,1/3,-z) z = 0.191183 C : 2c (0, 0, z) (0, 0, -z) z = 0.390430	0.8009
Ru$_2$C	Rhombohedral ($R3m$ /160)	21x21x21	a = 5.302, α = 30.46°	Ru: 1a (z, z, z) z = 0.703773 Ru: 1a (z, z, z) z = 0.520810 C : 1a (z, z, z) z = 0.281030	1.0951
Ru$_3$C	Hexagonal ($P\bar{6}m2$ /187)	25x25x10	a = b = 2.783, c = 7.126	Ru:1a (0, 0, 0) Ru: 2i (2/3,1/3,z) (2/3,1/3,-z) z = 0.307465 C : 1b (0, 0, 1/2)	0.9265

[a]E. Zhao *et al*. 2010 (GGA)   [b]Abidri *et al*. 2010 (LDA)   [c]Z. Zhao *et al*. 2010 (GGA)
[d]H.R. Soni *et al*., 2011(GGA)

Using evolutionary algorithm based structure search, the present work has shown the emergence of, in addition to the previously proposed zinc blende structure, two other lower energy structures for RuC stoichiometry. Among the three structures of RuC stoichiometry, it is clear from the formation energy values (table 5.1) that rhombohedral structure is the most stable one, the next being trigonal and zinc blende structures, in that order of stability. Figure 5.1 presents the variation of energy with unit cell volume for

these three systems. The symbols represent the energy values from DFT calculation and the solid lines correspond to the fits with Murnaghan equation of state (Murnaghan, 1944). The values of energy and volume are normalized to formula units.
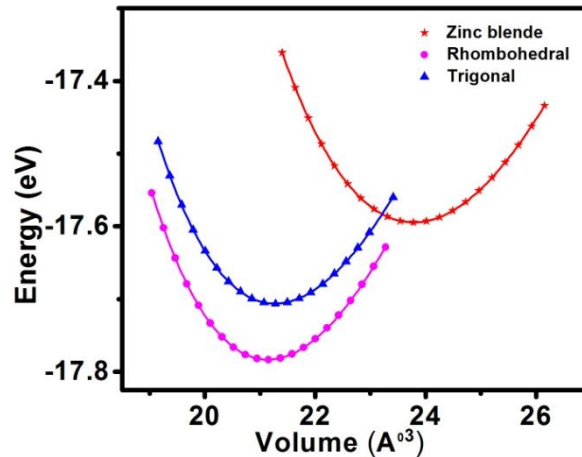
Fig. 5.1: Variation in energy with unit cell volume
for the three structures of RuC.

Figure 5.2 shows the variation of energy with pressure values calculated from the Murnaghan equation of state. The minimum of each of the energy–volume graphs in figure 5.1 corresponds to the zero pressure point of the respective energy–pressure graph in figure 5.2. Figure 5.3 shows the variation in enthalpy with pressure.
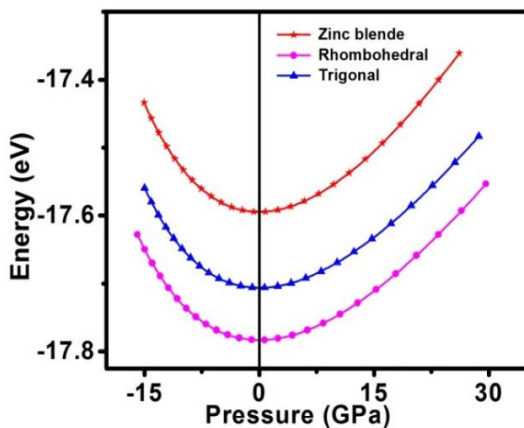
Fig. 5.2: Variation in energy with pressure
for the three structures of RuC.
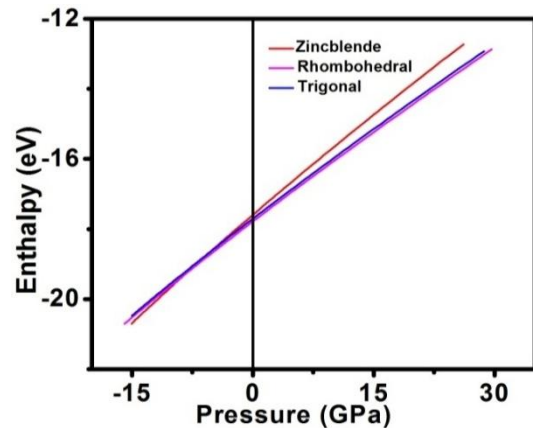
Fig.5.3: Variation in enthalpy with pressure
for the three structures of RuC.

Figures 5.1–5.3 further confirm that rhombohedral system is the most stable among these three as it has the minimum energy and enthalpy in the given volume and pressure range. The apparent transition of the trigonal system to zinc blende system at volumes well above the equilibrium volume corresponds to negative pressure on the trigonal unit cell and is not physically realizable. While this cross over in figure 5.1 takes place at negative pressure side for trigonal system it is at positive pressure side for zinc blende system and hence it is absent in the energy–pressure graphs in figure 5.2. In figure 5.3, for all positive pressure values, the rhombohedral system has the lowest enthalpy.

One previous study employing structure search by particle swarm optimization algorithm has reported the structure of $R\bar{3}m$ symmetry as the most stable one (Guang *et al*., 2012). Though it has been called hexagonal structure in that study, it is actually the hexagonal representation of rhombohedral structure with thrice the number of atoms in the unit cell. The lattice parameters of the hexagonal unit cell reported in this work are a_H = 2.785 Å and c_H = 18.886 Å. The relationship between the lattice parameters of the rhombohedral cell and the hexagonal supercell of the same structure are : $a_H = 2a_R \sin(\alpha/2)$ and $c_H = a_R\sqrt{3 + 6\cos\alpha}$. Using a_R and α values obtained for the Rhombohedral structure (table 5.1), we get a_H = 2.7856 Å and c_H = 18.891 Å, which are in excellent agreement with the values obtained by Guang *et al.* (2012). Thus, the present work independently confirms the previous report that rhombohedral structure ($R\bar{3}m$) is the lowest energy structure of RuC stoichiometry. While only the lowest energy structure of RuC stoichiometry has been reported in the previous work employing structure search (Guang *et al*., 2012), here three structures emerge within a narrow formation energy band for RuC stoichiometry and also structures of Ru_2C and Ru_3C stoichiometries are identified for the first time.

All the structures have positive formation energies that show that they are not thermodynamically stable, i.e. they cannot be spontaneously formed under ambient conditions. In order to synthesize them, sufficient energy should be supplied and possibly high temperature and pressure. The synthesis of Ruthenium Carbide (Kempter and Nadler, 1960; Kempter, 1964; Sanjay Kumar *et al*., 2012) under high pressure and high

temperature testifies to this result. Among the three structures of RuC stoichiometry, the rhombohedral structure has the minimum formation energy indicating that it is more likely to be formed during synthesis under suitable high energy conditions. The maximum difference in formation energy between the three structures is 94.4 meV/atom, corresponding to a temperature of 1133 K. This clearly shows that at the typical high temperatures (~2000 K) during the synthesis of Ruthenium Carbides, the formation of any of these three structures is possible for RuC stoichiometry at proper conditions. Though it is not possible to compare the formation energies between different stoichiometries it can be noted that the formation energy values of systems of Ru_2C and Ru_3C stoichiometries are close to those of RuC systems. The formation energies of these five systems lie within an energy band of width 225 meV/atom, corresponding to a temperature of 2700 K. This implies that the formation of Ru_2C and Ru_3C stoichiometries are also possible at high temperatures.

In the recent high pressure–high temperature synthesis of Ruthenium Carbides (Sanjay Kumar *et al*., 2012) it has been analyzed that the synthesized structure has the stoichiometry of Ru_2C with Fe_2N-type hexagonal ($P\bar{3}m1$) structure. In the present work, for Ru_2C stoichiometry only one fittest structure, rhombohedral, is obtained (table 5.1). The difference could be due to the fact that in the present work the structures are being determined in the ground state whereas the synthesis of Ruthenium Carbide has been carried out at high pressure and temperature. However, it is interesting to note that the trigonal structure obtained from the structure search done here in RuC stoichiometry is of the same space group as the structure deduced in this experiment. The inherent difficulties involved in the determination of stoichiometry and structure of the synthesised material in high pressure–high temperature experiments (Sanjay Kumar *et al*., 2012) suggest the possibility that the stoichiometry of the synthesised structure could be RuC. Similarly, in the first reported synthesis of Ruthenium Carbide (Kempter and Nadler, 1960; Kempter, 1964), the stoichiometry has been estimated as RuC and the structure as WC-type hexagonal ($P\bar{6}m2$). It has been proved in previous computational work (Z. Zhao *et al*., 2010) that this structure lacks dynamical stability in RuC

81

stoichiometry. Interestingly, the same structure emerges in the present structure search in Ru$_3$C stoichiometry and it is shown here (section 5.2.3.) that the structure is dynamically stable in this stoichiometry. It is significant that the present structure search has yielded the two reported structures from the synthesis of Ruthenium Carbides ($P\bar{6}m2$ and $P\bar{3}m1$) though in stoichiometries different from the reported ones. The reason for the mixing up of stoichiometries could be the possibility of any of these systems to be formed at the extreme experimental conditions of the synthesis. Therefore more detailed experimental analysis is required to carefully pinpoint both the stoichiometry and the structure. The results of an exhaustive structure search as in the present work provide possible candidate structures to be looked for in any synthesis at extreme conditions.

5.2.2. Elastic Constants

To study the mechanical stability of the Ruthenium Carbide systems, the elastic stiffness constants C_{ij} at the equilibrium lattice parameters are calculated. Then, using the equations (2.40)-(2.48) for elastic moduli for cubic, rhombohedral and hexagonal crystal classes the bulk moduli and rigidity moduli are calculated in Voigt and Reuss approximations and their average values are taken, according to Hill approximation. The elastic constants and the average values of B, G, Y (in GPa) and ν are tabulated in table 5.2. The data for zinc blende and rhombohedral systems of RuC stoichiometry, available from other computational works, are also tabulated for comparison. All the five systems obtained here satisfy the Born-Huang stability criteria (Born and Huang, 1956; Wallace, 1972; Nye, 1985; Mouhat and Coudert, 2014), given by Eqns.(2.37)-(2.39), and hence all of them are mechanically stable. Crystals in the rhombohedral class can be divided into two : Rhombohedral I with space groups 149 to 167 and Rhombohedral II with space groups 143 to 148. RuC–Rhombohedral and Ru$_2$C–Rhombohedral belong to the class Rhombohedral I (table 5.1) which has 6 independent elastic constants C_{11}, C_{12}, C_{13}, C_{14}, C_{33} and C_{44}. The other nonzero elastic constants in this class are $C_{24} = -C_{14}$, $C_{56} = C_{14}$ and $C_{66} = (C_{11}-C_{12})/2$. The pair of elastic constants (C_{24}, C_{14}) has to be of opposite sign for crystals belonging to the class Rhombohedral I. However, the mechanical stability of the

crystal depends on C^2_{14} and C^2_{13} which are positive. Hence negative sign of C_{14} (table 5.2) does not imply mechanical instability. The same situation arises for Rhombohedral II as well. It has 7 independent elastic constants C_{11}, C_{12}, C_{13}, C_{14}, C_{15}, C_{33} and C_{44}. The other nonzero elastic constants in this class are $C_{24} = -C_{14}$, $C_{25} = -C_{15}$, $C_{46} = -C_{15}$, $C_{56} = C_{14}$ and $C_{66} = (C_{11}-C_{12})/2$ (Mouhat and Coudert, 2014). The pair of elastic constants (C_{24}, C_{14}), (C_{25}, C_{15}) and (C_{46}, C_{15}) have to be of opposite sign for crystals belonging to the class Rhombohedral II. However, the mechanical stability of the crystal depends on C^2_{14} and C^2_{15} (Mouhat and Coudert, 2014) which are positive. Thus, for both the rhombohedral systems, some of the elastic constants have to be negative, but that would not violate mechanical stability provided the Born–Huang elastic stability criteria are satisfied.

Table 5.2: Elastic Properties of Ruthenium Carbides.

	RuC-Zinc blende		RuC-Rhombohedral		RuC-Trigonal	Ru$_2$C-Rhombohedral	Ru$_3$C-Hexagonal
	This work	**Other works**					
C_{11}	342.46	355[a], 373.1[b], 345.31[c]	522.51	(539[e])	529.34	546.37	547.47
C_{12}	220.93	221[a], 250.6[b], 216[c]	158.10	(152[e])	132.53	147.85	162.37
C_{13}			158.07	(178[e])	135.55	215.83	210.54
C_{14}			-38.99		23.95	3.14	
C_{33}			598.14	(581[e])	586.78	577.27	600.63
C_{44}	62.40	70[a], 58.1[b], 66.32[c]	138.37	(176[e])	86.88	120.42	121.37
B	261.44	266[a], 263[b], 259.11[c], 253[d]	287.45	(296[e])	272.21	313.23	316.99
G	61.74	69[a], 60.7[b], 65.65[c]	163.23	(186[e])	144.83	156.61	157.48
Y	171.70	190[a], 166.8[b]	411.75	(462[e])	369.05	402.71	405.32
N	0.391	0.38[a], 0.404[b]	0.261	(0.241[e])	0.274	0.286	0.287
B/G	4.24	3.95[c]	1.76	(1.59[e])	1.88	2.00	2.01

[a] E. Zhao *et al*. 2010 (GGA)   [b] Abidri *et al*. 2010 (LDA)   [c] Z. Zhao *et al*. 2010 (GGA)
[d] H.R. Soni *et al*. 2011 (GGA)   [e] Guang *et al.* 2012 (GGA)

Let's further consider the origin of the sign of C_{14} as far as the two Ruthenium Carbide systems belonging to the Rhombohedral I group are concerned. For any given system elastic constants are computed as linear combinations of force constants of the system, with the force constants depending upon the material as well as the specific

structure. The coefficients of these linear combinations depend, in addition, on the choice of the directions of the axes of the Cartesian reference frame. So the sign of C_{14} can depend on both the structure and the choice of the Cartesian reference frame. A System with rhombohedral symmetry can also be represented by a supercell with hexagonal symmetry. There is no unique setting of the hexagonal supercell with respect to the rhombohedral unit cell and this allows for various ways of choosing the Cartesian reference frame. Depending upon this choice of the relative orientation of the axes and the specific structure, the sign of C_{14} can be positive or negative for rhombohedral systems (for a detailed discussion, see Golesorkhtabar *et al.*, 2013). So it is possible that C_{14} is negative for RuC–Rhombohedral (space group : 166) while it is positive for Ru_2C–Rhombohedral (space group : 160). They are different structures though both of them belong to the class Rhombohedral I. However, as pointed out above, it is to be noted that the sign of C_{14} does in no way affect the mechanical stability.

The calculated values of B/G ratio for the given systems (table 5.2) are larger than 1.75, the critical value to separate brittleness and ductility, according to Pugh's criterion (Pugh, 1954). This indicates that these systems are all ductile.

5.2.3. Phonons

Phonon dispersions provide significant information about the dynamical properties of materials. Within harmonic approximation the phonon data is used for the calculation of free energy, entropy, specific heat and electron–phonon interaction. Within quasiharmonic approximation it is used for the calculation of thermal expansion, heat conduction etc. The presence of imaginary frequencies in the phonon spectrum indicates that the structure is dynamically unstable. Phonon data can also provide information about structural phase transformations, mainly arising from soft modes. The lattice dynamical properties of the five ruthenium carbide systems are calculated using the self consistent DFPT method (Baroni *et al.*, 1987, 2001) with 2x2x2 supercells. Here the dynamical matrix, that contains the details of the lattice dynamics of the system, can be calculated from the ground state electron charge density and its first derivative with

respect to ionic coordinates for any given geometry. The post-processing of the data has been done by PHONOPY code. The phonon dispersion curves and phonon density of states of these systems have been calculated and the results are presented in figures 5.4–5.8. The high symmetry points in the Brillouin zone for each system are selected using the ACONVASP online utility (Setyawan and Curtarolo, 2010). The negative side of the plots represents imaginary frequencies.
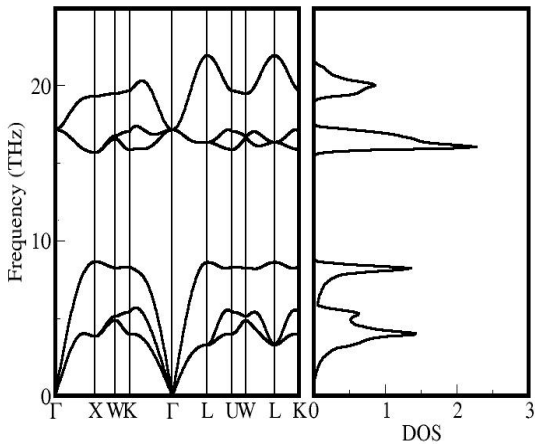
Fig. 5.4: Phonon dispersions & density of states of RuC–Zinc blende.
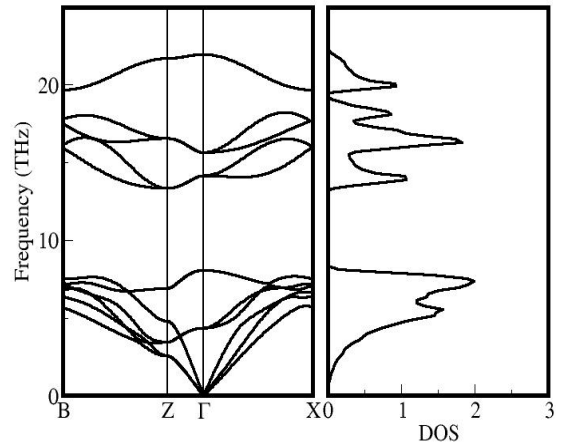
Fig. 5.5: Phonon dispersions & density of states of RuC–Rhombohedral
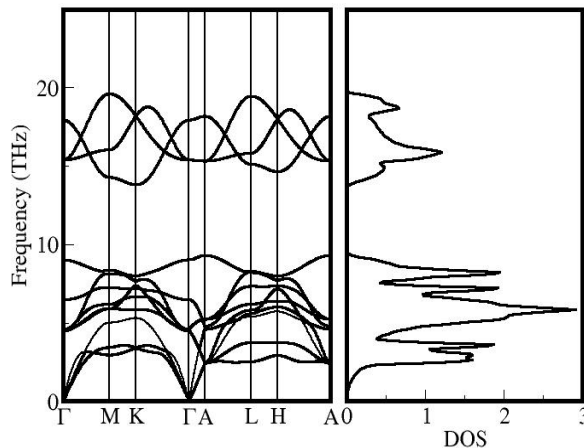
Fig. 5.6: Phonon dispersions & density of states of Ru$_3$C–Hexagonal.

For RuC–Zincblende (figure 5.4), RuC–Rhombohedral (figure 5.5) and Ru_3C–Hexagonal (figure 5.6) systems there are no imaginary frequencies in phonon dispersions confirming that these systems are dynamically stable. Phonon dispersion curves of RuC–Zinc blende structure at ambient pressure have been studied in two previous works (Z. Zhao *et al*., 2010; H.R. Soni *et al*., 2011). They have also predicted dynamical stability for this structure. The phonon dispersion curves obtained in the present work exactly correspond to those reported before. The phonon dispersion curves of RuC–Rhombohedral system at ambient pressure as obtained here agree well with the results obtained in Guang *et al*. (2012). For the Ru_3C–Hexagonal system phonon dispersions are being computed for the first time in the present work. There is a significant gap between the optic and acoustic phonon modes for all these systems.

For RuC–Trigonal and Ru_2C–Rhombohedral systems there are some imaginary frequencies near the Γ–point in phonon dispersions, implying that these systems are dynamically unstable. A recent computational work on the Ru_2C system reported from the high pressure-high temperature synthesis (Sanjay Kumar *et al*., 2012) has established that it is dynamically unstable at ambient pressure and temperature (Sun *et al*., 2013). However, it has been shown to be stabilized under pressure by means of Lifshitz transition mechanism (Sun *et al*., 2013). The possibility has already been pointed out that this particular system reported from the recent experimental synthesis could be RuC–Trigonal identified here. In the present work the dynamical stability of RuC–Trigonal and Ru_2C–Rhombohedral systems is investigated at different higher pressures. The results are presented in figures 5.7-5.8.

In the case of RuC–Trigonal the imaginary frequencies disappear at 50 GPa (figure 5.7). As no attempt has been made here for increasing the pressure at regular stages, it is possible that the stabilization of this system can be achieved at a lower pressure. In Sun *et al*. (2013), under the same computational environment, the stabilization of Ru_2C system has been observed in the pressure range 30–110 GPa. It is significant that the phonon dispersion curves reported in Sun *et al*. (2013) for Ru_2C

system look remarkably similar to those of RuC–Trigonal system presented here, indicating the possibility that the two systems could be the same.
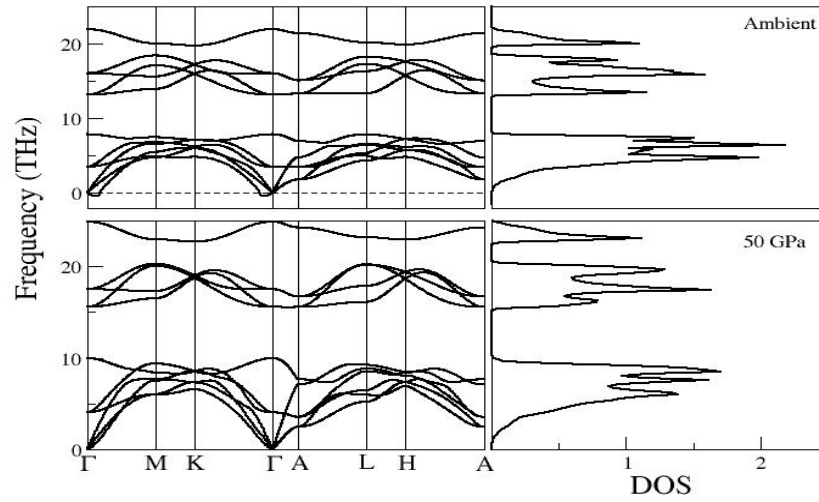
Fig. 5.7: Phonon dispersions & density of states of RuC–Trigonal.
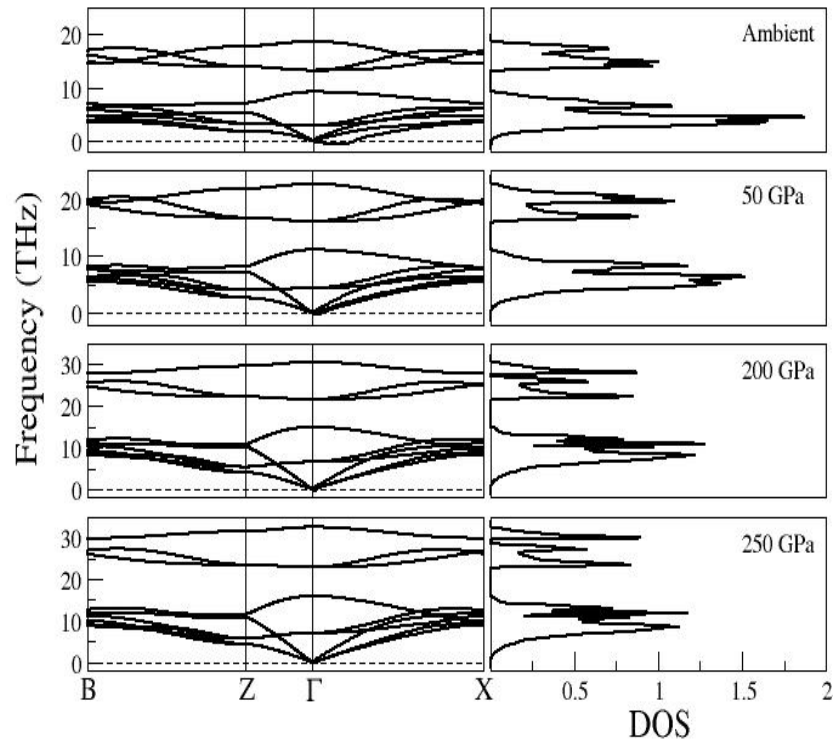
Fig. 5.8: Phonon dispersions & density of states of Ru$_2$C–Rhombohedral.

In the case of Ru$_2$C–Rhombohedral, the imaginary frequencies do not completely disappear, but they systematically decrease with pressure and become negligibly small at 200 GPa (figure 5.8). For some of the systems that may be synthesized only at high pressures, the instability at ambient pressure and stabilization under pressure can be a possibility, as in the case of RuC–Trigonal and Ru$_2$C–Rhombohedral.

Only the three systems established as stable ones at ambient pressure have been considered for the determination of the electronic structure and hardness in the subsequent sections of this work. Spin-polarized calculation is attempted and it is concluded that no significant magnetism is present in Ruthenium Carbides.

5.2.4. Electronic structure

The electronic energy bands along the high symmetry directions of the Brillouin zone and the partial density of states are presented in figures 5.9–5.11 for stable Ruthenium Carbide systems. The Fermi level is set to 0 eV.
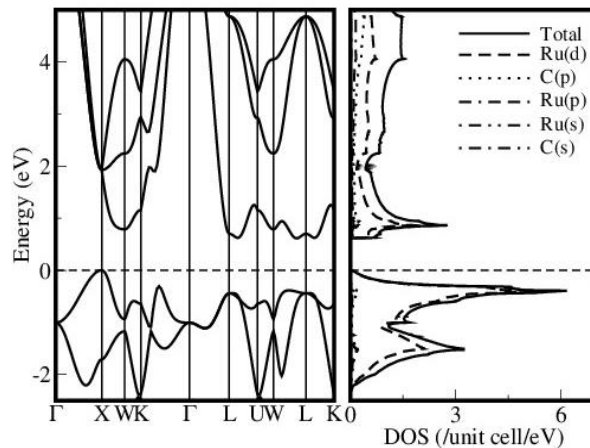
Fig.5.9: Electronic bands and partial density of states of RuC–Zinc blende.
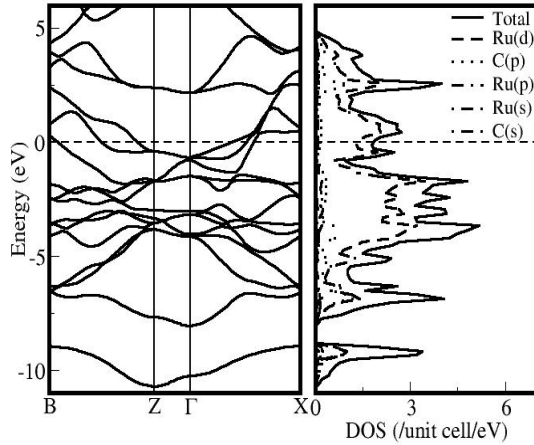
Fig. 5.10: Electronic bands and partial density of states of RuC–Rhombohedral.
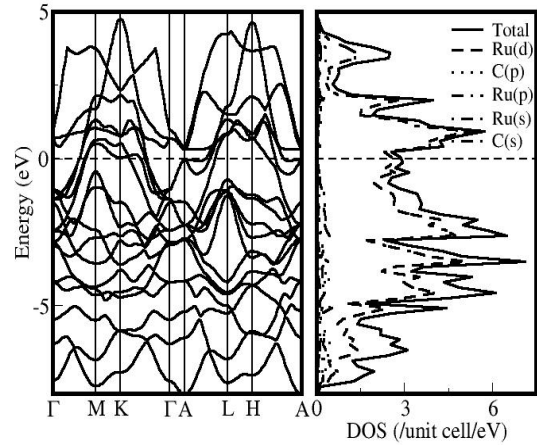
Fig. 5.11: Electronic bands and partial density of states of Ru₃C–Hexagonal.

It is evident from the electronic band structure that RuC–Zinc blende is semiconducting as there is a distinct gap between the valence and conduction bands (figure 5.9). It has an indirect band gap of 0.618 eV. Two previous works (Z. Zhao *et al.*, 2010; H.R. Soni *et al.*, 2011) had computed the electronic energy bands of RuC–Zinc blende system. Both had concluded that this structure was semiconducting with an indirect band gap of 0.6 eV (Z. Zhao *et al.*, 2010) or 0.71 eV (H.R. Soni *et al.*, 2011). It can be emphasized that density functional theory generally underestimates the band gap, so the experimental value of the band gap for this system could be higher than the present estimate. RuC–Zinc blende system is further interesting as it also exhibits ductile nature from the B/G value (table 5.2), but at the same time being a semiconductor. This is contrary to the general expectation that a ductile material could be conducting.

For the other two stable systems the valence and conduction bands overlap (figures 5.10, 5.11), which is the characteristic behaviour of metallic systems. According to the B/G values (table 5.2), these two systems are ductile, which is a metallic characteristic. Guang *et al.* (2012) has reported metallic nature for RuC–Rhombohedral system. In all the three systems, the major contributions to the electronic partial density of states are from Ru(d) states and C(p) states, the former being significantly higher. For the two stable systems in RuC stoichiometry, the variation in density of states is identical for Ru(d) states and C(p) states implying strong hybridization between them. It may be

interesting to investigate the possible phase transitions from conducting to semiconducting band structure among these two, particularly so since such structural transitions are energetically possible among them (table 5.1) during the synthesis. There is a pseudo–gap at the Fermi level for RuC–Rhombohedral (figure 5.10) system, indicating high stability. This is in agreement with the computed value of the lowest formation energy of this system in Ru_1C_1 stoichiometry (table 5.1).

5.2.5. Infrared Spectrum

Given the very small amount of the material produced in the two synthesis of Ruthenium Carbides, the determination of the stoichiometry has been a very delicate exercise. Therefore more detailed experimental analysis is required to carefully pinpoint both the stoichiometry and the structure. In the case of the semiconducting Zinc blende system in RuC stoichiometry the computation the dynamical quantity Born effective charge tensor and the generation of infrared (IR) spectrum can help in the structure determination in future experimental attempts. Counter intuitively, the principal (diagonal) elements of the BEC tensor are often not close to the formal charges of the atoms of the compound. The diagonal elements of the BEC tensor computed for RuC-Zinc blende system are presented in table 5.3 along with the formal charges on the ions.

Table 5.3: Born effective charge tensor for RuC-Zinc blende system (in |e|).

Ions	Z_{xx}^*	Z_{yy}^*	Z_{zz}^*	Z^{formal}
Ru	-5.4684	-5.4684	-5.4681	-4
C	5.4712	5.4712	5.4709	+4

For systems with cubic symmetry BEC tensor is diagonal and there are only two independent elements. According to the sum rule ensuring the charge neutrality, for every direction α and β, $\sum_l Z_{\alpha\beta}^*(l) = 0$. i.e., for every matrix element, the sum of the Born effective charges of all the ions in the cell must vanish (Gonze and Lee, 1997). The sum rule can be broken because of the finiteness of the number of plane waves or the discretization of the real-space integral (Gonze and Lee, 1997). For example, in the case

of CuInS$_2$ (Łażewski *et al.*, 2002), which is a semiconductor, the sum rule is broken for both diagonal and off-diagonal matrix elements. The sum rule is obeyed here for RuC-Zinc blende. For this system both the in-plane and perpendicular BEC values for Ru and C differ significantly from their formal charges. This indicates that the bonding is different from ionic. The corresponding BEC values of Ru and C atoms have almost the same numerical values and opposite signs. Taken together, these factors signify strong covalent bonding between Ru and C atoms.

The intensity of the IR active modes are calculated (Eq.2.77) in terms of the BECs and the phonon polarization vectors (Baroni *et al.*, 2001). The computed IR spectrum of RuC-Zinc blende system is given in figure 5.12. There are no experimental measurements of IR spectrum available for the Ruthenium Carbide systems for comparison. The present work is the first effort to compute the IR spectra of these systems.
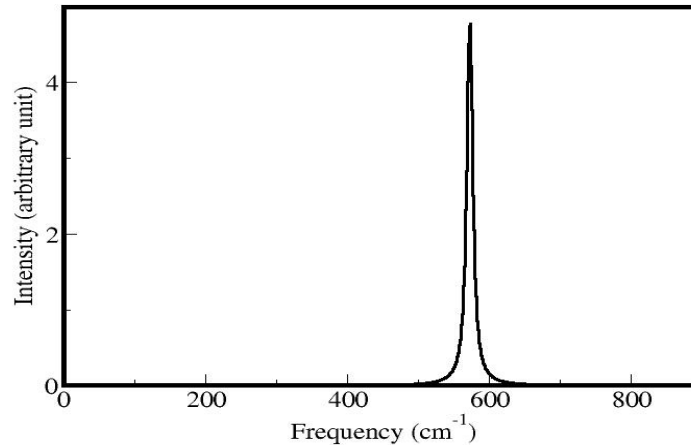
Fig.5.12: IR spectrum of RuC-Zinc blende.

RuC-Zinc blende system gives one peak at 572.8 cm^{-1}. It corresponds to a 3-fold degenerate mode T$_2$. Of these three modes, one corresponds to vibrations of both Ru and C atoms along z-direction alone and the other two correspond to vibrations of both atoms in the xy-plane. The amplitude of vibrations of C atom is one order of magnitude higher than that of Ru atom. C atom being lighter, it is expected to vibrate with higher amplitude and this is exhibited in the computed phonon amplitudes.

5.2.6. Hardness

With the growth of interest on novel superhard materials over the past several decades, it has become necessary to understand the microscopic features that control the hardness of materials. Many empirical models have been developed that aim to correlate hardness with different properties of materials. The hardness values of these Ruthenium Carbide systems are estimated here with three different models, one microscopic model and two macroscopic models.

5.2.6.1. Model Based on Bond Strength

Different models, that can be classified as microscopic models, have been proposed to estimate the intrinsic hardness of ideal crystals in terms of input parameters like structural data or properties of constituent elements (Šimůnek and Vackář, 2006; Šimůnek, 2007, 2009; X. J. Guo *et al*., 2008) . The model based on the bond strength, proposed by Šimůnek and Vackář (2006) and Šimůnek (2007, 2009), is considered here. The theory is discussed in detail in section 2.3.9.1. Substituting the atomic radii (Kittel, 1996) and distances in Å, Eqs. (2.78–2.80) give the hardness in GPa.

For Ru, $Z_1=8$ and $R_1=1.34$ Å, so $e_1=5.9702$. For C, $Z_2=4$ and $R_2=0.92$ Å, so $e_2 = 4.3478$. The counting scheme of the number of bonds in the unit cell is as follows: If a bond is shared by two atoms within the unit cell, it is counted as one; if a bond is shared between one atom within the unit cell and another atom outside the unit cell, its contribution is counted as half. For each structure, the number of neighbours of Ru (n_1) and C (n_2), the bond lengths of Ru–Ru bond (d_{11}), Ru–C bond (d_{12}) and C–C bond (d_{22}), and the number of these bonds in the unit cell (b_{11}, b_{12} and b_{22}, respectively), the volume of the unit cell (Ω) and the calculated value of hardness from different models are presented in table 5.4. In figures 5.13–5.15, the grey larger spheres represent Ru atoms and the brown smaller ones represent C atoms. The atoms identical to each other in their bonding environment are given the same label. The crystal visualization program VESTA (Momma and Izumi, 2011) is used to generate the images.
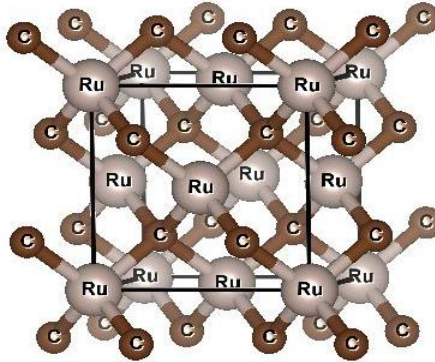
Fig. 5.13: RuC–Zinc blende structure.

Figure 5.13 represents RuC–Zinc blende structure. There are four Ru and four C atoms in the unit cell. The estimated hardness is 36.66 GPa (table 5.4). Estimation of hardness using the above semi–empirical formula has been previously done for this particular system (Abidri, 2010) yielding a value of 36.94 GPa. The estimate based on the semi–empirical model of X.J. Guo *et al.* (2008) has yielded a value of 42.8 GPa in another earlier computational work (Z. Zhao *et al*., 2010) on this system.

Table 5.4: Computational parameters for the bond strength model and the hardness values of Ruthenium Carbides from models based on bond strength (H_b), Pugh's ratio (H_P) and Debye temperature (H_D)

		RuC-Zinc blende	RuC-Rhombohedral	Ru$_3$C-Hexagonal
Ru	n_1	4	12	13, 12
C	n_2	4	4	6
Ru-Ru bond	d_{11} (Å)		2.8208	2.7482, 2.7502
	b_{11}		9	16
Ru-C bond	d_{12} (Å)	1.9765	2.0484	2.1130
	b_{12}	16	6	6
C-C bond	d_{22} (Å)		1.3995	
	b_{22}		1	
Volume	Ω (Å^3)	95.1273	42.2808	47.81
	H_b (GPa)	36.66	21.15	12.42
Hardness		(36.94[a], 42.8[b])	(28[c])	
	H_P (GPa)	3.30	17.82	14.93
	H_D (GPa)	3.36	15.45	20.24

[a]Abidri *et al*. 2010   [b]Z. Zhao *et al.* 2010   [c]Guang *et al.* 2012

Figure 5.14 represents RuC–Rhombohedral structure. There are two Ru and two C atoms in the unit cell. Each Ru atom is surrounded by six Ru atoms in the same plane, three Ru atoms above (below) and three C atoms below (above), so $n_1 = 12$. All these 12 neighbours lie outside the unit cell. Each C atom is bonded to three Ru atoms, either above or below (all lying outside the unit cell), and one C atom (lying within the unit cell), so $n_2 = 4$. Each Ru atom forms 9 Ru–Ru bonds, with atoms lying outside the unit cell. Taking half the contribution of these 18 Ru–Ru bonds, $b_{11} = 9$. Each of the four atoms in the unit cell forms 3 Ru–C bonds, with atoms lying outside. Taking half the contribution of these 12 Ru–C bonds, $b_{12} = 6$. As there is only one C–C bond, shared by C atoms within the unit cell, $b_{22} = 1$. There are two slightly different Ru–Ru bond lengths, hence the average value is taken for d_{11} (table 5.4). The estimated hardness is 21.15 GPa (table 5.4). The estimate based on linear correlations between the elastic moduli and hardness has given a value of 28 GPa for this system in a previous work (Guang, 2012).
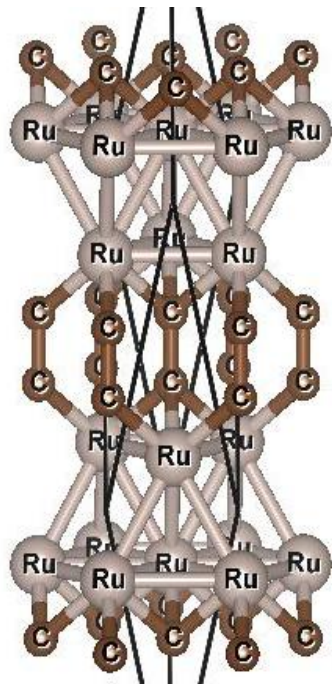
Fig.5.14: RuC–Rhombohedral structure.
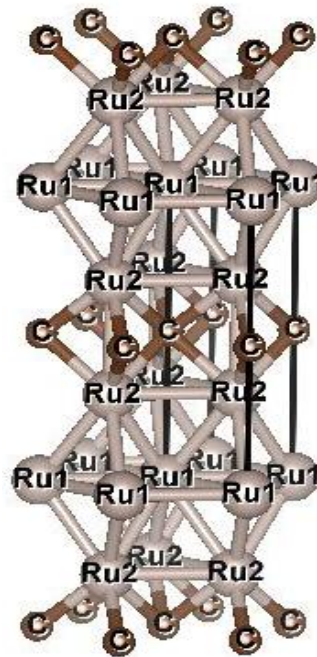
Fig. 5.15: Ru_3C–Hexagonal structure.

Figure 5.15 represents Ru_3C structure with three Ru atoms and one C atom in the unit cell. All the neighbours are not explicitly shown for every atom in the unit cell. The three Ru atoms in the unit cell belong to two types, one is labeled Ru1 and the other two are labeled Ru2. For Ru2 the orientation of the neighbours is similar to that described for Ru atoms in RuC–Rhombohedral structure (figure 5.14). In addition, there is an extra Ru–Ru bond between the two Ru2 atoms in the unit cell, so $n_1 = 13$ for these two Ru2 atoms with the average Ru–Ru bond length $d_{11} = 2.7482$ A^o. For Ru1, as it is surrounded only by other Ru atoms in the close–packing scheme, $n_1' = 12$, with the average bond length $d_{11}' = 2.7502$ A^o. Therefore the strength of Ru–Ru bond is estimated with the separate contributions from these two types of Ru–Ru neighbourhood and their average value is taken. The C atom is bonded to three Ru atoms both above and below, so $n_2 = 6$. Among the 12 Ru–Ru bonds formed by Ru1 atom, only one is shared by an atom within the unit cell; among the 10 Ru–Ru bonds formed by one Ru2 atom, two are shared by atoms within the unit cell; among the 10 Ru–Ru bonds formed by the other Ru2 atom, only one is shared by atoms within the unit cell. Not counting the bonds twice, $b_{11} = 16$. Among the 6 Ru–C bonds formed by the two Ru2 atoms together, two are shared by atoms within the unit cell; among the 6 Ru–C bonds formed by the C atom, two are shared by atoms within the unit cell. Not counting the bonds twice, $b_{12} = 6$. The estimated hardness is 12.42 GPa (table 5.4).

Thus, the two systems of RuC stoichiometry exhibit significantly high Vickers hardness (H_V) values, with that of RuC–Zinc blende approaching the superhard category ($H_V > 40$ GPa). As the metal to carbon ratio increases hardness decreases for Ru_3C, as expected from the nature of metallic bonds.

5.2.6.2. Model Based on Elastic Constants

Using Chen-Tian formula (Eq.2.82) based on elastic constants (Chen *et al.*, 2011; Tian *et al.*, 2012) and the data from table 5.2, the hardness of the Ruthenium Carbide systems are estimated and the values (H_P) are given in table 5.4. Except for the RuC–Zinc blende system, the hardness values obtained from the microscopic model based on bond strength and the macroscopic model based on Pugh's ratio are of the same order. As

RuC–Zinc blende system is a semiconductor (Fig.5.9), and since the model based on bond strength by Šimůnek and Vackář (2006) and Šimůnek (2007, 2009) is better suited for covalent crystals, the value of hardness from that model could be a better estimate of hardness for this system, compared to the value from the model based on Pugh's ratio. It can also be noted that another microscopic model based on the valence electron density (X. J. Guo *et al.*, 2008) has yielded a value (Z. Zhao *et al.*, 2010) close to the one from the model based on bond strength (table 5.4).

5.2.6.3. Model based on Debye temperature

The model is described in detail in section 2.3.9.3. In order to calculate the elastic wave velocities the elastic moduli from table 5.2 are used. The results of the calculations using Eqns.(2.83)-(2.87) are tabulated in table 5.5. Calculated values of Debye temperature from previous computational works have also been given for comparison. The values of Θ_D are consistent with the observed trends in bulk, shear and Young's moduli for the two systems of RuC stoichiometry. Together these values imply that rhombohedral system could be mechanically more stable among the three.

Table 5.5: Volumic density (in kg/m^3), transverse, longitudinal and average sound velocities (in m/s), and Debye temperature (in Kelvin).

	ρ	v_t	v_l	v_m	Θ_D
RuC−Zinc blende	7896	2796	6598	3161	412.36 (407.02[a])
RuC−Rhombohedral	8883	4287	7541	4765	646.46 (688[b])
Ru$_3$C−Hexagonal	10,948	3793	6938	4229	550.72

[a]Abidri *et al.*, 2010 (LDA)   [b]Guang *et al.*, 2012 (GGA)

As Debye temperature is derived from the elastic constants (Eqns.5.3–5.6), the hardness values obtained from this model can be expected to correspond to those from the model based on Pugh's ratio. With the fitting parameters a=2500 and b=200 and data from table 5.5, the hardness values (H$_D$) obtained from Eqn. (5.2) are given in table 5.4. As the Debye temperature of RuC–Zinc blende system is significantly smaller than the

values of other systems, any level of fitting based on this model will yield only a relatively small value of hardness for it. System of Ru_3C stoichiometry has higher molar mass and higher density compared to those of RuC stoichiometry (table 5.5). This causes an increase in hardness as given by the above formula for Ru_3C–Hexagonal. However, this trend is against the expectation that an increase in metallic component should result in a decrease in hardness, and such a variation is observed in the case of the hardness values obtained from the model based on bond strength (table 5.4).

It is concluded that the semi–empirical microscopic model based on bond strength by Šimůnek and Vackář (2006) and Šimůnek (2007, 2009) gives better estimates of hardness for Ruthenium Carbide systems compared to the two macroscopic models derived from elastic constants.

5.2.7. Thermodynamic Properties

From the phonon data, through the harmonic approximation, thermal properties due to phonons, such as internal energy, constant–volume heat capacity, Helmholtz free energy and entropy, are evaluated over a range of temperatures from the standard equations of statistical mechanics (Eqns.(2.69)-(2.73)) using the PHONOPY code. The results of the calculations are presented in figures 5.16–5.18.
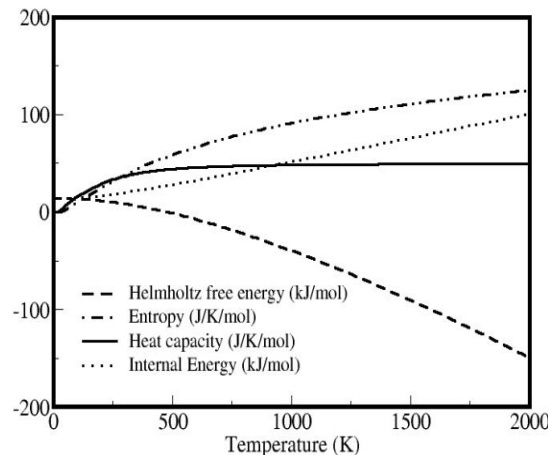
Fig. 5.16: Thermal properties of RuC–Zinc blende.
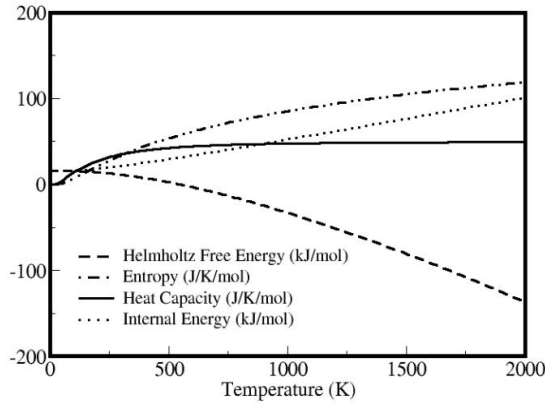
Fig 5.17: Thermal properties of RuC–Rhombohedral.
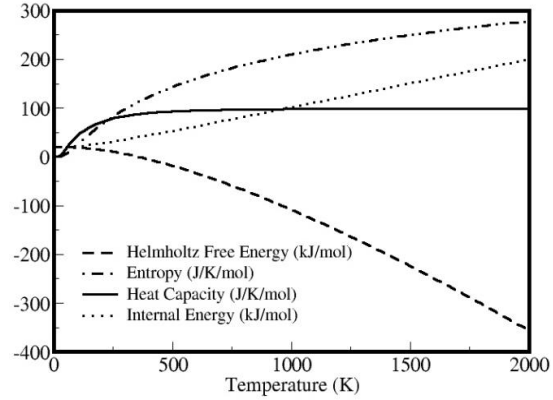
Fig. 5.18: Thermal properties of Ru₃C–Hexagonal.

The variations of F, S, E and C_v with temperature are similar for these three systems. The entropy S and the constant–volume heat capacity C_v exhibit only the expected pattern in their temperature variation. C_v obeys Debye–T^3 law at very low temperatures and Dulong–Petit law at very high temperatures. The results in the case of RuC–Zinc blende system are similar to those obtained in a previous work (H.R. Soni *et al*., 2011) while for RuC-Rhombohedral and Ru₃C-Hexagonal systems the thermodynamic properties are being computed for the first time here.

5.3. SUMMARY

Exhaustive structure search employing evolutionary algorithm is carried out for three stoichiometries of Ruthenium Carbides, RuC, Ru₂C and Ru₃C. Three lowest energy structures are obtained for RuC stoichiometry and one each for Ru₂C and Ru₃C stoichiometries. These include the two reported structures from the synthesis of Ruthenium Carbides ($P\bar{6}m2$ and $P\bar{3}m1$) and their emergence in stoichiometries different from the reported ones is plausible in the light of the high pressure and high temperature required for their synthesis. These five structures are fully relaxed and it is established that rhombohedral structure is energetically the most stable one in RuC stoichiometry. The mechanical stability of these five systems is confirmed by the elastic constants satisfying the corresponding stability criteria. Standard elastic properties are calculated for each system. From the Pugh's criterion, all these systems are found to be ductile. The

98

dynamical stability of three of the systems, RuC–Zinc blende, RuC–Rhombohedral and Ru_3C–Hexagonal, is clearly established from the phonon data. RuC–Trigonal system and Ru_2C–Rhombohedral system are dynamically unstable at ambient pressure, but both these systems can be stabilized under pressure. The electronic bands and DOS show that RuC–Zinc blende system is semiconducting with a band gap of 0.618 eV while the other two stable systems are metallic. The BEC tensor elements of RuC-Zinc blende system being discussed here give valuable information about the nature and strength of the bonding between different atoms. The computed IR spectrum can serve as bench mark for the experimental spectral analysis to be carried out on this system. Computations of dynamical quantities like Born effective charges and IR spectra from first principles can guide in the unambiguous determination of the stoichiometry and the structure by the comparison of the experimental measurements with the computational predictions. Using the semi–empirical model based on the bond strength, the hardness of the stable systems are estimated. The hardness of RuC–Zinc blende has a significantly large value of 36.66 GPa, very close to the superhard barrier of 40 GPa. The other stable system of RuC stoichiometry, i.e., RuC-Rhombohedral, also has fairly large value of hardness (21.15 GPa). As the metal to carbon ratio increases, hardness decreases for Ru_3C. Two other semi-empirical models of hardness, based on the elastic properties, are also employed for hardness estimation, but they are found to be inadequate for these systems. Standard thermodynamic properties of these systems are calculated from the phonon data, within the harmonic approximation. The positive formation energies of these systems show that they are not thermodynamically stable, i.e. high pressure and possibly high temperature are necessary for their synthesis.

Chapter 6

PRESSURE-INDUCED VARIATION OF THE STABILITY AND
PROPERTIES OF RUTHENIUM CARBIDES

6.1. INTRODUCTION

In the study of the ground state properties of Ruthenium Carbides (Harikrishnan *et al*., 2015a) it has been noted that the formation energies of all the Ruthenium Carbide systems obtained by the structure search are positive at ambient pressure (table 5.1), which suggest that high pressure and possibly high temperature would be required for their synthesis. Of the two reports of the synthesis of Ruthenium Carbide, the first has been at high temperature (Kempter and Nadler, 1960; Kempter, 1964) and the second, at high temperature and pressure (Sanjay Kumar *et al*., 2012). Our result that $P\bar{3}m1$ structure of RuC stoichiometry (RuC-Trigonal) is not dynamically stable at ambient pressure, but becomes stable at around 50 GPa (figure 5.7), clearly shows that the stability and properties of these systems can significantly change with pressure. Similarly, $R3m$ structure of Ru_2C stoichiometry (Ru_2C-Rhombohedral) is also shown to have dynamical instability at ambient pressure and stability at around 200 GPa (figure 5.8). Subsequently we have investigated using DFT how the structural, elastic, dynamical, electronic, thermodynamic properties and hardness of the three stable Ruthenium Carbide systems vary with pressure. As many of their potential industrial applications would be in extreme conditions, such a study would provide helpful indicators for the experimental works on these systems at high pressures.

6.2. RESULTS AND DISCUSSION
6.2.1. Formation Enthalpies and Structural Properties

In order to make an estimate of optimal synthesis conditions the enthalpies of

formation of the five Ruthenium Carbide systems have been calculated at different pressures, ranging from 0 to 300 GPa. Since enthalpies of Graphite and Ruthenium are also required for this purpose, they are also calculated accurately at each pressure using 19x19x7 and 31x31x20 k-grids, respectively, for Graphite and Ruthenium. The values of enthalpy per atom of Graphite and Ruthenium at different pressures are given in table 6.1.

Table 6.1: Enthalpy per atom of Ruthenium and Graphite (in eV) at different pressures

Pressure (GPa)	0	50	100	150	200	250	300
Graphite	-9.2320	-6.9551	-5.1170	-3.4643	-1.9348	-0.5005	0.8581
Ruthenium	-9.2751	-5.2001	-1.4999	1.9556	5.2296	8.3598	11.3712

Enthalpy of formation of Ruthenium Carbides at each pressure is calculated by the formula,

$$\Delta H_f = Enthalpy\ of\ Ru_aC_b - a\ \times (Enthalpy\ per\ atom\ of\ Ruthenium)$$
$$- b \times (Enthalpy\ per\ atom\ of\ Graphite) \qquad (6.1)$$

Enthalpies of formation ΔH_f of Ruthenium Carbides are calculated at different pressures and the results are given in table 6.2.

Table 6.2: Enthalpy of formation of Ruthenium Carbides (in eV) at different pressures

Pressure (GPa)	RuC-Zincblende	RuC-Rhombohedral	RuC-Trigonal	Ru_2C-Rhombohedral	Ru_3C-Hexagonal
0	0.9126	0.7240	0.8010	1.0950	0.9266
50	1.4346	0.5323	0.6293	0.5939	0.4153
100	2.0392	0.5599	0.6679	0.3707	0.1886
150	2.6089	0.6346	0.7497	0.2282	0.0438
200	3.1443	0.7307	0.8511	0.1305	-0.0558
250				0.0657	
300				0.0250	

Variation in enthalpy of formation with pressure is plotted in figure 6.1. For Ru_3C system the enthalpy of formation is negative at around 175 GPa. This implies that if sufficient

energy can be supplied to overcome the reaction barrier, Ru_3C-Hexagonal can be formed at 175 GPa. Though the enthalpies of formation of the other systems remain positive over the range of pressures considered here, some conclusions can be drawn from the trend in their variation with pressure
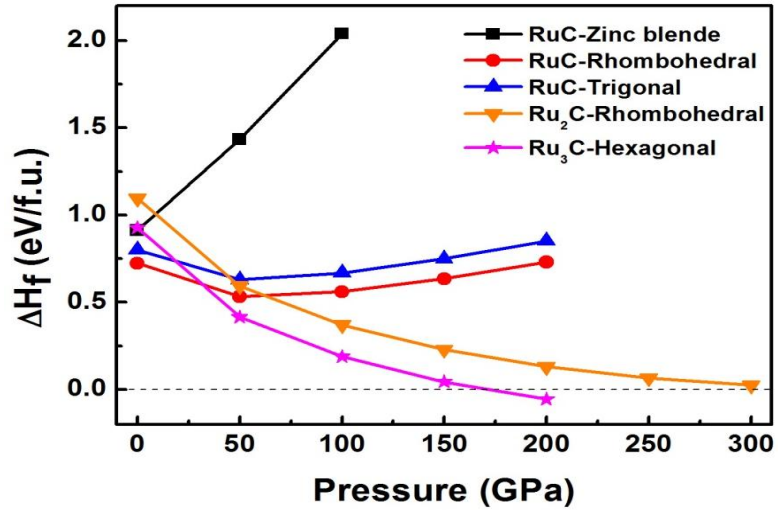
Fig.6.1: Variation in Enthalpies of Formation with Pressure

Since the enthalpy of formation of RuC-Zinc blende only increases with pressure, its synthesis would become increasingly difficult with increase in pressure. Hence RuC-Zinc blende cannot be synthesized by the increase of pressure. Its synthesis can be attempted at ambient pressure and high temperature. Thermal energy kT corresponding to enthalpy of formation per atom gives an estimate of the order of the temperature of synthesis. For RuC-Zinc blende ΔH_f per atom is 0.4564 eV which corresponds to a temperature of 5477 K. The melting temperature of Ruthenium is 2607 K. Though no data is available for the melting temperature of Ruthenium Carbides, it is quite unlikely to be as high as 5500 K. This implies that the synthesis of RuC-Zinc blende may not be possible at ambient pressure or at higher pressures. The enthalpy of formation of RuC-Rhombohedral is a minimum at around 50 GPa, with ΔH_f per atom of 0.2662 eV, which corresponds to a temperature of 3194 K. It can be concluded that the synthesis of RuC-Rhombohedral is most probable close to 50 GPa and 3200K. The formation enthalpy of

RuC-Trigonal follows the same trend as that of RuC-Rhombohedral. For Ru_2C-Rhombohedral ΔH_f is close to zero at 300 GPa, hence its synthesis is possible at this pressure if sufficient energy is supplied to overcome the reaction barrier. Though synthesis of Ru_3C-Hexagonal is possible at 175 GPa it may also be achieved at pressures as low as 50 GPa with the increase in temperature. At 50 GPa ΔH_f per atom of Ru_3C-Hexagonal is 0.1038 eV, which corresponds to 1246 K. This implies that Ru_3C-Hexagonal may be synthesized at 50 GPa when the temperature is about 1250 K. The above data at higher pressures have been generated using DFT under the condition of zero temperature. Accurate values of the temperature and pressure for synthesis would be governed by the Gibbs free energy G = H-TS, which depends on the entropy as well. Though the entropy is not calculated, it can be safely assumed that the change in the TS term with pressure would be small compared to that of the PV term. Hence it may be concluded that it is possible to synthesize these systems, with the exception of RuC-Zinc blende, at pressures lower than 50 GPa.

The first experimental synthesis of Ruthenium Carbides has been done at ambient pressure and at a temperature of 2873 K (Kempter and Nadler, 1960; Kempter, 1964). It is to be noted that the temperature is very close to the value of 2779 K, corresponding to ΔH_f per atom of Ru_3C system at ambient pressure. As pointed out before, the synthesis of Ru_3C system is possible at lower pressures or even ambient pressure provided the temperature is sufficiently high. It has been suggested earlier in our work (section 5.2.1) that $P\bar{6}m2$ structure reported in the first synthesis can be of Ru_3C stoichiometry, instead of the reported RuC stoichiometry. The second reported synthesis has been conducted at 5 GPa pressure and 2000 K (Sanjay Kumar *et al*., 2012). The proposed structure is $P\bar{3}m1$ in Ru_2C stoichiometry, and in a previous computational work (Sun *et al*., 2013) it has been shown to be dynamically unstable at ambient pressure while attaining stability in the pressure range 30-110 GPa. In the structure search undertaken in the present work, the same structure has emerged in RuC stoichiometry and the subsequent phonon analysis has shown that it is dynamically unstable at ambient pressure and attains stability at 50 GPa. The similarities in the phonon curves of the two systems suggest the possibility that

104

$P\bar{3}m1$ structure can be of RuC stoichiometry (figure 5.7). The trend in the variation of the formation enthalpies of RuC-Trigonal and Ru_2C-Rhombohedral correspond to the way they become dynamically stable on applying pressure (section 5.3). Only the other three systems dynamically stable at ambient pressure are considered for further investigation here.
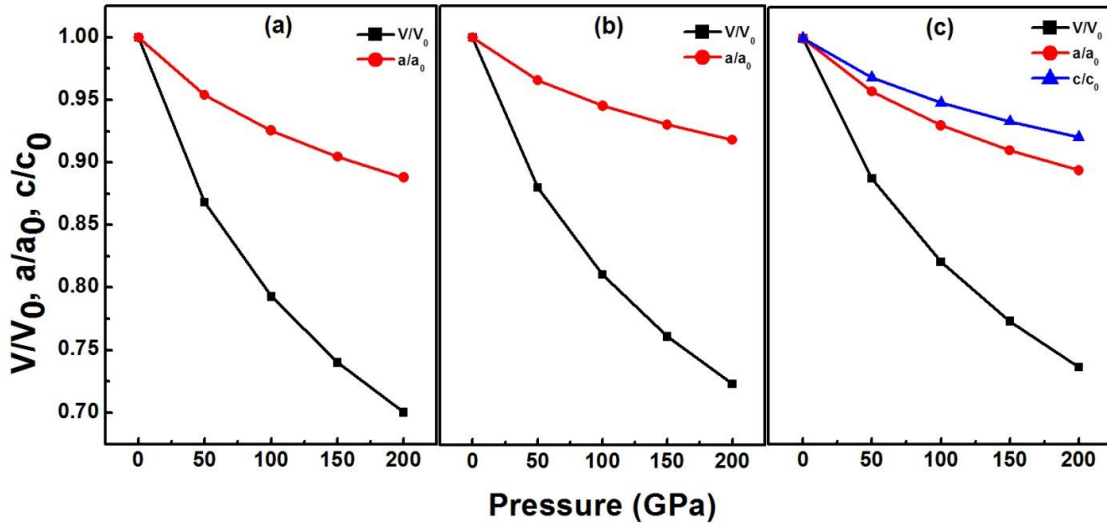
Fig. 6.2: Variation of normalized volume and lattice constants with pressure of (a) RuC-Zinc blende, (b) RuC-Rhombohedral and (c) Ru_3C-Hexagonal

Figure 6.2 shows the way the normalized volume (V/V_0, where V_0 is the volume at ambient pressure) and normalized lattice constants of the three stable systems of Ruthenium Carbides vary with pressure, when analyzed after the structure optimization at different pressures. The curve of the variation of volume with pressure is steeper for RuC-Zinc blende, indicating that it is more compressible than the other two systems. The variation of different bond lengths with pressure is given in Figure 6.3. The lattice constants and bond lengths monotonously decrease with pressure implying the absence of any structural phase transition in this pressure range.
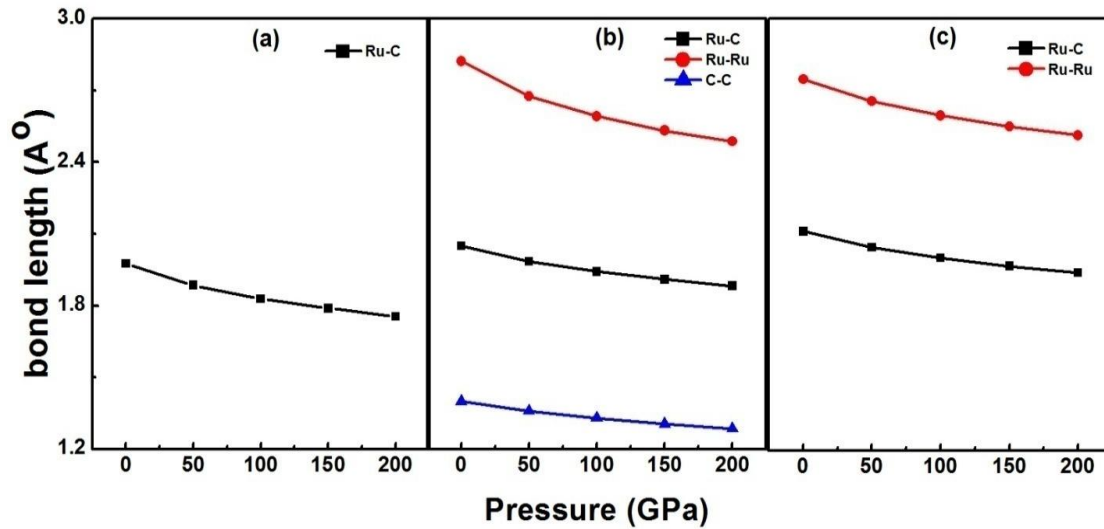
Fig. 6.3: Variation of Ru-C, Ru-Ru and C-C bond lengths with pressure of (a) RuC-Zinc blende, (b) RuC-Rhombohedral and (c) Ru$_3$C-Hexagonal

6.2.2. Elastic Constants

The elastic constants of RuC-Zinc blende, RuC-Rhombohedral and Ru$_3$C-Hexagonal are calculated at different pressures in the range 0-200 GPa using equations (2.34)-(2.36) and the variation of their independent elastic constants with pressure are presented in figures 6.4-6.6. We have retained the symbol $C_{\alpha\beta}$ for the modified elastic constants in the figure legends, the subsequent equations and the discussion.
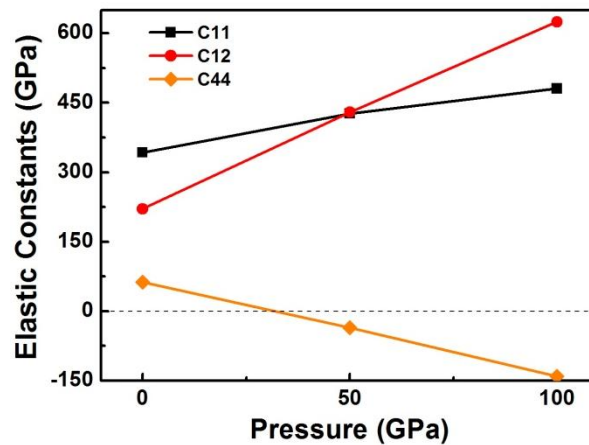
Fig. 6.4: Elastic constants vs. pressure for RuC-Zinc blende

106
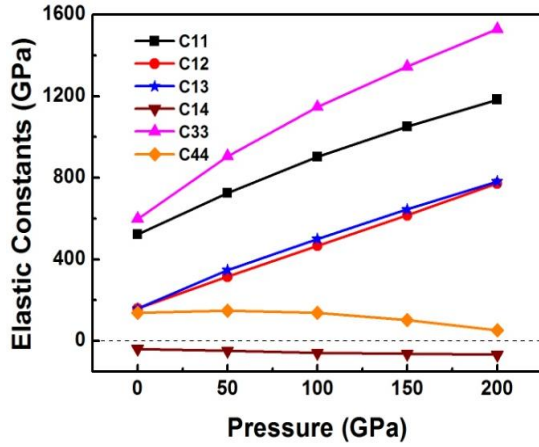
Fig. 6.5: Elastic constant vs. pressure for RuC-Rhombohedral
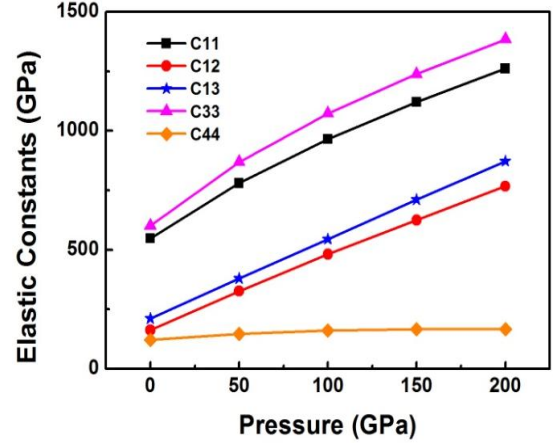
Fig. 6.6: Elastic constant vs. pressure for Ru$_3$C-Hexagonal

Most of the elastic constants exhibit a nonlinear variation with pressure. This is markedly different from the linear variation predicted by elasticity theory that uses the linear strain ϵ_{ij} in place of Lagrangian strain γ_{ij}. C_{11} and C_{33} are more sensitive to the change of pressure as compared to, say, C_{12} and C_{44}. This is because C_{11} and C_{33} represent resistance of the crystal to longitudinal strain by applying a longitudinal stress, and hence a pre-existing longitudinal strain which causes a change in volume of the crystal can easily produce a change in C_{11} or C_{33}. Elastic constants C_{12} and C_{44} are shear constants. Since a transverse strain can cause a change in shape without a change in volume, C_{12} and C_{44} can be less affected by pressure.

For mechanical stability, the elastic constants should satisfy the Born–Huang elastic stability criteria, as given by Eqns.(2.37)-(2.39). For RuC-Zinc blende C_{44} is negative at around 30 GPa (figure 6.4.), clearly indicating mechanical instability. Also, at 50 GPa, $C_{11} < C_{12}$ for this system, which is another indicator of mechanical instability. Along with our result of the steady increase of its enthalpy of formation (figure 6.1) this further proves that synthesis of RuC-Zinc blende cannot be achieved with increase of pressure. The elastic constants of RuC-Rhombohedral and Ru$_3$C-Hexagonal obtained here at different pressures satisfy Born–Huang stability criteria and hence they are mechanically stable in the pressure range 0-200 GPa.

RuC-Rhombohedral belongs to Rhombohedral I (table 5.1) group, with space groups 149 to 167, which has 6 independent elastic constants C_{11}, C_{12}, C_{13}, C_{14}, C_{33} and C_{44}. The other nonzero elastic constants are related to the above independent elastic constants as $C_{24} = -C_{14}$ and $C_{56} = C_{14}$. The pair of elastic constants (C_{24}, C_{14}) has to be of opposite sign. However, the mechanical stability of the crystal depends on C_{14}^2 and C_{13}^2 which are positive. Hence negative sign of C_{14} (figure 6.5) does not imply mechanical instability. However, for RuC-Rhombohedral C_{44} first increases up to 50 GPa and then steadily decreases, and the trend shows that it would be negative at 250 GPa, making the system mechanically unstable at this higher pressure. This is consistent with the variation in formation enthalpy for this system, which becomes minimum at 50 GPa and then increases steadily with pressure (figure 6.1).

Bulk modulus (B) and shear modulus (G) are calculated from $C_{\alpha\beta}$ with the standard formulae for the relevant crystal classes using the Voigt-Reuss-Hill approximation (Eqns.(2.40)-(2.48)). From B and G values, Young's modulus Y and Poisson's ratio ν are calculated. For different pressures (in GPa) the average values of B, G, Y (in GPa), ν and the Pugh's ratio B/G are tabulated in table 6.3. As RuC-Zinc blende becomes mechanically unstable at around 30 GPa, its elastic moduli at higher pressures are not considered here. The data for Zinc blende and Rhombohedral systems of RuC stoichiometry, available from other computational works at ambient pressure, are also tabulated for comparison. For RuC-Rhombohedral and Ru_3C-Hexagonal bulk modulus consistently increases with pressure whereas rigidity modulus first increases and beyond some pressure it decreases. This has resulted in quite high values of B/G for these two systems at higher pressures. The calculated values of B/G ratio for the three systems are larger than 1.75, which is the critical value to separate brittleness and ductility, according to Pugh's criterion. This indicates that these systems are all ductile. For RuC-Rhombohedral the decrease in both G and Y from 100 GPa onwards could be indicative of the trend towards mechanical instability. This is in correspondence with the variation of the elastic constant C_{44} of this system (figure 6.5), implying mechanical instability beyond 200 GPa.

Table 6.3: Elastic moduli of Ruthenium Carbides at different pressures. Pressure, B, G and Y are in GPa.

	Pressure	B	G	Y	ν	B/G
RuC-Zinc blende	0	261.44	61.74	171.70	0.391	4.24
RuC-Rhombohedral	0	287.45	163.23	411.75	0.261	1.76
	50	482.24	180.19	480.71	0.3339	2.676
	100	648.55	180.23	494.86	0.3728	3.598
	150	799.77	158.28	445.46	0.4072	5.053
	200	944.35	111.82	322.73	0.4430	8.445
Ru₃C-Hexagonal	0	316.99	157.48	405.32	0.2870	2.010
	50	509.19	189.08	504.76	0.3348	2.693
	100	680.25	203.77	555.82	0.3638	3.338
	150	837.90	207.44	574.89	0.3856	4.039
	200	988.04	206.06	577.99	0.4025	4.795

6.2.3. Phonons

Using the self consistent DFPT method the phonon modes of Ruthenium Carbide systems are calculated with supercells. PHONOPY code has been used for the post-processing. The phonon dispersion curves of these Ruthenium Carbide systems are calculated at different pressures and, to highlight the differences, only the results at well separated pressures are presented along with those at ambient pressure in figures 6.7–6.9. The ACONVASP online utility (Setyawan and Curtarolo, 2010) has been used for selecting the high symmetry points in the Brillouin zone for each system. It is clear from figure 6.7 that RuC-Zinc blende becomes dynamically unstable at 100 GPa. This further proves that along with its mechanical instability (figure 6.4) RuC-Zinc blende is dynamically unstable at 100 GPa. It is feasible that the system is dynamically stable at a pressure where it is mechanically unstable. Figures 6.8 and 6.9 show that RuC-Rhombohedral and Ru₃C-Hexagonal are dynamically stable in the pressure range 0-200 GPa, as there are no imaginary frequencies in their phonon dispersion curves. The frequencies of the bands increase with pressure, but the pronounced gap between the optic and acoustic phonon modes is consistently present at higher pressures for all these systems.
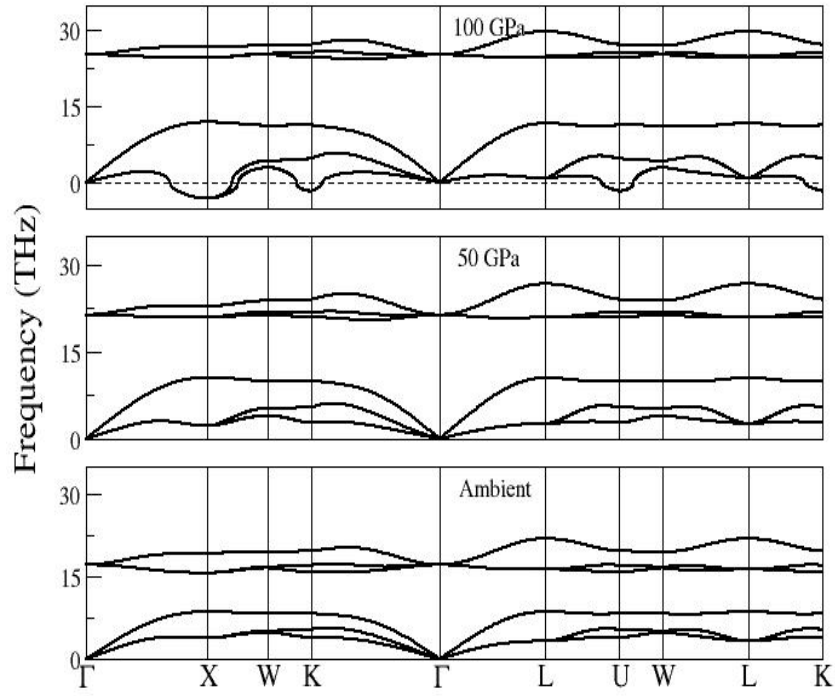
Fig.6.7: Phonon dispersions of RuC-Zinc blende
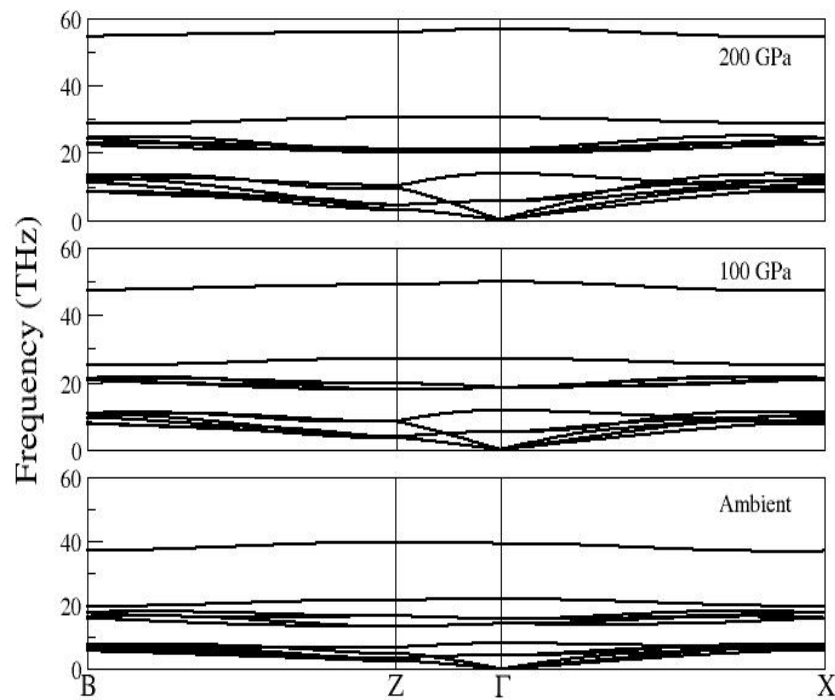
Fig.6.8: Phonon dispersions of RuC-Rhombohedral
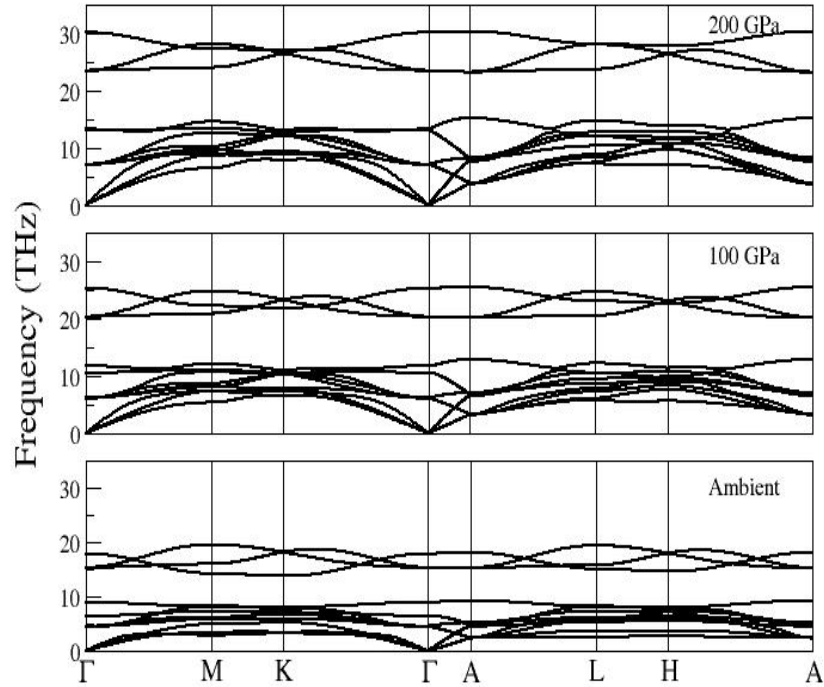
Fig.6.9: Phonon dispersions of Ru$_3$C-Hexagonal

6.2.4. Electronic Structure

The electronic energy band structure along the high symmetry directions of the Brillouin zone and the partial density of states at different pressures of stable Ruthenium Carbide systems are presented in figures 6.10–6.12. The Fermi level is set to 0 eV, represented by a dashed line in the plots. In these figures The black solid lines represent the total density of states (DOS), the red dashed lines represent the partial DOS due to Ru(d) states and the blue dotted lines represent the partial DOS due to C(p) states. The partial DOS due to other orbitals have been represented in distinct styles in black, but their contributions are too small to be distinguishable.

RuC–Zinc blende is semiconducting and it has an indirect band gap of 0.618 eV at ambient pressure (Harikrishnan *et al*., 2015a). With higher pressure the valence bands are shifted to lower energy values while the conduction bands are shifted to higher energy values, resulting in an increase in the band gap (figure 6.10). At 50 GPa band gap becomes 0.84 eV and at 100 GPa it is 0.92 GPa. Though RuC-Zinc blende is mechanically unstable at these pressures these computations provide the trend in the
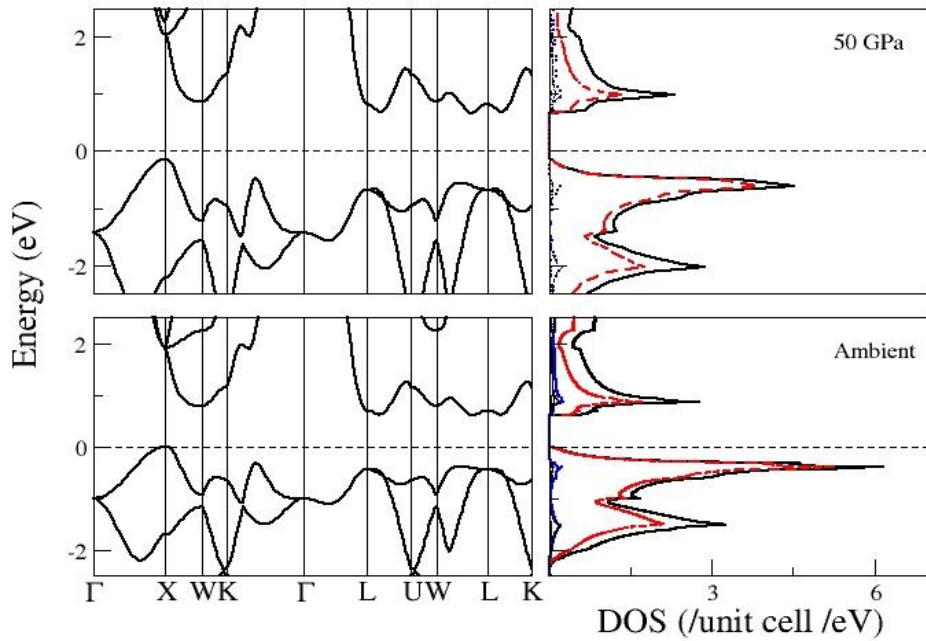
Fig. 6.10: Electronic bands and partial density of states of RuC-Zinc blende
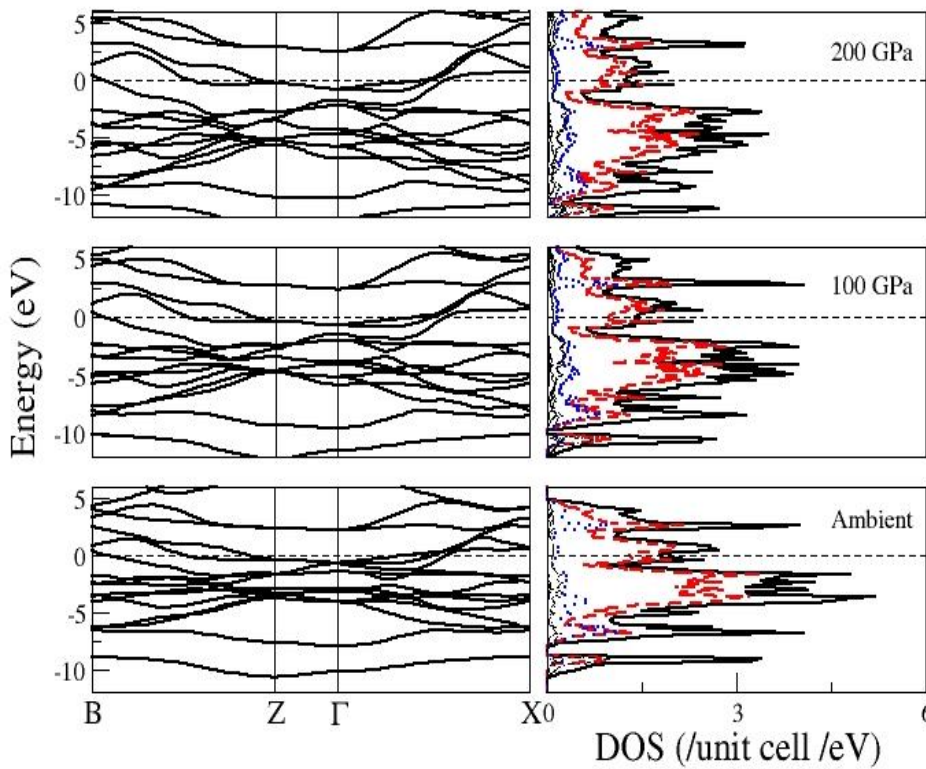
Fig.6.11: Electronic bands and partial density of states of RuC-Rhombohedral
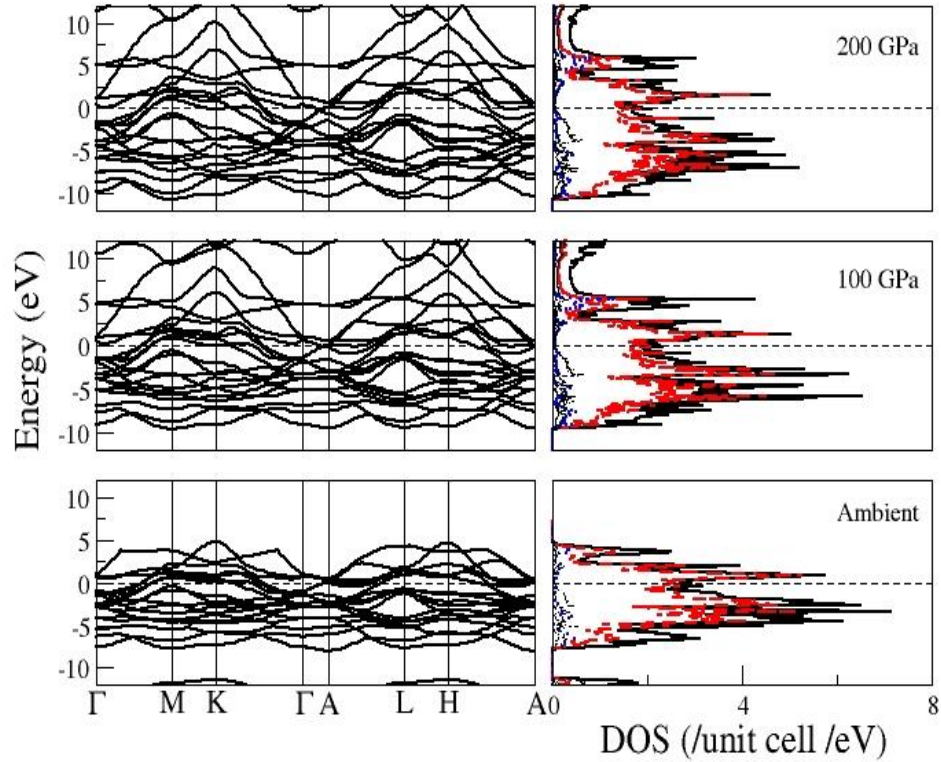
Figure 6.12: Electronic bands and partial density of states of Ru$_3$C-Hexagonal

variation of its band gap with pressure up to 30 GPa, beyond which it can be mechanically unstable. The other two stable systems are metallic as the valence and conduction bands overlap (figures 6.11, 6.12) at the Fermi level.

In all the three systems, Ru(d) state has the predominant contribution to the electronic partial density of states and C(p) state has the next higher share. This is a common feature of transition metal carbides in general. The identical variation in density of states between Ru(d) states and C(p) states of RuC-Zinc blende and RuC-Rhombohedral systems imply strong hybridization between these states, which is another common characteristic of transition metal carbides (Chauhan and Gupta, 2013). Even when the overlapping of the bands reveals the metallic nature of two of these systems, the presence of strongly hybridized p-d orbitals indicates the covalent character of the bonding between the atoms. For RuC–Rhombohedral and Ru$_3$C-Hexagonal the metallic nature is preserved up to 200 GPa. Here also as pressure-induced broadening of the bands takes place with conduction bands shifted to higher energy values and valence bands to

lower energy values. This causes the a reduction in the overlap between Ru(d) states and C(p) states, leading to a decreased hybridization. For RuC-Rhombohedral system a local valley in the DOS called the pseudo-gap, which is present at the Fermi level at ambient pressure, is shifted away to higher energy values as pressure increases (figure 6.11) and the DOS value becomes larger at the Fermi level. This implies a decreased stability for RuC-Rhombohedral as pressure increases to 200 GPa. This trend corresponds to earlier finding that the formation enthalpy of RuC-Rhombohedral increases beyond 50 GPa (figure 6.1). For Ru_3C-Hexagonal the shifting of the bands with pressure results in a pseudo-gap being formed at the Fermi level (figure 6.12), implying increased stability. This exactly corresponds to the fact that the formation enthalpy of this system becomes negative as pressure increases to 200 GPa (figure 6.1).

6.2.5. Infrared Spectra

We have computationally generated the infrared spectrum of RuC-Zinc blende system (Harikrishnan *et al*., 2015b) to provide a signature convenient for experimental verification. Here we study how the spectrum varies with pressure. The diagonal elements of the Born effective charge (BEC) tensor computed for RuC-Zinc blende system at ambient pressure and 50 GPa are presented in table 6.4 along with the formal charges on the ions.

Table 6.4: BEC tensor for RuC-Zinc blende system (in |e|) at different pressures

Pressure (GPa)	Ions	Z^*_{xx}	Z^*_{yy}	Z^*_{zz}	Z^{formal}
0	Ru	-5.4684	-5.4684	-5.4681	-4
	C	5.4712	5.4712	5.4709	+4
50	Ru	-5.4325	-5.4325	-5.4322	-4
	C	5.4363	5.4363	5.4363	+4

The significant deviation of the in-plane and perpendicular BEC values from their formal charges together with their opposite signs and equal magnitudes for R and C atoms

indicate strong covalent bonding between Ru and C atoms at ambient and higher pressures. The intensity of the infrared (IR) active modes is calculated (Eq.2.77) in terms of the BECs and the phonon polarization vectors (Baroni *et al*., 2001). The computed IR spectra of RuC-Zinc blende system at ambient pressure and 50 GPa are given in figure 6.13. No experimental measurements of IR spectra are available for the Ruthenium Carbide systems for comparison. The single peak, corresponding to a 3-fold degenerate mode T_2, at 572.8 cm^{-1} at ambient pressure shifts to 713.45 cm-1 as pressure increases to 50 GPa. This is expected as the phonon frequencies have increased with pressure. This computation provides the trend in the variation of IR spectrum of RuC-Zinc blende up to the limiting pressure of its mechanical stability.
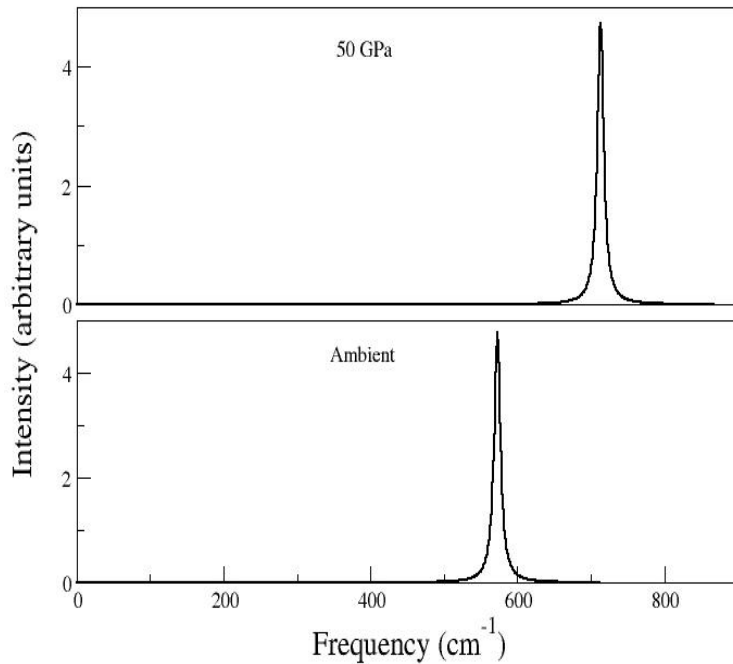
Fig. 6.13: IR spectrum of RuC-Zinc blende.

6.2.6. Hardness

Using the semi-empirical microscopic model of hardness based on the bond strength of a crystal proposed by Šimůnek and Vackář (2006) and Šimůnek (2007, 2009), we have estimated the hardness of the stable Ruthenium Carbide systems at ambient pressure (section 5.2.6.1). Here we further analyze how the hardness values of

these systems changes with pressure. For Ru_3C-Hexagonal system, we have slightly deviated here from the procedure adopted at ambient pressure of separately estimating their contributions to bond strength. Here we take the average of all Ru-Ru bond lengths in the unit cell and specify $n_1=13$. As two out of the three Ru atoms in the unit cell belong to this type and the difference in Ru-Ru bond lengths between the two types is very small, only an insignificant error is introduced by this approximation. As no structural transition is brought about by the pressure on these systems, the values of neighbours and the number of bonds per unit cell remain the same for all the pressures in the range 0-200 GPa. The only changes are in the bond lengths and the volume. For each pressure the average bond lengths of Ru–Ru bond (d_{11}), Ru–C bond (d_{12}) and C–C bond (d_{22}), the volume of the unit cell (Ω) and the calculated value of hardness are presented in table 6.5.

Table 6.5: The average bond lengths (in Å), unit cell volume (in Å^3) and the hardness (in GPa) at different pressures

	Pressure (GPa)	Ru-Ru bond d_{11}	Ru-C bond d_{12}	C-C bond d_{22}	Volume Ω	Hardness
RuC- Zinc blende	0		1.9765		95.127	36.66
	50		1.8856		82.576	44.27
RuC- Rhombohedral	0	2.8208	2.0484	1.3995	42.281	21.15
	50	2.6751	1.9839	1.3600	37.239	24.88
	100	2.5916	1.9412	1.3302	34.302	27.66
	150	2.5318	1.9087	1.3062	32.228	30.00
	200	2.4849	1.8823	1.2862	30.632	32.05
Ru_3C- Hexagonal	0	2.7482	2.1130		47.809	11.49
	50	2.6560	2.0462		42.439	13.38
	100	2.5959	2.0018		39.241	14.80
	150	2.5506	1.9680		36.968	15.98
	200	2.5139	1.9406		35.210	17.02

The bond lengths and volume decrease with pressure and this leads to consistent increase in hardness with pressure as predicted by this model. Hardness is maximum for RuC-Zinc blende at 50 GPa, where its value reaches the superhard region ($H_V > 40$ GPa). However, it has been shown in the previous sections that the synthesis of RuC-Zinc blende at ambient pressure or around 50 GPa may not be experimentally achievable and it is mechanically unstable around this pressure. The higher value only shows that the hardness of RuC-Zinc blende increases up to a pressure of around 30 GPa, the possible limiting pressure of its mechanical stability. RuC-Rhombohedral, which is the ground state structure of RuC stoichiometry, seems to be the suitable candidate for a superhard material among Ruthenium Carbide systems. Its hardness reaches a significantly high value of 30 GPa at the pressure of 150 GPa, where its synthesis can be achieved with sufficiently high temperature. The increased metallic component causes the hardness to decrease for Ru_3C stoichiometry, as expected.

6.2.7. Thermodynamic Properties

Within the harmonic approximation thermal properties due to phonons, such as internal energy (E), constant–volume heat capacity (C_v), Helmholtz free energy (F) and entropy (S) are evaluated from phonon data over a range of temperatures from the standard equations of statistical mechanics (Eqns.(2.69)-(2.73)) using the PHONOPY code. These properties are calculated for different pressures in the range 0-200 GPa and the results at well separated pressures are presented along with those at ambient pressure in figures 6.14–6.16. The Helmholtz free energy (F) and the internal energy (E) increase with pressure while the entropy (S) and the specific heat at constant volume C_v decrease. As entropy is derived as the negative of the temperature derivative of free energy, the pronounced variation of the free energy with pressure is reflected in entropy. Similarly, as specific heat is derived as the temperature derivative of internal energy, both are influenced to a lesser degree by the application of pressure. These three systems exhibit similar variations of F, S, E and C_v with temperature. Both the entropy and the specific heat follow the expected pattern in their temperature variation, both becoming zero as

117
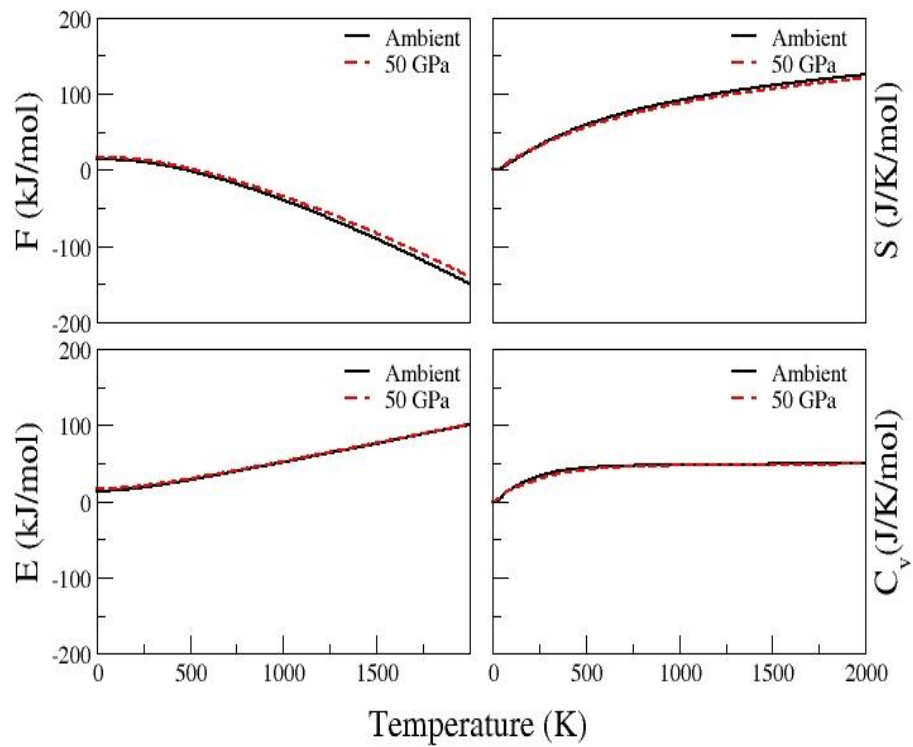
Fig.6.14: Thermal properties of RuC-Zinc blende.
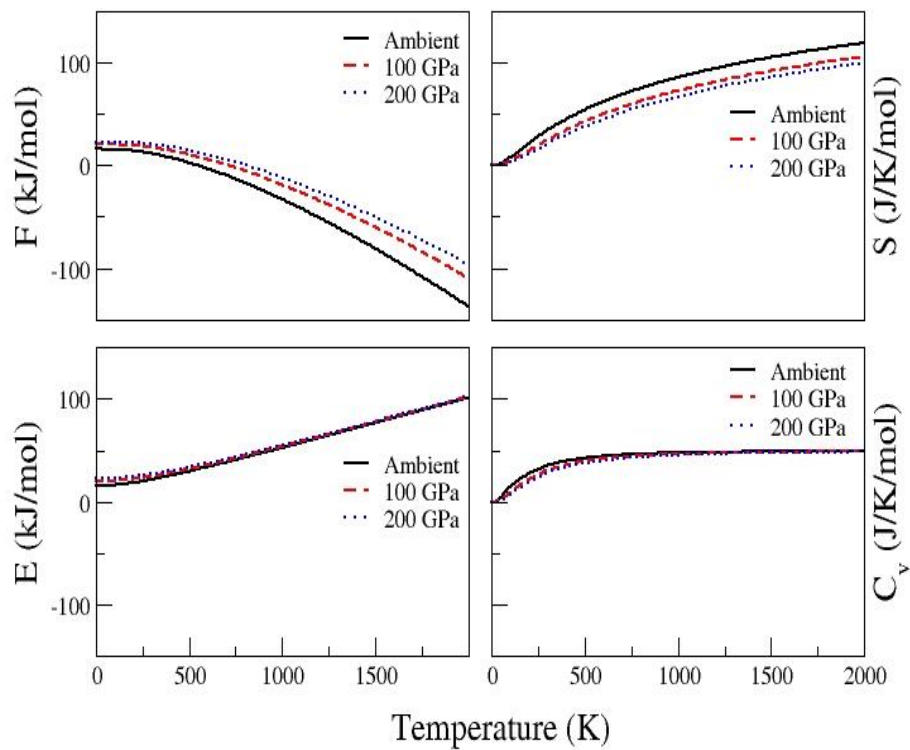
Fig. 6.15: Thermal properties of RuC-Rhombohedral.
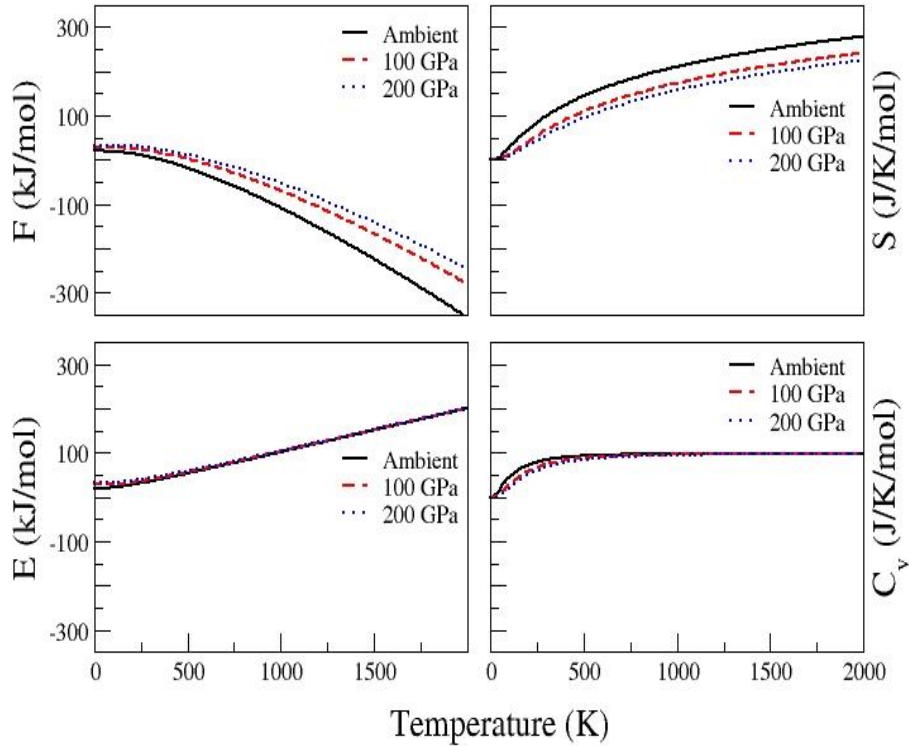
Fig.6.16: Thermal properties of Ru$_3$C-Hexagonal.

temperature approaches zero value. In the given pressure range specific heat at constant volume obeys Dulong–Petit law at very high temperatures and Debye–T^3 law at very low temperatures.

6.3. SUMMARY

The five structures obtained from the evolutionary algorithm based structure search of Ruthenium Carbide systems in the stoichiometries RuC, Ru$_2$C and Ru$_3$C are relaxed at different pressures in the range 0-300 GPa. The trend in the variation of formation enthalpies with pressure and the thermal energy corresponding to formation enthalpy per atom imply that the synthesis of RuC-Zinc blende may not be achievable at ambient pressure and higher pressures. The other four systems can be synthesized at different pressures and sufficiently high temperatures. In particular, Ru$_2$C-Rhombohedral can be synthesized at around 300 GPa and Ru$_3$C-Hexagonal at around 175 GPa. The monotonous decrease in the normalized unit cell volume and the lattice constants with

pressure show that no structural transition is present for these up to a pressure of 200 GPa. The variation of properties with pressure in the range 0-200 GPa is further investigated for three of these systems that are dynamically stable at ambient pressure. From the computed values of elastic constants at different pressures, it is established that RuC-Zinc blende system does not satisfy the Born-Huang criteria for mechanical stability close to 30 GPa whereas RuC-Rhombohedral and Ru_3C-Hexagonal systems are mechanically stable and ductile in the range 0-200 GPa. The analysis of phonons proves that RuC-Zinc blende is dynamically unstable at 100 GPa while the other two systems retain dynamical stability up to 200 GPa. The spreading of electronic bands and partial density of states with pressure show that the band gap increases with pressure for the semiconducting RuC-Zinc blende system. The pressure-induced shift in the pseudo-gap at the Fermi level of the density of states is unfavourable for RuC-Rhombohedral while it is advantageous for Ru_3C-Hexagonal. The IR spectrum of RuC-Zinc blende system is generated using the phonon data and the computed Born effective charge tensor of this system at 50 GPa and it is noted that the IR frequency increases with pressure. The hardness values of the three systems are estimated using a semi-empirical model based on bond strength and it is observed that hardness of all these systems consistently increases with pressure. Hardness of RuC-Zinc blende increases towards the superhard regime up to the limiting pressure of 30 GPa beyond which it can be mechanically unstable while hardness of RuC-Rhombohedral becomes a high value of 30 GPa at the pressure of 150 GPa. The variation with pressure in Helmholtz free energy, internal energy, entropy and specific heat at constant volume of the three systems is estimated from the phonon data within the harmonic approximation.

Chapter 7

CONCLUSIONS AND FUTURE WORK

7.1. CONCLUSIONS

7.1.1. $B_{12}C_3$ Stoichiometry

The ground state structure of $B_{12}C_3$ has been an active problem because of the absence of experimental detection of structure with Cm symmetry as predicted by DFT calculations. In an attempt to settle this issue an exhaustive structure search is done in $B_{12}C_3$ and six distinct structures are obtained. Their ground state properties are investigated by DFT calculations. The conclusions derived from this work are the following :

- The first independent confirmation using structure search is obtained that $B_{11}C^p(CBC)$ is the ground state structure of $B_{12}C_3$ stoichiometry.

- It is established that mechanically and dynamically stable structures with base-centered monoclinic symmetry can be at thermodynamical equilibrium at temperatures up to 660 K. This provides direction and motivation for the experimentalists for further attempting the search for monoclinic symmetry in the ground state of $B_{12}C_3$ in experimental measurements.

- The very good correlation between the experimental IR spectrum and the cumulative spectrum of four of the systems with Cm symmetry obtained from structure search implies that signatures of Cm symmetry can be detected among the experimental data.

- The negative formation energy and the good correlation with the experimental data of elastic moduli, band gap and IR spectrum for the structure with 30-atom unit cell yielded by the structure search raises the possibility of such structures with larger cells in the ground state structure of $B_{12}C_3$. It may even be possible

that a significant mode of the existence of even $B_{11}C^p$(CBC), the established ground state structure of this stoichiometry, could be through its presence as a structural component in such larger unit cells.

- The hardness of four of the $B_{12}C_3$ systems are close to the superhard regime, underlying their technological importance.

7.1.2. $B_{13}C_2$ Stoichiometry

There has been no consensus on the ground state structure of $B_{13}C_2$ stoichiometry. Also the discrepancy between the metallic nature of $B_{13}C_2$ predicted by the DFT calculations and its semiconducting nature recorded by the experiments has been a long standing problem in this stoichiometry. The two problems are intertwined, as the computation of electronic structure is based on the crystal structure of the system. The work done in $B_{12}C_3$ stoichiometry using supercells has indicated that superlattice ordering could be the key to solving these twin problems in $B_{13}C_2$ as well. To settle these two problems a structure search using supercells is done in $B_{13}C_2$ and for the lowest energy structure obtained the ground state properties are calculated using DFT. The conclusions from this work are the following :

- The 30-atom-cell structure $(B_{12})(B_{11}C^p)$(CBC)-C-B-B has many of the features of the two major structural candidates proposed in the literature for $B_{13}C_2$. It has both B_{12} cage and the CBC chain from the B_{12}(CBC) structure supported by DFT calculations; it has $(B_{11}C^p)$ cage from $B_{11}C^p$(CBB) structure supported by a group of experimentalists for its capacity to explain some of the trends in the transport properties. The major difference is the absence of (CBB) chain and the configuration of the different structural units. The formation energy of this structure, though positive, is easily accessible in the normal synthesis conditions of $B_{13}C_2$. These features make it a good candidate for the ground state structure of $B_{13}C_2$.

- The semiconducting property of this structure convincingly establishes that this structure with larger unit cell could be the actual ground state structure of $B_{13}C_2$

or, at the least, one of the closest kin. Thus the present work has conclusively solved the problem of the discrepancy between the DFT calculations and the experimental observations over the semiconducting nature of $B_{13}C_2$.

- The good correlation with the experimental data of bond lengths, elastic moduli, band gap and the IR spectrum for this system further strengthens its status as a potential ground state structure.

- The remarkable success of this 30-atom-cell structure in explaining many of the experimental data on $B_{13}C_2$ provides the first definitive evidence that structures with larger unit cells, that cannot be reduced to any smaller cells, are associated with crystals of $B_{13}C_2$ stoichiometry even at the ground state.

7.1.3. Ruthenium Carbides at ambient pressure

The widely varying structures proposed for Ruthenium Carbides from experimental reports of synthesis, computational modeling and crystal structure search have not resulted in any conclusive structural candidates to be pursued in experiments. To arrive at definitive results about the structure and properties of Ruthenium Carbide over different stoichiometries structure search is performed in RuC, Ru_2C and Ru_3C stoichiometries and the ground state properties of the resulting structures are evaluated using DFT. The following are the conclusions from this work :

- In RuC stoichiometry rhombohedral structure ($R\bar{3}m$) is the ground state structure, with mechanical and dynamical stability. Zinc blende structure is also present in RuC stoichiometry as a higher energy possibility. Both structures reported from experimental synthesis ($P\bar{6}m2$ and $P\bar{3}m1$) have emerged from structure search at stoichiometries different from the reported ones. This is plausible in the light of the high pressure and/or high temperature required for their synthesis and the difficulty in identifying the structure with only a small amount of sample being synthesized.

- Though Trigonal system ($P\bar{3}m1$) in RuC stoichiometry and Rhombohedral system ($R3m$) in Ru_2C stoichiometry are dynamically unstable at ambient pressure both can be stabilized under pressure.

- RuC–Zinc blende system is semiconducting with a band gap of 0.618 eV while the other two stable systems, RuC-Rhombohedral and Ru_3C-Hexagonal are metallic.

- RuC–Zinc blende has a significantly large hardness of 36.66 GPa, very close to the superhard regime. RuC-Rhombohedral has fairly large value of hardness of 21.15 GPa. As the metal to carbon ratio increases, hardness decreases for Ru_3C.

7.1.4. Ruthenium Carbides at High Pressures

The two experimental reports of the synthesis of Ruthenium Carbides have been at high temperature in the first case, and at high pressure and high temperature in the second case. Two of the systems obtained in the structure search in RuC and Ru_2C stoichiometries have been stabilized at high pressure in our work (Harikrishnan *et al*., 2015a) as well as in a previous computational work (Sun *et al*., 2013). Many of the industrial applications of transition metal carbides, in general, are in extreme conditions and this could very well be applicable for Ruthenium Carbides too. A study of the variation of stability and properties of Ruthenium Carbides with pressure would provide helpful indicators and benchmarks for future experimental investigations. It would also help in the optimum utilization of experimental resources. With this motivation we have conducted a detailed analysis of the pressure-induced variation of the structural, elastic, dynamical, electronic, thermodynamic properties and hardness of the three stable Ruthenium Carbide systems with pressure and deduced the following conclusions :

- RuC-Zinc blende system cannot be synthesized by increasing the pressure. Even at ambient pressure it may not be synthesized by increasing the temperature. It is conclusively proved that this system is mechanically unstable at around 30 GPa and dynamically unstable at around 100 GPa. RuC-Zinc blende, one of the most

124

extensively studied system in the theoretical modeling of Ruthenium Carbides in RuC stoichiometry, can be dropped from the status of potential structural candidate in future experimental investigations.

- RuC-Rhombohedral system is stable in the pressure range 0-200 GPa. Beyond 200 GPa it could be mechanically unstable. The optimum pressure for its synthesis is 50 GPa, but it can be synthesized even at ambient pressure by providing sufficiently high temperature.

- Ru_3C-Hexagonal system is stable in the pressure range 0-200 GPa and even beyond that. Its formation energy is nearly zero at around 175 GPa. Even at lower values of pressure it can be synthesized by increasing the temperature to the required limit. Its stability is further indicated by the formation of a pseudo-gap in its electronic density of states at the Fermi level with the application of pressure.

- No structural phase transition is possible for these three systems in the pressure range 0-200 GPa.

- Hardness of RuC-Zinc blende increases to nearly superhard regime in the pressure range 0-30 GPa and the hardness of RuC-Rhombohedral increases to 30 GPa at the pressure of 150 GPa. For high pressure applications beyond 30 GPa RuC-Rhombohedral is a better candidate than RuC-Zinc blende.

7.2. FUTURE WORK

This work has shown the paths for extending the investigation in the case of both Boron Carbides and Ruthenium Carbides. The following are the main avenues to be pursued :

- More experimental signatures like Raman spectrum, NMR spectrum etc. can be computed and compared with the experimental measurements to look for the presence of monoclinic symmetry in the ground state of $B_{12}C_3$. While computing these spectra the cumulative effect of different structural models should be taken into account, as shown in this work.

- The presence of structures with larger unit cells consisting of 30 atoms, 45 atoms, 60 atoms etc. should be pursued at the ground state of $B_{12}C_3$ stoichiometry. The indication that even an established structural model like $B_{11}C^p$(CBC) could be mostly present in the composition of $B_{12}C_3$ as a structural unit of such larger-cell systems should be further investigated in detail.

- With the convincing evidence of the existence of structures with larger unit cells in the ground state of $B_{13}C_2$ stoichiometry, more detailed investigation for such larger-cell systems should be carried out in this stoichiometry.

- It has become clear that exhaustive crystal structure search is the sure route to the solutions of many of the problems identified in Boron Carbide systems. Structure search can be attempted in the entire homogeneity range of Boron Carbides addressing unsolved problems at both boron-rich and carbon-rich ends. A special emphasis should be on the structures with larger unit cells, instead of confining the search on the cells accommodating the minimum number of atoms in each stoichiometry.

- Structure search can be attempted in RuC_2 and RuC_3 stoichiometries looking for harder variants of Ruthenium Carbides. It is expected that with the increase in carbon concentration, the hardness could be higher for these stoichiometries.

Appendix I

PARAMETERS EVOLUTIONARY ALGORITHM

% In this file the parameters of the evolutionary algorithm can be set. Please keep the format as it is - only change the values!!!

USPEX : calculationMethod (USPEX, VCNEB, META)

```
*******************************************
*     TYPE OF RUN AND SYSTEM          *
*******************************************
```

1   : calculationType (1 = bulk, 2 = clusters, 4 = varcomp bulk, 11 = molecular crystals)

% Possible symmetry of the randomly created structures; space groups fo crystals, point groups for clusters

% symmetries

2-230

% endSymmetries

% optimisation criteria

enthalpy : optType (optimise by: enthalpy, volume, hardness, struc_order, aver_dist, mag_moment)

% numbers of ions of each type

% numIons

12 3

% EndNumIons

% Here come the atomic numbers of the atoms involved

% atomType

5 6

% EndAtomType

% For hardness/softmutation, define the next few parameters (valence, etc)

% valencies

3 4

% endValencies

% bonds with valence strength above this value are always included into hardness formula. Need either matrix (like minDist) or a single value

%%%%%%%%%%%%%%%

% goodBonds

0.15

% EndGoodBonds

%%%%%%%%%%%%%%%

1   : checkConnectivity   % 1 = default; 0 - use only for large systems, switches off hardness calculation and connectivity criteria in softmutation

```
*****************************************
*          POPULATION          *
*****************************************
```

30   : populationSize (how many individuals per generation)

30   : initialPopSize (how many individuals in the first generation - if =0 then equal to the size specified above)

25   : numGenerations (how many generations shall be calculated)

25   : stopCrit (max number of generations with the same best structure before stoppage)

```
*****************************************
* SURVIVAL OF THE FITTEST AND SELECTION *
*****************************************
```

3   : keepBestHM (how many structures should survive and compete in the next generation)

1   : reoptOld (should the old structures be reoptimized? 1:yes, 0:no)

0.6   : bestFrac (What fraction of current generation shall be used to produce the next generation)

1   : dynamicalBestHM

```
*****************************************
*        VARIATION OPERATORS          *
*****************************************
```

0.50 : fracGene (fraction of generation produced by heredity)

0.10 : fracRand (fraction of generation produced randomly from space groups specified by user)

1.0   : percSliceShift (fraction of heredity-produced structures with shifts in all dimensions)

0.2   : fracPerm

0.1   : fracAtomsMut (fraction of the generation produced by softmutation)

% the following parameter describes the maximal atomic displacement amplitude in softmutation

2.5   : mutationDegree

% softMutOnly (what generations are produced by softmutation only, format : 1-3 5 7-9 15 etc)

0

% EndSoftOnly

200   : softMutTill (starting from this generation we use coormutation as atom mutation

% percentage of structures produced by lattice mutation = 1.0-(FracGene+FracPerm+FracRotMut)

% so don't need to specify explicitly

0.50 : mutationRate (standard deviation of the epsilons in the strain matrix)

1.00 : DisplaceInLatmutation

****

*   CONSTRAINTS   *

****

1.7   : minVectorLength (minimal length of any lattice vector)

%%%%%%%%%%%%%%

% IonDistances

0.8 0.8

0.8 0.8

% EndDistances

%%%%%%%%%%%%%%

% Above is the inter-atomic distance matrix of the different ion types. IMPORTANT: If only 1 value present, this is taken as DISTANCE, NOT radius!!!

%%%%%%%%%%%%%%%

****

*   CELL   *

****

% The following is what you know about the lattice. If you know the lattice vectors,

% type them in as 3x3 matrix. If not, type the estimated volume.

% Latticevalues (this word MUST stay here, type values below)

110.00

% Endvalues (this word MUST stay here)

% splitInto (possible number of atoms per one subcell)

1

% EndSplitInto

```
*****************************************

*          RESTART              *

*****************************************
```

1   : pickUpYN (if pickUpYN~=0 , then a previous calculation will be continued)

7   : pickUpGen (at which generation shall the previous calculation be picked up? If = 0 , then a new calculation is started)

0   : pickUpFolder (number of the results folder to be used. If = 0 , then the highest existing number is taken)

```
*****************************************

*  DETAILS OF AB INITIO CALCULATIONS   *

*****************************************
```

abinitioCode (which code from CommandExecutable shall be used for calculation? vasp (1), siesta (2), gulp (3), etc)

1 1 1 1

ENDabinit

% numProcessors (how many processors per calculation)

12 12 12 12

% EndProcessors

%Resolution for KPOINTS - one number per step or just one number in total)

% KresolStart

0.14 0.10 0.08 0.06

% Kresolend

200:00 : wallTime (max time for each calculation)

30   : numParallelCalcs (how many parallel calculations shall be performed)

%%%%%%%%%%%%%%%%

% What follows is the unix command to call optimizer - exactly as you would type it in the terminal, supported: vasp, siesta, gulp, mol_gulp, mol_siesta, MD, NeuralNetworks, mol_dmacrys, cp2k, QuantumEspresso, mol_dlpoly, mol. VASP, ASE, ATK

% commandExecutable

mpirun -np 4 /home/msg/valsa/vasp-bin/vasp.5.2.12-col-acml-ifort >> log

siesta

./job3_gulpNP

job2

siesta<input.fdf

./meam-lammps_han test.tcl

timelimit -t 400 ./OptimizeNN.x > log

timelimit -t 400 ./dmacrys <mol.res.dmain >output

mpirun -np 4 cp2k.popt cg.inp > cp2k_output

mpirun -np 4 pw.x < qe.in > output

reserved for DL POLY executable

molecular VASP

ASE executable

atkpython < ATK.in > ATK.out

% EndExecutable

%%%%%%%%%%%%%%%%

1   : doSpaceGroup (0 - no space group, 1 - calculate space groups)

****

*   HARDWARE-RELATED   *

****

2   : remoteRegime (0 - no remote, 1 - from Talc, 2 - remote using specially prepared file, see manual)

igc_neha : whichCluster (on which cluster are calculations performed? E.g. SIESTAlocal, xcom, MVS50k, BJremote, Skif, ABAX, CFN, nonParallel, neolith)

24   : maxErrors (how many errors is one individual allowed to produce before he is killed)

****

%   REMOTE SETTINGS (only if REMOTE>1)   *

****

valsa   : username (user name to login to remote supercomputer)

/home/msg/valsa/ : remotePath (user home folder at supercomputer)

22   : portNumber

USPEX-9.1.0/Hari/B4C-15-ns2   : localFolder (TALC folder)

30r : remoteFolder (remote folder)

****

%   FINGERPRINTS SETTINGS   *

****

0.05 : sigmaFing

0.10 : deltaFing

10.0 : RmaxFing

0.080 : toleranceFing (if distance is less than tolerance - structures are identical)

0.080 : toleranceBestHM

0.2   : maxDistHeredity

****
*

*   END OF INPUT   *

****
*

ATOMIC POSITIONS

Table A II.1: Atomic positions of Boron Carbide systems with 15-atom unit cell in $B_{12}C_3$ stoichiometry.

	$B_{11}C^p$(CBC)	$B_{11}C^e$(CBC)	14-atom-cage	$B_{10}C^{pe}_2$(CBB)	$B_{11}C^e$(BCC)
2b	B1, B12 (0.3265, 0.3377, 0.1565)	B2, B11 (-0.3732, 0.3373, -0.0526)	B4, B8 (-0.2306, 0.2851, 0.3674)	B1, B11 (0.4050, 0.2549, 0.3452)	B1, B2 (-0.1480, 0.2474, -0.4595)
2b	B2, B11 (-0.3424, 0.3392, 0.1350)	B3, B12 (0.0207, 0.2566, 0.1504)	B5, B10 (-0.4553, 0.1365, -0.4658)	B2, B3 (-0.3745, 0.1618, -0.4692)	B3, B10 (0.4626, 0.2554, -0.0677)
2b	B3, B6 (0.0520, 0.2543, 0.3460)	B4, B9 (-0.2047, 0.1624, -0.0359)	B6, B12 (0.1343, 0.2818, -0.2282)	B4, B5 (-0.2022, 0.3363, -0.4395)	B5, B11 (0.0715, 0.3369, -0.2735)
2b	B7, B8 (-0.0658, 0.2566, -0.0501)	B7, B10 (0.3978, 0.2435, -0.2462)	B7, B11 (-0.0148, 0.1295, 0.1041)	B8, B9 (-0.4789, 0.2562, -0.2553)	B6, B8 (0.2407, 0.1642, -0.2533)
1a	B4 (-0.1981, 0, -0.1680)	B5 (-0.0332, 0, -0.3724)	B1 (-0.2359, 0, 0.1559)	B7 (0.4539, 0, -0.1121)	B4 (0.3972, 0, 0.0637)
1a	B5 (0.1843, 0, 0.4628)	B6 (-0.2330, 0, -0.3584)	B2 (0.4867, 0, -0.1232)	B10 (0.2749, 0, 0.2334)	B9 (0.4151, 0, 0.4095)
1a	B9 (-0.0135, 0, 0.4893)	B8 (0.0441, 0, 0.2859)	B3 (-0.2340, 0, -0.1954)	C1 (-0.3635, 0, -0.1577)	B12 (0.2179, 0, 0.4281)
1a	C1 (-0.0018, 0, -0.1730)	C2 (0.1449, 0, 0.2584)	B9 (0.0474, 0, 0.3325)	C3 (0.4704, 0, 0.2295)	C3 (-0.4204, 0, 0.0253)
1a	C2 (-0.3797, 0, -0.4677)	C1 (-0.4188, 0, 0.3404)	C2, C3 **2b** (0.4000, 0.2913, -0.4981)	C2 (0.0957, 0, -0.0635)	B7 (-0.2350, 0, 0.3068)
1a	B10 (0.4950, 0, -0.3614)	B1 (0.4571, 0, 0.4454)		B6 (-0.0369, 0, 0.0318)	C1 (-0.0997, 0, 0.2320)
1a	C3 (0.3733, 0, -0.2452)	C3 (0.3290, 0, -0.4526)	C1 0.2718, 0, 0.2373)	B12 (-0.1782, 0, 0.1268)	C2 (0.0245, 0, 0.1410)

Table A II.2: Atomic positions of the Bravais cell of $(B_{11}C^p)(B_{10}C^{pe}_2)(CBC)(CBB)$ in $B_{12}C_3$ stoichiometry. Each atom occupies 1a site.

Atoms	Wyckoff Positions	Atoms	Wyckoff Positions
B_1	-0.34318, 0.04598, 0.19888	B_{16}	0.49497, 0.20614, 0.02361
B_2	-0.14530, 0.04827, -0.02557	B_{17}	-0.00414, -0.29266, -0.47891
B_3	-0.02977, -0.45218, 0.22199	B_{18}	0.10371, -0.19518, 0.20795
B_4	0.32552, 0.38216, 0.17112	B_{19}	-0.39534, -0.20879, -0.28881
B_5	0.10155, 0.29262, 0.21158	B_{20}	0.32721, -0.29702, 0.16488
B_6	-0.33774, -0.45144, 0.33744	B_{21}	0.47247, 0.04293, -0.27515
B_7	0.35199, -0.45603, 0.46887	B_{22}	0.48771, -0.11627, 0.02700
B_8	-0.16957, -0.11093, -0.32771	B_{23}	0.16294, 0.05008, -0.15507
B_9	-0.27934, 0.30096, -0.01263	B_{24}	-0.27748, -0.20692, -0.01032
B_{10}	0.15385, -0.45620, -0.30833	C_1	0.04125, 0.05052, 0.08490
B_{11}	0.21546, 0.29098, 0.49010	C_2	-0.32932, 0.04813, -0.47581
B_{12}	0.28624, 0.02178, -0.40972	C_3	-0.21102, -0.45411, 0.10643
B_{13}	-0.39748, 0.30199, -0.29191	C_4	0.21963, -0.21798, 0.47074
B_{14}	-0.17297, 0.20997, -0.32820	C_5	0.16729, -0.45083, 0.01884
B_{15}	-0.00612, 0.38713, -0.47795	C_6	-0.45979, -0.45079, -0.42406

Table A II.3: Atomic positions of the 60-atom Bravais cell of $(B_{12})(B_{11}C^P)(CBC)$-C-B-B in $B_{13}C_2$ stoichiometry

Atoms	Wyckoff Positions		Atoms	Wyckoff Positions	
	4b : (x, y, z), (x+1/2, y+1/2, z), (x, -y, z), (x+1/2, -y+1/2, z)				
	2a : (x, 0, z), (x+1/2, 1/2, z)				
B1, B12, B27, B38	4b	0.28381, 0.33583, 0.58648	B17, B43	2a	0.52946, 0, 0.42585
B2, B13, B28, B39	4b	0.01855, 0.33514, 0.07018	B18, B19, B44, B45	4b	0.17724, 0.33968, 0.38851
B3, B16, B29, B42	4b	0.17628, 0.24061, 0.18598	B20, B46	2a	0.42822, 0, 0.21777
B4, B30	2a	0.77404, 0, 0.23916	B21, B47	2a	0.67979, 0, 0.05047
B5, B25, B31, B51	4b	0.02401, 0.25005, 0.28412	B22, B48	2a	0.82225, 0, 0.42955
B6, B11, B32, B37	4b	0.27853, 0.23894, 0.78227	B24, B50	2a	0.03248, 0, 0.77359
B7, B33	2a	0.95722, 0, 0.33823	B26, B52	2a	0.22820, 0, 0.99693
B8, B9, B34, B35	4b	0.94077, 0.26580, 0.69589	C1, C5	2a	0.26391, 0, 0.17075
B10, B36	2a	0.67788, 0, 0.70553	C2, C6	2a	0.77075, 0, 0.89642
B14, B40	2a	0.94659, 0, 0.57498	C3, C7	2a	0.51501, 0, 0.63435
B15, B23, B41, B49	4b	0.93381, 0.16465, 0.90701	C4, C8	2a	0.19723, 0, 0.81857

Appendix III

HARDNESS MODEL

Computational parameters of the hardness model based on bond strength for the Boron Carbide systems in $B_{12}C_3$ and $B_{13}C_2$ stoichiometries are given in two tables here.

Table A III.1: Computational parameters of the bond strength model for the hardness of Boron Carbide systems in $B_{12}C_3$ stoichiometry

Type of Bond			$B_{11}C^p$ (CBC)	$B_{11}C^e$ (CBC)	$B_{10}C^{pe}_2$ (CBB)	$B_{11}C^e$ (BCC)	14-atom cage
$B^{pol.}/B^{eq.}$	Intericosahedron	$b_{11}^{(3)}$	2	3	2	3	3
n_1=6		$s_{11}^{(3)}$	0.04936	0.04966	0.04902	0.04991	0.05015
	Equatorial hexagon	$b_{11}^{(4)}$	6	4	4	4	26
		$s_{11}^{(4)}$	0.04897	0.04898	0.04884	0.04875	0.04680
	Polar-equatorial	$b_{11}^{(5)}$	15	15	12	15	
		$s_{11}^{(5)}$	0.04777	0.04776	0.04764	0.04808	
	Polar triangle	$b_{11}^{(6)}$	4	6	4	6	
		$s_{11}^{(6)}$	0.04722	0.04785	0.04718	0.04729	
$C^{pol.}/C^{eq.}$	Intericosahedron	$b_{12}^{(3)}$	1		1		2
n_2=6		$s_{12}^{(3)}$	0.05682		0.05732		0.05764
n_1=6	Equatorial hexagon	$b_{12}^{(4)}$		2	2	2	10
		$s_{12}^{(4)}$		0.05497	0.05556	0.05551	0.05433
	Polar-equatorial	$b_{12}^{(5)}$	3	3	6	3	
		$s_{12}^{(5)}$	0.05375	0.05335	0.05399	0.05432	
	Polar triangle	$b_{12}^{(6)}$	2		2		
		$s_{12}^{(6)}$	0.05353		0.05402		
B^{end}	Intrachain	$b_{11}^{(1)}$			1		
n_1=4		$s_{11}^{(1)}$			0.25355 (n_1'=2)		
n_1'=2,6		$b_{12}^{(1)}$				1	
n_2=2,6		$s_{12}^{(1)}$				0.30104 (n_2=2)	
	Chain-icosahedron	$b_{11}^{(2)}$			2	2	
		$s_{11}^{(2)}$			0.07612 (n_1'=6)	0.07352 (n_1'=6)	
		$b_{12}^{(2)}$			1	1	
		$s_{12}^{(2)}$			0.08890 (n_2=6, $d_{12}^{(2)}$=1.5714)	0.08861 (n_2=6, $d_{12}^{(2)}$=1.5765)	
C^{end}	Intrachain	$b_{12}^{(1)}$	2	2	1		
n_2=4		$s_{12}^{(1)}$	0.29433 (n_1=2)	0.29183 (n_1=2)	0.29159 (n_1=2)		
n_2'=2,6		$b_{22}^{(1)}$				1	
n_1=2,6		$s_{22}^{(1)}$				0.40115 (n_2'=2)	
	Chain-icosahedron	$b_{12}^{(2)}$	6	5	3	3	4
		$s_{12}^{(2)}$	0.08788 (n_1=6)	0.08750 (n_1=6)	0.08775 (n_1=6, $d_{12}^{(2)}$=1.5921)	0.08516 (n_1=6, $d_{12}^{(2)}$=1.6406)	0.08975 (n_1=6)
		$b_{22}^{(2)}$		1			
		$s_{22}^{(2)}$		0.11775 (n_2'=6)			
Volume (Å^3)		Ω	105.23	105.66	105.66	107.49	104.55
Hardness (GPa)		H^b	37.74	37.84	37.10	38.00	33.07

Table A III.2: Computational parameters of the bond strength model for the hardness of $(B_{12})(B_{11}C^p)(CBC)\text{-}C\text{-}B\text{-}B$ in $B_{13}C_2$ stoichiomtery

Type of Bond				
$B^{pol.}/B^{eq.}$	intericosahedron		$b_{11}^{(6)}$	4
$n_1=6$			$s_{11}^{(6)}$	0.04790
	polar-equatorial	B_{12} cage	$b_{11}^{(7a)}$	18
			$s_{11}^{(7a)}$	0.04757
		$B_{11}C^p$ cage	$b_{11}^{(7b)}$	15
			$s_{11}^{(7b)}$	0.04811
	equatorial hexagon	B_{12} cage	$b_{11}^{(8a)}$	6
			$s_{11}^{(8a)}$	0.04842
		$B_{11}C^p$ cage	$b_{11}^{(8b)}$	6
			$s_{11}^{(8b)}$	0.04682
	polar triangle	B_{12} cage	$b_{11}^{(9a)}$	6
			$s_{11}^{(9a)}$	0.04697
		$B_{11}C^p$ cage	$b_{11}^{(9b)}$	4
			$s_{11}^{(9b)}$	0.04600
$C^{pol.}$	intericosahedron		$b_{12}^{(6)}$	1
$n_2=6, n_1=6$			$s_{12}^{(6)}$	0.05752
	polar-equatorial	$B_{11}C^p$ cage	$b_{12}^{(7b)}$	3
			$s_{12}^{(7b)}$	0.05394
	polar triangle	$B_{11}C^p$ cage	$b_{12}^{(9b)}$	2
			$s_{12}^{(9b)}$	0.05095
C^{end}	Intra chain		$b_{12}^{(1)}$	2
$n_2=4, n_1=2, 6$			$s_{12}^{(1)}$	0.29429 ($n_1=2$)
	Chain-icosahedron		$b_{12}^{(2)}$	6
			$s_{12}^{(2)}$	0.08705 ($n_1=6$)
$B22^{int.}$	interstitial-		$b_{11}^{(3)}$	7
$n_1=7, n_1'=6$	icosahedron		$s_{11}^{(3)}$	0.04488
$C3^{int.}$	interstitial-		$b_{12}^{(4)}$	4
$n_2=4, n_1=6$	icosahedron		$s_{12}^{(4)}$	0.08526
$B7^{int.}$	interstitial-		$b_{11}^{(5)}$	4
$n_1=5, n_1'=6$	icosahedron		$s_{11}^{(5)}$	0.05780
Volume (Å^3)			Ω	220.11
Hardness(GPa)			H^b	33.76

REFERENCES

Abidri, B., Rabah, M., Rached, D., Baltache, H., Rached, H., Merzoug, I. and Djili, S. (2010). "Full potential calculation of structural, elastic properties and high-pressure phase of binary noble metal carbide: Ruthenium carbide." *J. Phys. Chem. Solids*, 71, 1780-1784.

Abrahams, S. C. and Hsu, F. S. L. (1975). "Debye temperatures and cohesive properties." *J. Chem. Phys.*, 63, 1162-1165.

Amberger, E. and Stumpf, W. (1981). *Gmelin Handbook of Inorganic Chemistry*, ed. K.-C. Buschbeak, Pp. 112–238, Springer, Berlin.

Anderson, O. L. (1963). "A simplified method for calculating the debye temperature from elastic constants." *J. Phys. Chem. Solids,* 24(7), 909-917.

Armstrong, D. R., Balland, J., Pukins, P. G and Kirfel, A. (1983). "The Nature of the chemical bonding in boron barbide. IV. Electronic band structure of boron carbide, $B_{12}C_2$, and three models of the structure $B_{12}C_3$." *Acta Cryst. B*, 39, 324–329.

Aselage, T. L., Emin, D. and McCready, S. S. (2000). "Bipolaron hopping conduction in boron carbides." *Phys. Status Solidi. B*, 218(1), 255–258.

Aselage, T.L. and Tissot, R.G. (1992). "Lattice constants of boron carbide." *J. Am. Ceram. Soc.*, 75(8), 2207–2212.

Aydin, S. and Simsek, M. (2009). "Hypothetically superhard boron carbide structures with a $B_{11}C$ icosahedron and three-atom chain." *Phys. Status Solidi B*, 246 (1), 62–70.

Balakrishnarajan, M. M., Pancharatna, P.D. and Hoffmann, R. (2007). "Structure and bonding in boron carbide: The invincibility of imperfections." *New J. Chem.*, 31(4), 473–485.

Baroni, S., de Gironcoli, S., Corso, A.D. and Giannozzi, P. (2001). "Phonons and related properties of extended systems from density-functional perturbation theory." *Rev. Mod. Phys*., 73, 515-562.

Baroni, S., Giannozzi, P. and Testa, A. (1987). "Green's-function approach to linear response in solids." *Phys. Rev. Lett.,* 58(18), 1861-1864.

Blochl, P.E. (1994). "Projector augmented-wave method." *Phys. Rev. B,* 50, 17953-17980.

Born, M. and Huang, K. (1956). *Dynamical theory of crystal lattices*, Clarendon, Oxford.

Bylander, D. M., Kleinman, L. and Lee, S.B. (1990). "Self-consistent calculations of the energy bands and bonding properties of $B_{12}C_3$." *Phys. Rev. B*, 42(2), 1394–1403.

Bylander, D.M. and Kleinman, L. (1991). "Structure of $B_{13}C_2$." *Phys. Rev. B*, 43(2), 1487–1491.

Calandra, M., Vast, N., Mauri, F. (2004). "Superconductivity from doping boron icosahedra." *Phys. Rev. B*, 69(22), 224505-01-05.

Ceperley, D. M. and Alder, B. J. (1980). "The homogeneous electron gas; Ground state of the electron gas by a stochastic method." *Phys. Rev. Lett.*, 45, 566-569.

Chauhan,M. and Gupta, D.C. (2013). "Electronic, mechanical, phase transition and thermo-physical properties of TiC, ZrC and HfC: High pressure computational study." *Diamond Relat. Mater*., 40, 96-106.

Chen, X-Q, Niu, H, Li, D. and Li, Y. (2011). "Modeling hardness of polycrystalline materials and bulk metallic glasses." *Intermetallics*, 19, 1275–1281.

Chung, H. Y., Weinberger, M.B., Levine, J.B., Kavner, A., Yang, J. M., Tolbert, S. H. and Kaner, R. B. (2007). "Synthesis of ultra-incompressible superhard rhenium diboride at ambient pressure." *Science,* 316(5823), 436-439.

Crowhurst, J.C., Goncharov, A. F., Sadigh, B., Evans, C. L., Morrall, P. G., Ferreira, J. L. and Nelson, A. J. (2006). "Synthesis and characterization of the nitrides of Platinum and Iridium." *Science,* 311(5765), 1275-1278.

Deus, P. and Schneider, H. A. (1983). "Estimation of the debye temperature of diamond-like semiconducting compounds from bulk modulus and microhardness." *Cryst. Res. Technol.*, 18(4), 491-500.

Dieter, G. E. (1988). *Mechanical Metallurgy*, SI Metric edn., McGraw-Hill.

Domnich, V., Gogotsi, Y., Trenay, M. and Tanaka, T. (2002). "Nanoindentation and Raman spectroscopy studies of boron carbide single crystals." *Appl. Phys. Lett.*, 81(2), 3783-3785.

Domnich, V., Reynaud, S., Haber, R. A. and Chhowalla, M. (2011). "Boron carbide: Structure, properties, and stability under stress." *J. Am. Ceram. Soc.*, 94(11), 3605-3628.

Ektarawong, A., Simak, S. I., Hultman, L., Birch, J. and Alling, B. (2015). "Configurational order-disorder induced metal-nonmetal transition in $B_{13}C_2$ studied with first-principles superatom-special quasirandom structure method." *Phys. Rev. B*, 92, 014202-1-12.

Ektarawong, A., Simak, S. I., Hultman, L., Birch, J. and Alling, B. (2014). "First-principles study of configurational disorder in B_4C using a superatom-special quasirandom structure method." *Phys. Rev. B*, 90, 024204-1-11.

Emin, D. (1988). "Structure and single-phase regime of boron carbides." *Phys. Rev. B*, 38(9), 6041–6055.

Fan, C. Z., Zeng, S.Y., Zhan, Z. J., Liu, R. P., Wang, W.K., Zhang, P. and Yao, Y.G. (2006). "Low compressible noble metal carbides with rocksalt structure: *Ab initio* total energy calculations of the elastic stability." *Appl. Phys. Lett.,* 89, 071913-071916.

Fanchini, G., McCauley, J. W. and Chhowalla, M. (2006). "Behavior of disordered boron carbide under stress." *Phys. Rev. Lett.*, 97(3), 035502-1-4.

Feng, Y. J., Seidler, G. T., Cross, J. O., Macrander, A. T. and Rehr, J. J. (2004). "Role of inversion symmetry and multipole effects in nonresonant X-ray Raman scattering from icosahedral B_4C." *Phys. Rev. B*, 69(12), 125402-1-8.

Field, J. E. (1992). *The properties of natural and synthetic diamond,* Academic, London.

Fock, V. (1930). "Näherungsmethode zur Lösung des quantenmechanischen Mehrkörperproblems." Z. *Phys.*, 61, 126-148.

Fu, H., Penga, W. and Gaob, T. (2009). "Structural and elastic properties of ZrC under high pressure." *Mater. Chem. Phys.,* 115, 789-794**.**

Gieske, J. H., Aselage, T. L. and Emin, D. (1991). "Elastic properties of boron carbides." *Boron-Rich Solids. AIP Conf. Proc*., 231, 376–379.

Gilan, J. J. (2009). *Chemistry and physics of mechanical hardness Wiley series on processing of engineering materials,* John Wiley & Sons, New Jersey.

Gilman, J. J., Cumberland, R. W. and Kaner, R. B. (2006). "Design of *hard* crystals." *Int. J. Refract. Met. Hard Mater.,* 24, 1-5.

Glass, C.W., Oganov, A.R. and Hansen, N. (2006). "USPEX – Evolutionary crystal structure prediction." *Comput. Phys. Commun.,* 175, 713-720.

Golesorkhtabar, R., Pavone, P., Spitaler, J., Puschnig, P. and Draxl, C. (2013). "ElaStic: A tool for calculating second-order elastic constants from first principles." *Comput. Phy. Commun.,* 184, 1861-1873.

Gonze, X. and Lee, C. (1997). **"**Dynamical matrices, Born effective charges, dielectric permittivity tensors,and interatomic force constants from density-functional perturbation theory." *Phys. Rev. B*, 55(6), 10355-10368.

Grasso, S., Hu, C., Vasylkiv, O., Suzuki, T. S., Guo, S., Nishimura, T. and Sakkaa, Y. (2011) "High-hardness B_4C textured by a strong magnetic field technique." *Scripta Mater*., 64, 256–259.

Gregoryanz, E., Sanloup, C., Somayazulu, M., Badro, J., Fiquet, G., Mao, H. K. and Hemley, R. J. (2004). "Synthesis and characterization of a binary noble metal nitride." *Nat. Mater.,* 3(5), 294-297.

Grossman, J. C., Mizel, A., Cote, M., Cohen, M. L. and Louie, S.G., (1999). "Transition metals and their carbides and nitrides: Trends in electronic and structural properties." *Phys. Rev. B,* 60, 6343-6347.

Guang, Z. M., Yan, Y. H., Tai, Z. G. and Hui, W. (2012). "The ground-state structure and physical properties of RuC: first-principles calculations." *Chin. Phys. B,* 217, 076103-076109.

Guillermet, A.F. and Grimvall, G. (1989). **"**Cohesive properties and vibrational entropy of 3d-transition-metal compounds: *MX* (NaCl) compounds (*X*=C, N, O, S), complex carbides, and nitrides**.**" *Phys. Rev. B,* 40, 10582-10593.

Guo, X. J., Li, L., Liu, Z. Y., Yu, D., He, J., Liu, R., Xu, B., Tian, Y. and Wang, H. T. (2008). "Hardness of covalent compounds: Roles of metallic component and d-valence electrons." *J. Appl. Phys.,* 104(2), 023503-1-7.

Guo, X., Xu, B., He, J., Yu, D., Liu, Z. and Tian, Y. (2008). "Structure and mechanical properties of osmium carbide: First-principles calculations." *Appl. Phys. Lett.,* 93, 041904-041907.

Haguland, J., Grimvall, G., Jalborg, T. and Guillermet, A.F. (1991). "Band structure and cohesive properties of 3d-transition-metal carbides and nitrides with the NaCl-type structure." *Phys. Rev. B*, 43, 14400-14408.

Haguland, J., Guillermet, A.F., Grimvall, G. and Korling M. (1993). "Theory of bonding in transition-metal carbides and nitrides." *Phys. Rev. B,* 48, 11685-11691.

Hao, J., Tang, X., Li, W.J. and Li, Y.W. (2014). "First-principle calculations of high-pressure phase transformations in RuC." *Europhys. Lett*., 105(4), 46004-46008.

Hao, A., Zhou, T., Zhu, Y., Zhang, X. and Liu, R. (2011). "First-principles investigations on electronic, elastic and thermodynamic properties of ZrC and ZrN under high pressure." *Mater. Chem. Phys.,* 129, 99-104.

Harikrishnan, G., Ajith, K.M., Sharat Chandra, Valsakumar, M.C. (2015a). "Evolutionary algorithm based structure search for hard ruthenium carbides." *Modelling Simul. Mater. Sci. Eng.,* 23, 085006-1-24.

Harikrishnan, G., Ajith, K.M., Sharat Chandra, Valsakumar, M.C. (2015b). "Vibrational spectra of ruthenium carbide structures yielded by the structure search employing evolutionary algorithm." *Mater. Sci. Semicond. Process.,* 40, 484-490.

Hartree, D. R. (1928). "The wave mechanics of an atom with a non-Coulomb central field. Part I. Theory and methods." *Proc. Camb. Phil. Soc.*, 24, 89-110.

Hayun, S., Paris, V., Dariel, M.P., Frage, N. and Zaretzky, E. (2009). "Static and dynamic mechanical properties of boron carbide processed by spark plasma sintering." *J. Eur. Ceram. Soc.*, 29, 3395–3400.

Heine, V. (1971). "The Pseudopotential Concept." *Solid State Phys.*, 24, 1-36.

Hill R. (1952). "The elastic behaviour of a crystalline aggregate." *Proc. Phys. Soc., London*, 65, 349-354.

Hoard, J. L. and Hughes, R. E. (1967). *Elemental boron and compounds of high boron content: Structure, properties, and polymorphism. The chemistry of boron and its compounds*, ed. E. L. Muetterties, Wiley, New York.

Hohenberg, P. and Kohn, W. (1964). "Inhomogeneous electron gas." *Phys. Rev.*, 136, B864.

Hosmane, N. S., Maguire, J. A. and Yinghuai, Z. (2006). "Polyhedral boron cage compounds: an account." *Main Group Chem.*, 5(4), 251–265.

Hugosson, H.W., Eriksson, O., Jansson, U. and Johansson, B. (2001). "Phase stabilities and homogeneity ranges in 4d-transition-metal carbides: A theoretical study." *Phys. Rev. B,* 63, 134108-134119.

Huhn, W. P. and Widom, M. (2013). **"**A free energy model of boron carbide." *J. Stat. Phys*. 150, 432-441.

Hynes, T. V. and Alexander, M. N. (1971). "Nuclear magnetic resonance study of b-rhombohedral boron and boron carbide." *J. Chem. Phys*., 54, 5296–5310.

Ivanovskii, A. L. (2009). "Platinum group metal nitrides and carbides: Synthesis, properties and simulation." *Russ. Chem. Rev.,* 78(4), 303-318.

Ivashchenko, V.I., Shevchenko, V.I. and Turchi, P.E.A. (2009). "First-principles study of the atomic and electronic structures of crystalline and amorphous B_4C." *Phys. Rev. B*, 80(23), 235208-1-9.

Jiménez, I., Sutherland, D. G. J., van Buuren, T., Carlisle, J.A., Terminello, L.J. and Himpsel, F.J. (1998). "Photoemission and X-ray-absorption study of boron carbide and its surface thermal stability." *Phys. Rev. B*, 57(20), 13167–13174.

Kaner, R. B., Gilman, J. J. and Tolbert, S. H. (2005). "Materials *science –* Designing super hard materials." *Science,* 308, 1268-1269.

Kavitha, M., Priyanga, G.S., Rajeswarapalanichamy, R. and Iyakutti, K. (2015). "First principles study of the structural, electronic, mechanical and superconducting properties of WX (X=C, N)." *J. Phys. Chem. Solids*, 77, 38-49.

Kempter, C.P. (1964). "Further investigation of RuC and OsC." *J. Chem. Phys*., 41, 1515-1516.

Kempter, C.P. and Nadler, M.R. (1960). "Preparation and crystal structures of RuC and OsC." *J. Chem. Phys.,* 33, 1580-1581.

Kirfel, A., Gupta, A. and Will, G. (1979). "The nature of the chemical bonding in boron carbide, $B_{13}C_2$. I. Structure refinement." *Acta Cryst. B*, 35, 1052-1059.

Kittel, C. (1996). *Introduction to solid state physics*, Pp. 78, Table 9, Wiley, New York.

Kohn, W. and Sham, L. J. (1965). "Self-consistent equations including exchange and correlation effects." *Phys. Rev*., 140(4A), A1133-A1138.

Kresse, G. and Furthmuller, J. (1996). "Efficient iterative schemes for *ab initio* total-energy calculations using a plane-wave basis set." *Phys. Rev. B,* 54, 11169-11186.

Kresse, G. and Hafner, J., 1993. "*Ab initio* molecular dynamics for liquid metals." *Phys. Rev. B,* 47, 558-561.

Kresse, G. and Joubert, D. (1999). "From ultrasoft pseudopotentials to the projector augmented-wave method." *Phys. Rev. B,* 59, 1758-1775.

Kuhlmann, U., Werheit, H. and Schwetz, K. A. (1992). "Distribution of carbon atoms on the boron carbide structure elements," *J. Alloy. Compd.,* 189, 249–258.

Kwei, G. H. and Morosin, B. (1996). "Structures of the boron-rich carbides from neutron powder diffraction: Implications for the nature of the inter-icosahedral chains." *J. Phys. Chem.,* 100, 8031–8039.

Łażewski, J., Jochym, P. T. and Parlinski, K. (2002). "Band structure, born effective charges, and lattice dynamics of $CulnS_2$ from *ab initio* calculations." *J. Chem. Phys.,* 117(6), 2726-2731.

Lazzari, R., Vast, N., Besson, J.M., Baroni, S. and Dal Corso, A. (1999). "Atomic structure and vibrational properties of icosahedral B_4C boron carbide." *Phys*. *Rev*. *Lett*., 83(16) 3230–3233.

Levine, J.B., Tolbert, S.H. and Kaner, R.B. (2009). "Advances in the search for superhard ultra-incompressible metal borides." *Adv. Funct. Mater.,* 19, 3519-3533.

Li, X., Zhang, X., Qin, J., Zhang, S., Ning, J., Jing, R., Ma, M. and Liu, R. (2014). "First-principles calculations of structural stability and mechanical properties of tungsten carbide under high pressure." *J. Phys*. *Chem*. *Solids*, 75, 1234-1239.

Lu, J., Hong, F., Lin, W.J., Ren, W., Li, Y.W. and Yan, Y. (2015). "Novel ultra-incompressible phases of Ru_2C." *J. Phys. Condens. Mater.,* 27, 175505-1-6.

Lyakhov, A. O., Oganov, A. R. and Valle, M. (2011). *Crystal structure prediction using evolutionary approach. Modern Methods of Crystal Structure Prediction*, ed. A.R. Oganov chapter 7,Wiley-VCH, Weinheim, Germany.

Manghnani, M. H., Wang, Y., Li, F., Zinin, P. and Rafaniello, W. (2000). *Elastic and vibrational properties of B_4C to 21 GPa, Science and technology of high pressure*, eds. M. H. Manghnani, W. J. Nellis, and M. F. Nicol., Pp. 945–948, Universities Press, Hyderabad.

Mauri, F., Vast, N., and Pickard, C. J. (2001). "Atomic structure of icosahedral B_4C boron carbide from a first principles analysis of NMR spectra." *Phys. Rev. Lett*., 87(8), 085506-1- 4.

Mehl, M. J., Kein, B. M. and Papaconstantopoulos, D. A. (1994). *Intermetallic compounds : Principles and practice,* eds. J. H. Westbrook, R. L. Fleischer, John Wiley & Sons, London.

Methfessel, M. and Paxton, A.T. (1989). "High-precision sampling for brillouin-zone integration in metals." *Phys. Rev. B,* 40, 3616-3621.

Mishra,V., and Chaturvedi, S. (2013). "FP-APW calculations of equation of state and elastic properties of a and b phases of tungsten carbide at high pressure." *J. Phys. Chem. Solids,* 74, 509-517.

Momma, K. and Izumi, F. (2011). "VESTA 3 for three-dimensional visualization of crystal, volumetric and morphology data." *J. Appl. Cryst.,* 44, 1272-1276.

Monkhorst, H. J. and Pack, J. D. (1976). "Special points for brillouin-zone integrations." *Phys. Rev. B,* 13, 5188-5192.

Morosin, B., Aselage, T. L. and Feigelson, R. S. (1987). "Crystal structure refinements of rhombohedral symmetry materials containing boron-rich icosahedra." *Mater. Res. Soc. Symp. Proc*. 97, 145-149.

Morosin, B., Kwei, G. H, Lawson, A. C., Aselage, T. L. and Emin, D. (1995). "Neutron powder diffraction refinement of boron carbides. Nature of inter-icosahedral chains." *J. Alloy. Compd.* 226, 121-125.

Morosin, B., Mullendore, A.W., Emin, D. and Slack, G.A. (1986). "Rhombohedral crystal structure of compounds containing Boron-rich icosahedra." *Boron-Rich Solids. AIP Conf. Proc.*, 140, 70–86.

Mouhat, F. and Coudert, F-X. (2014). "Necessary and sufficient elastic stability conditions in various crystal systems." *Phys. Rev. B*, 90, 224104-01-04.

Murnaghan, F. D. (1944). "The compressibility of media under extreme pressures." *Proc. Natl. Acad. Sci. U.S.A.,* 30, 244-247.

Murthy, S. R. (1985). "Elastic properties of boron carbide." *J. Mater. Sci. Lett.*, 4(5), 603–605.

Nelmes, R. J., Loveday, J. S., Wilson, R. M., Marshall, W. G., Besson, J. M., Klotz, S., Hamel, G., Aselage, T. L. and Hull, S. (1995). "Observation of inverted-molecular compression in boron carbide." *Phys. Rev. Lett.,* 74(12), 2268–2271.

Nye, J. F. (1985). *Physical Properties of Crystals: Their Representation by Tensors and Matrices*, Oxford University Press, Oxford.

Oganov, A. R. (2010). *Modern methods of crystal structure prediction*, Wiley-VCH Weinheim, Germany.

Oganov, A. R. and Glass, C.W. (2006). "Crystal structure prediction using *ab initio* evolutionary techniques: Principles and applications." *J. Chem. Phys.,* 124, 244704-244719.

Ono, O., Kikegawa, T. and Ohishi, Y. (2005). "A high-pressure and high-temperature synthesis *of* platinum carbide." *Solid State Commun.* 133, 55-59.

Page, Y. L. and Saxe, P. (2001). "Symmetry-general least-squares extraction of elastic coefficients from *ab initio* total energy calculations." *Phys. Rev. B,* 63, 174103-01-08

Page, Y. L. and Saxe, P. (2002). "Symmetry-general least-squares extraction of elastic data for strained materials from *ab initio* calculations of stress." *Phys. Rev. B,* 65, 104104-01-14.

Perdew, J. P., Burke, K. and Ernzerhof, M. (1997). "Generalized gradient approximation made simple [Phys. Rev. Lett. 77, 3865 (1996)] - Errata."*Phys. Rev. Lett.*, 78, 1396.

Perdew, J. P., Burke, K. and Ernzerhof, M. (1996). "Generalized gradient approximation made simple." *Phys. Rev. Lett*. 77, 3865- 3870.

Perdew, J. P. and Zunger, A. (1981). "Self-interaction correction to density-functional approximations for many-electron systems." *Phys. Rev. B*, 23, 5048-5079.

Pugh, S.F. (1954). "Relations between the elastic moduli and the plastic properties of polycrystalline pure metals." *Philos. Mag.*, 45, 823-843.

Rathod, N., Gupta, S.K., Shinde, S. and Jha, P.K. (2013). **"**First-principles investigation of thermophysical properties of cubic ZrC under high pressure." *Int. J. Thermophys.*, 34, 2019-2026.

Reuss, A. (1929). "Berechnung der Fließgrenze von Mischkristallen auf Grund der Plastizittitsbedingung fiir Einkristalle." *Math. Mech.*, 9, 49-58**.**

Saal, J. E. Shang, S. and Liu, Z. K. (2007). "The structural evolution of boron carbide via *ab initio* calculations." *Appl. Phys. Lett.*, 91(23), 231915-1-3.

Samara, G. A., Tardy, H. L., Venturini, E. L., Aselage, T. L. and Emin, D. (1993). "AC Hopping conductivities, dielectric-constants, and reflectivities of boron carbides." *Phys. Rev. B*, 48(3), 1468–1477.

Sanjay Kumar, N.R., Chandra Shekar, N.V., Sharat Chandra, Basu, J., Divakar R. and Sahu P.Ch. (2012). "Synthesis of novel Ru_2C under high pressure–high temperature conditions." *J. Phys. Condens. Mater.,* 24, 362202-362208.

Schmechel, R. and Werheit, H. (1997). "Evidence of the superposition of Drude type and Hopping type transport in boron-rich solids." *J. Solid State Chem.*, 133 (1), 335–341.

Schmechel, R. and Werheit, H. (1999). "Correlation between structural defects and electronic properties of icosahedral boron-rich solids." *J. Phys. Condens. Mat.*, 11, 6803–6813.

Schreiber, E., Anderson, O. L. and Soga, N. (1973). *Elastic constants and their measurements,* McGraw-Hill, New York.

Schwetz, K. A. and Grellner, W. (1981). "The influence of carbon on the microstructure and mechanical properties of sintered boron carbide." *J. Less Common Met.*, 82, 37–47.

Setyawan, W. and Curtarolo, S. (2010). "High-throughput electronic band structure calculations: Challenges and tools." *Comp. Mater. Sci.,* 49, 299-312.

Shirai, K. (2010). "Electronic structures and mechanical properties of boron and boron-rich crystals (Part I)." *J. Superhard Mater.*, 32(3), 205–225.

Shirai, K., Sakuma, K. and Uemura, N. (2014). "Theoretical study of the structure of boron carbide $B_{13}C_2$." *Phys. Rev. B*, 90, 064109-1-10.

Šimůnek, A. (2007). "How to estimate hardness of crystals on a pocket calculator." *Phys. Rev. B,* 75, 172108-172112.

Šimůnek, A. (2009). "Anisotropy of hardness from first principles: The cases of ReB_2 and OsB_2." *Phys. Rev. B,* 80, 060103-060107.

Šimůnek, A. and Vackář, J. (2006). "Hardness of covalent and ionic crystals: First-principle calculations." *Phys. Rev. Lett.,* 96, 085501-085505.

Sin'ko, G. V. and Smirnov, N. A. (2002). "Ab *initio* calculations of elastic constants and thermodynamic properties of bcc, fcc, and hcp Al crystals under pressure." *J. Phys. Condens. Matter*, 14, 6989-7005.

Smith, D., Dworking, A. S. and Van Artsdalen, E. R. (1955). "The heats of combustion and formation of boron carbide." *J. Am. Chem. Soc.,* 77, 2654-2656.

Soni, H.R., Gupta, S.K. and Jha, P.K. (2011). "*Ab initio* total energy calculation of the dynamical stability of noble metal carbides." *Physica B,* 406, 3556-3561.

Soni, P., Pagare, G. and Sanyal, S.P. (2011). "Structural, high pressure and elastic properties of transition metal monocarbides: A FP-LAPW study." *J. Phys. Chem. Solids*, 72, 810-816.

Stein, H., Aselage, T. L. and Emin, D. (1991). "Infrared absorption in boron carbides: Dependence on isotopes and carbon concentration." *Boron-Rich Solids. AIP Conf. Proc.*, 231, 322–325.

Sun, W., Chakraborty, S. and Ahuja, R. (2013). "Stabilizing a hexagonal Ru_2C *via* Lifshitz transition under pressure." *Appl. Phys. Lett.*, 103, 251901(1)-251901(4).

Suri, A.K., Subramanian, C., Sonber, J. K. and Murthy, T. (2010). "Synthesis and consolidation of boron carbide: A review." *Int. Mater. Rev.*, 55(1), 4–40.

Tallant, D.R., Aselage, T.L., Campbell, A.N. and Emin, D. (1989). "Boron carbide structure by Raman spectroscopy." *Phys. Rev. B*, 40(8), 5649–5656.

Thevenot, F. (1990). "Boron carbide – A comprehensive review." *J. Eur. Ceram. Soc.*, 6, 205– 225.

Tian, Y., Xu, B. and Zhao Z. (2012). "Microscopic theory of hardness and design of novel superhard crystals." *Int. J. Refract. Met. Hard Mater.* 33, 93–106.

Togo, A., Oba, F. and Tanaka, I. (2008). "First-principles calculations of the ferroelastic transition between rutile-type and $CaCl_2$-type SiO_2 at high pressures." *Phys. Rev. B*, 78, 134106-01-09.

Toth, L.E. (1971). *Transition Metal Carbides and Nitrides*, Academic, New York.

Varshney, D. and Shriya, S. (2013). "Elastic, mechanical and thermodynamic properties at high pressures and temperatures of transition metal monocarbides." *Int. J. Refract. Met. Hard Mater.* 41, 375-401.

Vast, N., Sjakste, J. and Betranhandy, E. (2009). "Boron carbides from first principles." *J. Phys. Conf. Ser.*, 176, 012002-1-18.

Veprek, S., Zeer, A. and Riedel, R. (2000). *Handbook of ceramic hard materials.* ed. R. Riedel, Wiley, New York.

Voigt, W. (1928). *Lehrbook Der Kristallphysik*, Teubner, Leipsig.

Wallace, D. C. (1972). *Thermodynamics of crystals*, Wiley, New York.

Wang, D. Y., Yan, Q., Wang, B., Wang, Y. X., Yang, J. and Yang, G. (2014). **"**Predicted boron-carbide compounds: A first-principles study." *J. Chem. Phys*. 140, 224704-1-8.

Watt, J. P. (1980). "Hashin-Shtrikman bounds on the effective elastic moduli of polycrystals with monoclinic symmetry" *J. Appl. Phys.*, 51(3), 1520-1524.

Watt, J. P. and Peselnick, L. (1980). "Clarification of the Hashin-Shtrikman bounds on hexagonal, trigonal, and tetragonal symmetries." *J. Appl. Phys.,* 51, 1525-1530.

Werheit, H. (2006). "On excitons and other gap states in boron carbide." *J. Phys. Condens. Mat.*, 18(47), 10655–106662.

Werheit, H., Au, T., Schmechel, R., Shalamberidze, S.O., Kalandadze, G.I. and Eristavi, A.M. (1999). "IR-active phonons and structure elements of isotope-enriched boron carbide." *J. Solid State Chem.*, 154, 79–86.

Werheit, H. and de Groot, K. (1980). "Metal-insulator transition in boron carbide." *Phys. Status Solidi. B*, 97(1), 229–238.

Werheit, H., Laux, M., Kuhlman, U., and Telle, R. (1991). "Optical interband transitions of boron carbide." *Phys. Stat. Sol. B.,* 172, K81-K86.

Werheit, H., Leithe-Jasper, A., Tanaka, T., Rotter, H. W. and Schwetz, K. A. (2004). "Some properties of single-crystal boron carbide." *J. Solid State Chem.,* 177, 575-579.

Widom, M. and Huhn, W. P. (2012). "Prediction of orientational phase transition in boron carbide." *Solid State Sci.,* 14, 1648-1652.

Widom, M. and Mihalkovi*c̀*, M. (2009). "Relative stability of α and β boron." *J. Phys. Conf. Ser*., 176, 012024-1-10.

Wood, C. and Emin, D. (1984). "Conduction mechanism in boron carbide." *Phys. Rev. B*, 29(8), 4582–4587.

Wood, C., Emin, D. and Gray, P. E. (1985). "Thermal conductivity of boron carbides." *Phys. Rev. B*, 31(10), 6811–6814.

Yakel, H. L. (1975). "The Crystal structure of a boron-rich boron carbide." *Acta Cryst. B*, 31, 1797–1806.

Yin, Z. Z., Ju, P., Fen, Z., Lin, M. C., Ju, C., Bin, C. G. and Dong, C. (2010). "Pressure and temperature effects on NaCl-type transition metal carbide from first-principles calculations" *Physica B*, 405, 4620-4626.

Young, A. F., Sanloup, C., Gregoryanz, E., Scandolo, S., Hemley, R. J. and Mao, H. K. (2006). "Synthesis of novel transition metal nitrides IrN_2 and OsN_2." *Phys. Rev. Lett.,* 96(15), 155501-01-04.

Zaoui, A. and Ferhat, M. (2011). "Dynamical stability and high pressure phases of platinum carbide." *Solid State Commun.*, 151, 867-869.

Zhao, E., Wang, J. and Wu, Z. (2010). "Structural stability and phase transition in OsC and RuC." *J. Comput. Chem.,* 31, 2883-2888.

Zhao, Z., Wang, M., Cui, L., He, J., Yu, D. and Tian, Y. (2010). "Semiconducting Superhard Ruthenium Monocarbide." *J. Phys. Chem. C,* 114, 9961-9964.

Zheng, J.C. (2005). "Super-hard hexagonal transition metal and its carbide and nitride: Os, OsC, and OsN." *Phys. Rev. B,* 72, 052105-052109.

PUBLICATIONS

Refereed International Journals

1. **Harikrishnan, G.**, Ajith, K.M., Sharat Chandra, Valsakumar, M.C. (2015). "Evolutionary algorithm based structure search for hard ruthenium carbides." *Modelling Simul. Mater. Sci. Eng.,* 23, 085006-1-24.

2. **Harikrishnan, G.**, Ajith, K.M., Sharat Chandra, Valsakumar, M.C. (2015). "Vibrational spectra of ruthenium carbide structures yielded by the structure search employing evolutionary algorithm." *Mater. Sci. Semicond. Process.,* 40, 484-490.

3. **Harikrishnan, G.**, Ajith, K.M., Sathish Natarajan, Sharat Chandra, Valsakumar, M.C. (2016). "Pressure-induced variation of structural, elastic, vibrational, electronic, thermodynamic properties and hardness of Ruthenium Carbides." J. *Phys. Chem. Solids*., 94, 47-58.

4. **Harikrishnan, G.**, Ajith, K.M., Sharat Chandra, Valsakumar, M.C. (2016). "Evolutionary algorithm based structure search and first-principles study of hard $B_{12}C_3$ polytypes." *J. Alloys Compd.* **Manuscript under review.**

5. **Harikrishnan, G.**, Ajith, K.M., Sharat Chandra, Valsakumar, M.C. (2016). "Evolutionary algorithm based structure search and first-principles study of semiconducting $B_{13}C_2$." *Phys. Rev. B.* **Manuscript under review.**

Curriculum Vitae

Name	:	Harikrishnan G
Nationality	:	Indian
Occupation	:	Assistant Professor of Physics
Official Address	:	Dept. of Physics, Govt. College Madappally, Vadakara, Kerala, India. PIN – 673102
		Website : http://www.gcm.edu.in Email : madappallycollege@rediffmail.com Ph : +91-496-2512587, Fax : +91-496-2512587
E-mail	:	gharikrishnan2007@gmail.com,
Phone	:	+91 9447855840

Educational Qualifications

Course	University/ Board	Year	Percentage of Marks	Class
M.Phil Physics	University of Calicut	2000	74	First Class
M.Sc Physics	University of Calicut	1998	76	Second Rank
NET	UGC-CSIR	1998	N.A.	N.A.
B.Sc Physics	University of Calicut	1996	97	First Rank
Pre-Degree	University of Calicut	1993	86	Distinction
SSLC	Board of Public Exams, Kerala	1991	93	Distinction

Teaching Experience

Institution	Classes Taught	Period	
		From	To
Mahatma Gandhi College, Iritty, Kannur, Kerala, India	B.Sc	June 2000	January 2007
Govt. College Madappally, Vadakara, Kerala, India	B.Sc and M.Sc	January 2007	August 2016

Research Experience

- Joined for Ph.D at National Institute of Technology Karnataka (NITK), Surathkal, Karnataka, India in December 2010.

- Obtained the UGC Fellowship for full-time research under Faculty Improvement Programme in May 2012.
- Started working in the collaborative research project, the structure and ground state properties of Boron Carbides and Ruthenium Carbides, at IGCAR, Kalpakkam, Tamil Nadu, India in May 2012.
- Used the evolutionary algorithm-based code USPEX for structure determination.
- Used the DFT-based code VASP for structural relaxation and for the computation of ground state properties like formation energies, electronic bands and DOS, phonon bands and DOS, elastic constants, hardness etc.
- Used the DFT-based code Quantum ESPRESSO for the computation of total energies and structural relaxation, in connection with the USPEX work.

Projects / Workshops / Seminars

Programme	Institution	Year
Collaborative research project using Density Functional Theory based computations	Indira Gandhi Centre for Atomic Research, Kalpakkam	2012-2013
National Workshop on Applied Materials and Density Functional Theory	University of Calicut	2012
UGC- Refresher Course in Materials Science	University of Calicut	2011
Discussion Meeting on Impact of Quantum Effects on Our Classical World View (sponsored by TIFR)	Mahatma Gandhi University	2011
Lecture Workshop on Statistical Mechanics (sponsored by Indian Academy of Science)	Nehru Arts & Science College, Kanhangad, Kerala	2011
UGC- Refresher Course in Mathematical Sciences	University of Calicut	2009
SERC School on Theoretical High Energy Physics	Hyderabad Central University	2007
UGC- Refresher Course in Physics	University of Calicut	2003